NUREG/CR-3995

Hydrodynamics of Counter-Current Two Phase Flow Through Porous Media

Prepared by J. S. Marshall, V. K. Dhir

School of Engineering and Applied Sciences
University of California, Los Angeles

Prepared for
U.S. Nuclear Regulatory
Commission

NOTICE

Availability of Reference Materials Cited in NRC Publications

Most documents cited in NRC publications will be available from one of the following sources:

1. The NRC Public Document Room, 1717 H Street, N.W.
   Washington, DC 20555
2. The NRC/GPO Sales Program, U.S. Nuclear Regulatory Commission,
   Washington, DC 20555
3. The National Technical Information Service, Springfield, VA 22161

Although the listing that follows represents the majority of documents cited in NRC publications, it is not intended to be exhaustive.

Referenced documents available for inspection and copying for a fee from the NRC Public Document Room include NRC correspondence and internal NRC memoranda; NRC Office of Inspection and Enforcement bulletins, circulars, information notices, inspection and investigation notices; Licensee Event Reports; vendor reports and correspondence; Commission papers; and applicant and licensee documents and correspondence.

The following documents in the NUREG series are available for purchase from the NRC/GPO Sales Program: formal NRC staff and contractor reports, NRC-sponsored conference proceedings, and NRC booklets and brochures. Also available are Regulatory Guides, NRC regulations in the *Code of Federal Regulations*, and *Nuclear Regulatory Commission Issuances*.

Documents available from the National Technical Information Service include NUREG series reports and technical reports prepared by other federal agencies and reports prepared by the Atomic Energy Commission, forerunner agency to the Nuclear Regulatory Commission.

Documents available from public and special technical libraries include all open literature items, such as books, journal and periodical articles, and transactions. *Federal Register* notices, federal and state legislation, and congressional reports can usually be obtained from these libraries.

Documents such as theses, dissertations, foreign reports and translations, and non-NRC conference proceedings are available for purchase from the organization sponsoring the publication cited.

Single copies of NRC draft reports are available free, to the extent of supply, upon written request to the Division of Technical Information and Document Control, U.S. Nuclear Regulatory Commission, Washington, DC 20555.

Copies of industry codes and standards used in a substantive manner in the NRC regulatory process are maintained at the NRC Library, 7920 Norfolk Avenue, Bethesda, Maryland, and are available there for reference use by the public. Codes and standards are usually copyrighted and may be purchased from the originating organization or, if they are American National Standards, from the American National Standards Institute, 1430 Broadway, New York, NY 10018.

GPO Printed copy price: $6.50

NUREG/CR-3995
R2

Hydrodynamics of Counter-Current Two Phase Flow Through Porous Media

Manuscript Completed: May 1984
Date Published: December 1984

Prepared by
J. S. Marshall, V. K. Dhir

School of Engineering and Applied Sciences
University of California, Los Angeles
Los Angeles, CA 90024

Prepared for
Division of Accident Evaluation
Office of Nuclear Regulatory Research
U.S. Nuclear Regulatory Commission
Washington, D.C. 20555
NRC FIN G-04-81-025

ABSTRACT

Understanding of the hydrodynamic characteristics and flow limitations of two phase flow through porous media is necessary to evaluate the coolability of a top flooded degraded nuclear reactor core. In the present work, an analytical and experimental investigation of counter-current two phase flow through 80-100 cm deep porous layers composed of both uniform size spherical particles (nominal diameters 1-19 mm), mixtures of these particles, and mixtures of spherical particles and non-spherical "sharps" has been performed. The porous layers were formed in a 20 cm diameter plexiglass tube. Water and air were used as the test fluids, with superficial velocities ranging from 0-19.5 mm/s and 0-163 mm/s, respectively. Bed porosity, mean particle diameter, flooding limits, and void fraction and pressure gradient at flooding were investigated. An analytical approach based upon geometrical models was used to derive expressions for porosity and mean particle diameter. An empirical correlation has been found for the flooding data which is slightly different than that found in the literature. The effect of coupling of the overlying liquid layer with the bed and of axial gas injection upon the flooding limit were also studied. The results of these hydrodynamic investigations were applied to obtain dryout heat flux in bottom and volume heated particulate beds.

Table of Contents

LIST OF FIGURES

Figure		Page

Figure		Page

Figure		Page

LIST OF TABLES

Table		Page

NOMENCLATURE

Roman Letters

A	cross-sectional area (m^2)
a	surface area of packing per unit volume (m^2/m^3)
B	dimensionless two phase weighting parameter
C	constant (section 3.3)
D	diameter (m)
$\overline{D}$	mean diameter (m)
$D_{k,\ell}$	boundary of regions k and ℓ (m)
d_j	mean diameter of region j (m)
g	gravitational acceleration (m/s^2)
H	height (m)
h_{fg}	latent heat of evaporation (J/kg)
j	superficial velocity (m/s) $j \equiv Q/A$
L	bed height (m)
M	mixture set array
m	mass (kg)
N	number of particle sizes
n	diameter array counter
P	pressure (N/m^2)
q	dryout heat flux (W/m^2)
$\dot{Q}_v$	maximum energy removal rate per unit volume (W/m^3)
Q	volumetric flow rate (m^3/s)
Re	Reynolds number

S	dimensionless porosity weighting factor
x	volume fraction
XU_j	relative fraction of used particles from region j
XUT	total relative fraction of used particles
XUTT	total absolute fraction of used particles
V	volume (m^3)
z	axial direction (m)

Greek Letters

$\bar{\alpha}_{ac}$	average active void fraction
β	number ratio
$\beta_{r,min}$	minimum ratio of $\beta_j/\beta_{sat,j}$
γ	diameter ratio
ϵ	porosity
η	inertial relative permeability multiplier
κ	viscous relative permeability multiplier
μ	dynamic viscosity $(N \cdot s/m^2)$
ρ	density (kg/m^3)
ω	dimensionless mixing relaxation parameter

Subscripts

a	atmospheric
add	additional
crit	critical
f	frictional
fl	flooding

g	gas
i	initial (Appendix D)
ℓ	liquid
max	maximum
meas	measured
min	minimum
o	overlying layer
p	particle
s	static
sat	saturated
sep	separated
t	total
1	larger particle size (section 3.2.2)
2	smaller particle size (section 3.2.2)
1,2,3,4	region number (section 3.2.3)

Superscripts

*	nondimensional

Chapter 1

INTRODUCTION

In the event of nuclear reactor core degradation, several scenarios can be envisioned in which the core material may be considered to behave as a porous layer (1). The most efficient means of cooling such a degraded core is by bottom flooding, where the liquid flow rate is limited only by the amount of driving head available. However, if an impervious blockage forms at the bottom of the reactor core or if the debris drops into the reactor cavity, bottom flooding would no longer be possible and the debris must be cooled from above. The maximum amount of energy which can be removed from a top flooded debris bed depends on the counter-current flooding limit through the bed, which in turn depends upon the bed porosity and mean particle diameter. Since the debris bed would be composed of particles of various sizes and shapes, an a priori evaluation of porosity and mean particle diameter is required. In this work, analytical and experimental studies of mean particle diameter, porosity, counter-current flooding limits, and void fraction and pressure gradient at and before flooding are performed for beds composed of both uniform size spherical particles and mixtures of various size particles. The effect of overlying liquid layer coupling with the bed, axial gas injection, and bed stratification upon the flooding limit is also investigated. The results of these hydrodynamic studies are then applied to evaluate the dryout heat flux for bottom and volume heated particulate beds.

During the past several years, experimental and analytical studies of dryout heat flux in bottom and volume heated beds have appeared in the literature (1). Almost all of the models for dryout heat flux are based on counter-current flow limitations through particulate beds. In these models either the results for limiting velocities are borrowed from the literature (2) or are obtained by making some assumptions about the void fraction (3,4) while accounting for the particle drag experienced by the vapor and liquid phases. Also, in some of the studies (2,4) no clear distinction between dryout in bottom and volume heated beds or consideration to the interaction between the overlying layer and the bed has been made. The dryout heat fluxes observed in volume heated beds are generally higher than those observed in bottom heated beds (5). The purpose of this work is to study experimentally the flooding limit in particulate beds and then apply this to determine dryout heat flux in bottom and volume heated beds. Studies of bed porosity and mean particle diameter in beds composed of mixtures of various size particles are also performed in order to make this work more applicable to the cooling of a degraded nuclear reactor core.

Chapter 2

EXPERIMENTAL APPARATUS AND PROCEDURE

The experimental apparatus was designed so that the porosity, mean particle diameter, limiting phase velocities, average void fraction, and local pressure at several locations along the test section can be determined for beds composed of various size particles. Mean particle diameter was obtained from measurements of the single phase liquid pressure drop through the bed. In all of the experiments, air and water were used as the test fluids with superficial velocities ranging from 0 to 163 mm/s and 0 to 19.5 mm/s, respectively.

2.1 Discription of the Apparatus

Experiments on counter-current two phase flow through porous media were conducted with ambient temperature air-water flow through a cylindrical test section. A schematic diagram of the experimental apparatus is given in Figure 2.1. The basic components of the setup are: a plexiglass test section, a water reservoir, and a centrifugal pump. Instrumentation consists of water manometers, air and liquid flow meters, and an inlet air pressure gage. Electric solenoid valves were installed in the inlet and exit water lines and the inlet air line for rapid flow cut-off. The test section, a 20.3 cm inner diameter and 167 cm long plexiglass tube, is formed of 15.2 cm long sections joined by flanges. The test section is placed on an outlet header with a slotted aluminum plate and a perforated brass sheet sandwiched inbetween. Upon the brass sheet, a 3.175 mm inner

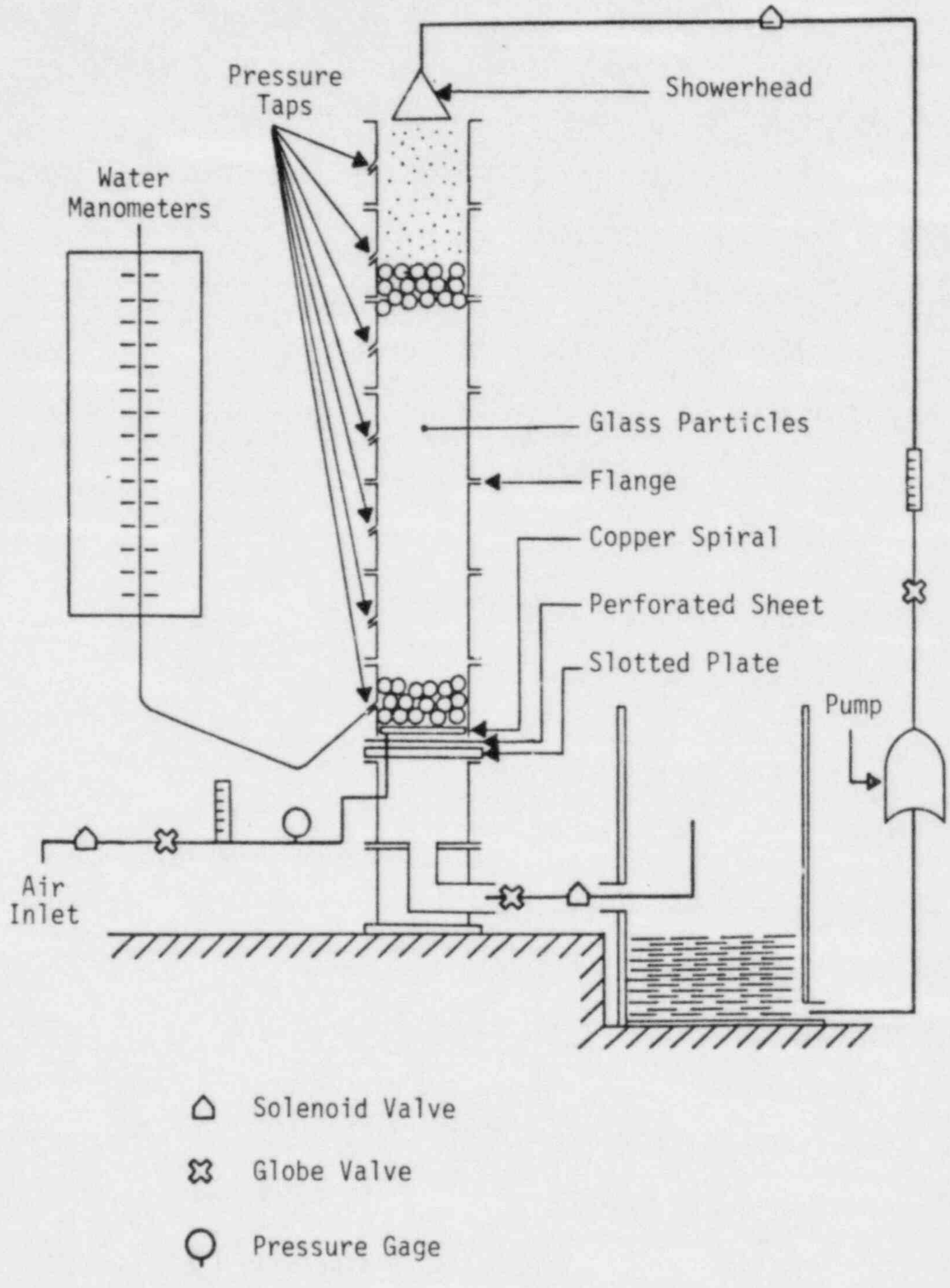

Figure 2.1 Schematic of the Experimental Apparatus

diameter copper tubing wound in the form of a spiral is placed. On the top side of the spiral, 0.794 mm diameter holes are drilled in a pattern which provides a uniform gas flow when the spiral is connected to an air supply. Water is sprinkled down on the particulate bed from a showerhead placed at the top of the test section. Eight pressure taps, made of 3.2 mm inside diameter plexiglass tubing, are placed along the bed height at 15.2 cm intervals and are connected to water manometers. Ten additional pressure taps are placed at 2 cm intervals near the top of the bed. Short glass tubes, measuring 2.0 mm in outside diameter and 1.0 mm in inside diameter, with glass wool loosely glued to the outside surface are inserted into the pressure taps. These porous plugs act to dampen oscillations in local pressure and detain air bubbles from entering the water manometer lines. Water exits through the outlet header and into a containing reservoir. A globe valve is inserted in the water exit line to control the water height in the test section and is referred to later as the water drainage valve. A 30 cm long pipe is connected perpendicularly upward at the end of the water exit line to insure that no air enters the line. This condition is necessary for void fraction measurements. A fixed scale is placed along the length of the test section to provide easy measurement of bed and overlying liquid layer heights.

In order to simulate volumetric vapor production in the bed, experiments were performed in which air was injected at various locations along the bed height. Five air injection locations were used, each spaced by 15.2 cm. These locations correspond to the first five pressure taps. Each injection location was connected to a separate air flow meter and then to a common source of compressed air.

2.2 Procedure

Before counter-current flow experiments were performed, measurements of particle material density and mean particle diameter were made for each particle size. Particle material density was determined by the volume of water displaced when a predetermined weight of particles was added to a 2000 ml graduated cylinder initially half filled with water. Particle mean diameter was determined by measuring the minimum and maximum diameters of 40 samples from each particle size using a one inch micrometer.

A certain amount of particles was then weighed and poured into the test section to obtain a particular height. Particulate beds were formed in a pool of water to minimize particle impact velocities. The porosity was determined from measurements of the bed height, bed weight, and particle material density. After formation of the bed, a predetermined liquid flow rate was established. Readings of the water manometers were noted to determine the single phase liquid pressure drop through the bed. Air was then gradually added to the test section in increments while keeping the liquid flow rate constant. An overlying two phase air-water layer between 10 cm to 40 cm in depth was allowed to form above the bed to eliminate effects of the free surface on void fraction in the upper section of the bed. Readings of the water manometers and overlying layer height were noted at each incremental air flow rate. The volume of air in the bed and overlying layer was found by simultaneously closing the water inlet and exit lines and the air inlet line. The effects of air compression on the air flow rate and non-instantaneous closure of the solenoid valves on overlying layer height drop were tested and accounted for. Experiments were terminated at air flow rates at which flooding was observed to occur.

2.3 Data Reduction

The density of the particle material (glass) was obtained from the following equation:

$$\rho_p = \frac{m_p}{\Delta V_\ell} \tag{2-1}$$

where ΔV_ℓ is the volume of liquid displaced by a known mass of particles m_p. The porosity of the particulate bed was calculated as

$$\epsilon = 1 - \frac{m_p}{\rho_p A L} \tag{2-2}$$

where m_p is the total mass of particles in the bed, ρ_p is the particle material density, L is the bed height, and A is the cross-sectional area. For an overlying layer of known hydrostatic head, ΔP_o, and depth, H_o, the average void fraction within the overlying layer, $\bar{\alpha}_o$, was obtained from the equation

$$\bar{\alpha}_o = \frac{\rho_\ell - \frac{\Delta P_o}{gH_o}}{\rho_\ell - \rho_g} \tag{2-3}$$

The active void fraction, discussed in reference (6), is defined as the fraction of pore area occupied by moving gas. The fraction of the pore occupied by non-moving gas is termed in (6) as the inactive void fraction. Since in this study only the active void fraction is considered, it is often written simply as "void fraction" where the "active" is implied. The average active void fraction in the particulate bed was obtained by simultaneously stopping the incoming air flow and incoming and exiting water flows. This resulted in a reduced overlying layer height, H_1. By a volume balance on air, the average active void fraction was calculated by the equation

$$\bar{\alpha}_{ac} = \frac{(H_o - H_1) - \bar{\alpha}_o H_o}{\varepsilon L} \tag{2-4}$$

The frictional pressure gradient was calculated from a known total pressure gradient by the following equation:

$$\frac{dP_f}{dz} = \frac{dP_t}{dz} - \left[(1-\bar{\alpha}_{ac})\rho_\ell + \bar{\alpha}_{ac}\rho_g\right] g \tag{2-5}$$

Chapter 3

RESULTS OF HYDRODYNAMIC STUDIES

Pressure drop, void fraction, porosity, and flooding data were obtained for beds composed of uniform size spherical particles, mixtures of spherical particle sizes, and mixtures of spherical particles and non-spherical "sharps". Glass particles with nominal diameters of 1, 3, 6, 10, 15, and 19 mm were used. The sharps were passed through a sieve with a 5.66x5.66 mm cross-section but were retained on a sieve with a 4x4 mm cross-section. The porosity varied between 0.38 and 0.42 for beds composed of uniform size spherical particles and between 0.18 and 0.38 for beds composed of mixtures of spherical particles. Particulate bed heights of between 80 cm and 98 cm were used. Superficial velocities were varied from 0 to 19.5 mm/s for water and from 0 to 163 mm/s for air.

3.1 Mean Particle Diameter

3.1.1 Mean Particle Diameter for Beds Composed of Nearly Uniform Size Spherical Particles

The observed frictional pressure gradients for single phase liquid flow through beds composed of 3, 6, 10, and 19 mm nominal diameter particles are shown in Figure 3.1. The single phase liquid frictional pressure gradient is given by the Kozeny-Carmen equation as

$$\frac{dP_f}{dz} = \frac{150(1-\varepsilon)^2}{\varepsilon^3 D_p^2} \mu_\ell j_\ell + \frac{1.75(1-\varepsilon)}{\varepsilon^3 D_p} \rho_\ell j_\ell^2 \qquad (3\text{-}1)$$

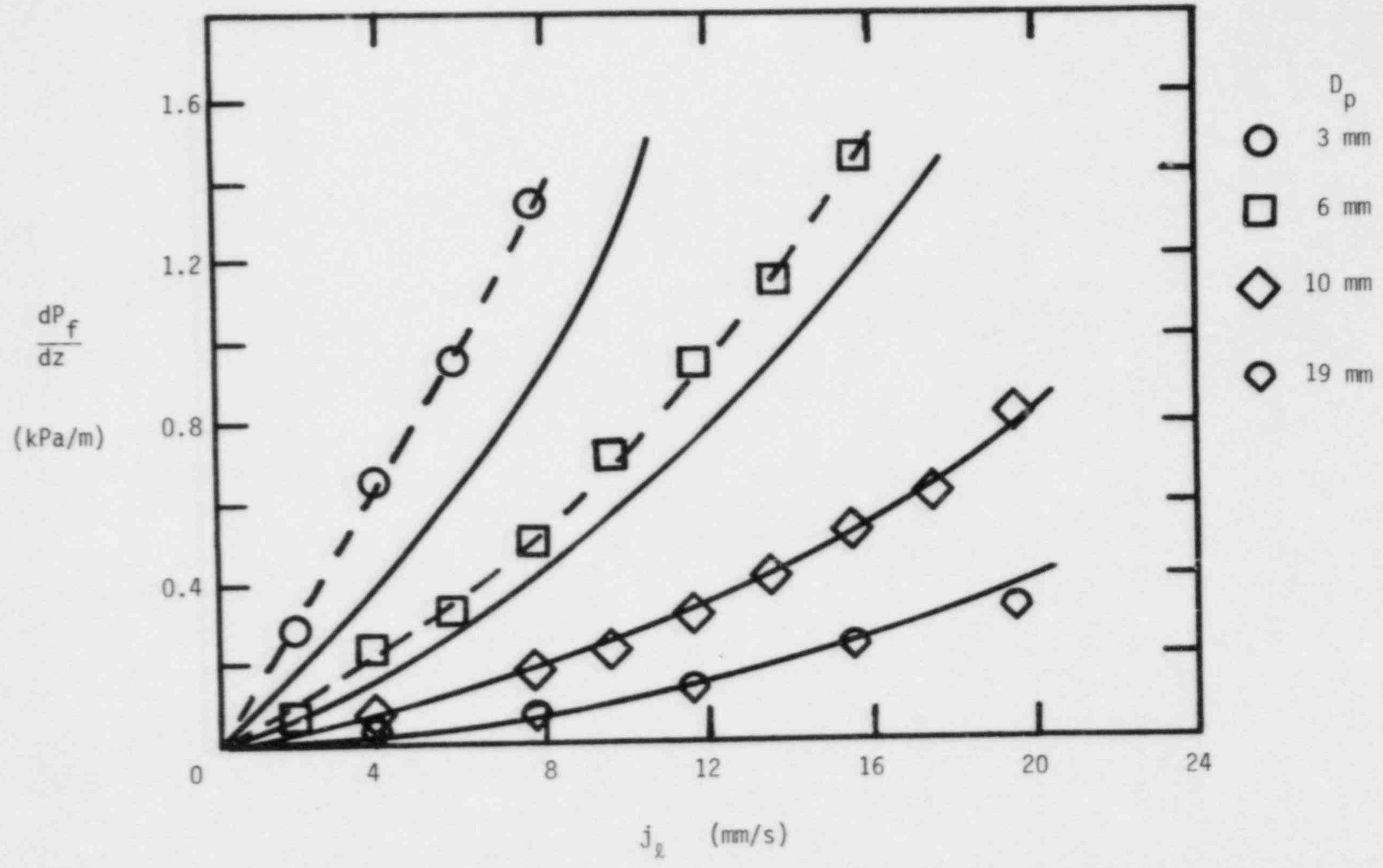

Figure 3.1 Single Phase Liquid Frictional Pressure Gradients

The arithmetic mean particle diameter for each nominal particle size was determined by measuring the diameters of a set of 40 particles and taking an average. Another value for mean particle diameter can be obtained by using the experimentally obtained frictional pressure gradient and solving for diameter in equation (3-1). A comparison between these two methods for determining the mean particle diameter is given in Table 3.1. In Table 3.1, the measured arithmetic mean particle diameters are seen to be within 14% of those calculated using equation (3-1). The range of variation of measured diameters in Table 3.1 is simply the minimum and maximum of the micrometer readings for each nominal particle size. The solid lines in Figure 3.1 represent the pressure gradients predicted from equation (3-1) using the measured arithmetic mean particle diameters, and the dotted lines represent a best fit to the data. The diameter measuring technique was not very accurate for small diameter particles, thus the predicted pressure gradients are slightly higher than the observed pressure gradients for 3 mm and 6 mm nominal diameter particles.

3.1.2 Mean Particle Diameter for Single Phase Liquid Flow Through Beds Composed of Mixtures of Particle Sizes

The mean particle diameter for single phase liquid flow through beds composed of mixtures of particle sizes may be calculated by imagining the bed to be formed of stratified layers of each constituent particle size. In selecting a mean particle diameter

Table 3.1 Mean Diameters of Beds Composed of Uniform Size Spherical Particles

Nominal Diameter (mm)	Kozeny-Carmen Mean Diameter (mm)	Measured Arithmetic Mean Diameter (mm)	Range of Variation (mm)
3	2.1	2.8	1.9-3.4
6	5.0	5.8	5.6-6.1
10	10.0	10.0	9.8-10.3
15	13.0	14.7	14.4-14.9
19	21.7	19.1	18.4-19.7

for the mixture, the pressure gradient through a bed composed of uniform size spherical particles of diameter equal to the mean particle diameter of the mixture and with a porosity equal to the actual mixture porosity must be the same as the actual pressure gradient through the mixture at any given superficial liquid velocity. Using the Kozeny-Carmen equation (3-1) and equating the pressure drops through the layered bed and the mean diameter bed, we get the relation

$$AL\left[\frac{150(1-\epsilon)^2}{\epsilon^3\bar{D}_p^{\,2}}\,\mu_\ell j_\ell + \frac{1.75(1-\epsilon)}{\epsilon^3\bar{D}_p}\,\rho_\ell j_\ell^{\,2}\right]$$

$$= \sum_{i=1}^{N} AL_i\left[\frac{150(1-\epsilon)^2}{\epsilon^3 D_{p,i}^{\,2}}\,\mu_\ell j_\ell + \frac{1.75(1-\epsilon)}{\epsilon^3 D_{p,i}}\,\rho_\ell j_\ell^{\,2}\right] \qquad (3\text{-}2)$$

From the definition of the volume fraction, we can write

$$x_i = \frac{AL_i}{AL} \qquad (3\text{-}3)$$

Dividing (3-2) by $1.75(1-\epsilon)\rho_\ell j_\ell^{\,2}/\epsilon^3$, the following relation can be obtained for the mean diameter:

$$\frac{1}{\bar{D}_p} + \frac{86(1-\epsilon)\mu_\ell}{\rho_\ell j_\ell}\,\frac{1}{\bar{D}_p^{\,2}} = \sum_{i=1}^{N}\left[\frac{x_i}{D_{p,i}} + \frac{86(1-\epsilon)\mu_\ell}{\rho_\ell j_\ell}\,\frac{x_i}{D_{p,i}^{\,2}}\right] \qquad (3\text{-}4)$$

Notice that in equation (3-4), the mean diameter is a function of the liquid superficial velocity. Defining the Reynolds number as

$$Re_\ell = \frac{\rho_\ell j_\ell \bar{D}_p}{\mu_\ell} \quad , \tag{3-5}$$

equation (3-4) can be written as

$$\left[1 + \frac{86(1-\varepsilon)}{Re_\ell}\right] \frac{1}{\bar{D}_p} = \sum_{i=1}^{N} \left[1 + \frac{86(1-\varepsilon)}{Re_\ell} \frac{\bar{D}_p}{D_{p,i}}\right] \frac{x_i}{D_{p,i}} \tag{3-6}$$

For $Re_\ell >> 86(1-\varepsilon)$, equation (3-6) can be approximated as

$$\frac{1}{\bar{D}_p} = \sum_{i=1}^{N} \frac{x_i}{D_{p,i}} \tag{3-7}$$

Alternatively for $Re_\ell << 86(1-\varepsilon)$, equation (3-6) becomes

$$\frac{1}{\bar{D}_p^{\,2}} = \sum_{i=1}^{N} \frac{x_i}{D_{p,i}^{\,2}} \tag{3-8}$$

Equations (3-8) and (3-7) represent the bounds of the mean particle diameter as j_ℓ goes to zero and infinity, respectively.

The experimental values of the mean particle diameter from the Kozeny-Carmen equation are compared with the predictions of equations (3-7) and (3-8) in Table 3.2. The experimental values of the mean particle diameter represent an average of data taken for superficial liquid velocities ranging from 1.9 to 19.5 mm/s. For most of this range the Reynolds number is of the same order as $86(1-\varepsilon)$; thus the mean particle diameter is expected to be found somewhere inbetween the predictions of equations (3-7) and (3-8). In Table 3.2, the predictions of equation (3-7) are seen to be between 4% to 50% higher than those of equation (3-8). The exper-

Table 3.2 Mean Diameters for Mixtures of Sperical Particles

Nominal Diameters of Constituent Particles (mm)	Volume Fractions of Constituent Particles	Kozeny-Carmen Mean Diameter (mm)	Mean Diameter from Equation (3-7) (mm)	Mean Diameter from Equation (3-8) (mm)
6,10	0.28,0.72	7.8	8.3	8.0
6,15	0.16,0.84	10.3	11.9	10.7
6,10,15,19	0.20,0.30,0.30,0.20	9.9	10.5	9.6
3,6,10,15,19	0.16,0.21,0.21,0.21,0.21	5.4	6.2	5.7
1,3,6,10,15,19	0.10,0.15,0.25,0.25, 0.15,0.10	3.1	4.2	2.8

imental data in Table 3.2 agrees with the predictions of equation (3-8) to within 10%, but differs from the predictions of equation (3-7) by as much as 35%. In some instances, the experimental data does not fall between the theoretical limits obtained from equations (3-7) and (3-8). This deviation is caused by experimental uncertainty in the pressure gradient and constituent particle diameters.

3.1.3 Mean Particle Diameter for Two Phase Flow Through Beds Composed of Mixtures of Particle Sizes

The mean particle diameter for two phase flow through beds composed of mixtures of particle sizes can be obtained in a manner similar to that used for single phase liquid flow. Equating the two phase pressure drop through the layered bed and the mean diameter bed, we can write

$$AL\left[\frac{150(1-\varepsilon)^2}{\kappa_g\varepsilon^3\bar{D}_p^2}\mu_g j_g + \frac{1.75(1-\varepsilon)}{\eta_g\varepsilon^3\bar{D}_p}\rho_g j_g^2 - \frac{150(1-\varepsilon)^2}{\kappa_\ell\varepsilon^3\bar{D}_p^2}\mu_\ell j_\ell - \frac{1.75(1-\varepsilon)}{\eta_\ell\varepsilon^3\bar{D}_p}\rho_\ell j_\ell^2\right] = \sum_{i=1}^{N} AL_i\left[\frac{150(1-\varepsilon)^2}{\kappa_g\varepsilon^3 D_{p,i}^2}\mu_g j_g + \frac{1.75(1-\varepsilon)}{\eta_g\varepsilon^3 D_{p,i}}\rho_g j_g^2 - \frac{150(1-\varepsilon)^2}{\kappa_\ell\varepsilon^3 D_{p,i}^2}\mu_\ell j_\ell - \frac{1.75(1-\varepsilon)}{\eta_\ell\varepsilon^3 D_{p,i}}\rho_\ell j_\ell^2\right] \quad (3\text{-}9)$$

In equation (3-9), the superficial liquid velocity is taken as positive for counter-current flow. Dividing equation (3-9) by $\eta_g\varepsilon^3\rho_g j_g^2/1.75(1-\varepsilon)$ and rearranging gives

$$\left[\left(\frac{86(1-\varepsilon)\eta_g\mu_g}{\kappa_g\rho_g j_g}\right)\frac{1}{\bar{D}_p^{\,2}}+\frac{1}{\bar{D}_p}\right]-\left(\frac{\eta_g\rho_\ell j_\ell^{\,2}}{\eta_\ell\rho_g j_g^{\,2}}\right)\left[\left(\frac{86(1-\varepsilon)\eta_\ell\mu_\ell}{\kappa_\ell\rho_\ell j_\ell}\right)\frac{1}{\bar{D}_p^{\,2}}+\frac{1}{\bar{D}_p}\right]$$

$$=\sum_{i=1}^{N}x_i\left\{\left[\left(\frac{86(1-\varepsilon)\eta_g\mu_g}{\kappa_g\rho_g j_g}\right)\frac{1}{D_{p,i}^{\,2}}+\frac{1}{D_{p,i}}\right]-\left(\frac{\eta_g\rho_\ell j_\ell^{\,2}}{\eta_\ell\rho_g j_g^{\,2}}\right)\left[\left(\frac{86(1-\varepsilon)\eta_\ell\mu_\ell}{\kappa_\ell\rho_\ell j_\ell}\right)\frac{1}{D_{p,i}^{\,2}}+\frac{1}{D_{p,i}}\right]\right\}$$

(3-10)

The results of numerous studies (6,7) indicate that η_g/κ_g and η_ℓ/κ_ℓ are nearly equal to one. The Reynolds number for liquid is given in equation (3-5) and the Reynolds number for gas can be written as

$$Re_g = \frac{\rho_g j_g \bar{D}_p}{\mu_g} \qquad (3\text{-}11)$$

The relative importance of the gas and liquid phases in evaluating the mean particle diameter is determined by a two phase weighting parameter B, defined as

$$B \equiv \frac{\eta_g\rho_\ell j_\ell^{\,2}}{\eta_\ell\rho_g j_g^{\,2}} \qquad (3\text{-}12)$$

Using equations (3-11) and (3-12) and assuming that $\eta_g/\kappa_g = \eta_\ell/\kappa_\ell = 1$, equation (3-10) can be rewritten as

$$\left[\left(1+\frac{86(1-\varepsilon)}{Re_g}\right)-B\left(1+\frac{86(1-\varepsilon)}{Re_\ell}\right)\right]\frac{1}{\bar{D}_p}$$

$$=\sum_{i=1}^{N}x_i\left[\left(1+\frac{86(1-\varepsilon)}{Re_g}\frac{\bar{D}_p}{D_{p,i}}\right)-B\left(1+\frac{86(1-\varepsilon)}{Re_\ell}\frac{\bar{D}_p}{D_{p,i}}\right)\right]\frac{1}{D_{p,i}} \qquad (3\text{-}13)$$

This is the general mean diameter equation for two phase flow.

For $\rho_\ell j_\ell^{\,2} << \rho_g j_g^{\,2}$, the two phase weighting parameter B goes to zero and equation (3-13) can be written as

$$\left[1 + \frac{86(1-\varepsilon)}{Re_g}\right]\frac{1}{\overline{D}_p} = \sum_{i=1}^{N}\left[1 + \frac{86(1-\varepsilon)}{Re_g}\frac{\overline{D}_p}{D_{p,i}}\right]\frac{x_i}{D_{p,i}} \tag{3-14}$$

It can easily be shown that equation (3-14) goes to the limit of equation (3-7) for $Re_g >> 86(1-\varepsilon)$ and that of equation (3-8) for $Re_g << 86(1-\varepsilon)$. Similarly for $\rho_\ell j_\ell^2 >> \rho_g j_g^2$, B becomes very large and equation (3-13) can be written as

$$\left[1 + \frac{86(1-\varepsilon)}{Re_\ell}\right]\frac{1}{\overline{D}_p} = \sum_{i=1}^{N}\left[1 + \frac{86(1-\varepsilon)}{Re_\ell}\frac{\overline{D}_p}{D_{p,i}}\right]\frac{x_i}{D_{p,i}} \tag{3-15}$$

This equation is equivalent to equation (3-6) for single phase liquid flow. The limits of equations (3-7) and (3-8) are again obtained for $Re_\ell >> 86(1-\varepsilon)$ and $Re_\ell << 86(1-\varepsilon)$, respectively. The predictions of equations (3-7) and (3-8) are thus seen to represent the upper and lower bounds of the mean particle diameter for two phase flow through porous media. By estimating the ranges of the superficial gas and liquid velocities, one can determine an appropriate mean particle diameter using either the general weighting equation (3-13) or one of the limiting equations (3-7) and (3-8).

3.2 Porosity

3.2.1 Porosity of Beds Composed of Uniform Size Spherical Particles

Pore size in beds composed of uniform size spherical particles is known to vary between a minimum and a maximum determined by the set of stable geometrical configurations of the particles. The minimum pore size is given by a rhombohedral configuration, shown in Figure 3.2a, and results in a porosity of 0.259 (8). Scheidegger (8) points out that the configuration giving the greatest pore size has not yet been discovered. However, for purposes of this study, the maximum pore size can be assumed to be given by a cubic configuration (9), as shown in Figure 3.2b. A cubic configuration gives a porosity of 0.476. The porosity of the entire bed thus varies statistically between 0.259 and approximately 0.476, and the probability of obtaining any given porosity between these limits is given by a skewed normal distribution with a mean value of 0.40 (8). It should be noted that for "large" diameter particles ($D \geq 1$ mm) porosity is not a function of particle size. Several investigators (9,10) have detected increased porosities for "small" diameter particles ($D < 1$ mm) due to bridging. This study will be restricted to "large" particles ($D \geq 1$ mm), such that the porosity can be assumed to be independent of particle size. Pore size is also known to increase in the proximity of container walls, thus the mean porosity of a bed can increase either with increase in the particle diameter or decrease in the container diameter.

3.2.2 Porosity of Beds Composed of Mixtures of Two Size Particles

A few general terms and concepts must be defined before we proceed with the study of porosity of mixtures of particle sizes. It was previously stated that porosity of beds composed of a single

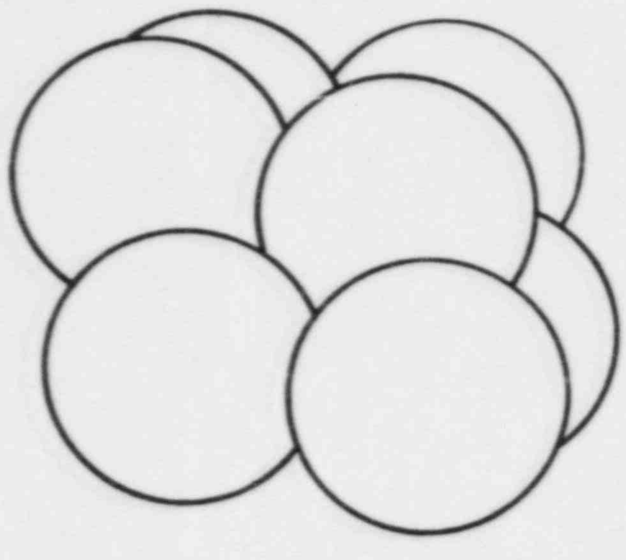

a. Rhombohedral Array

b. Cubic Array

Figure 3.2

particle size ($D \geq 1$ mm) is independent of the particle diameter. On this assumption, porosity of beds composed of mixtures of different particle sizes must also be independent of the absolute diameters of the constituent particles but dependent instead upon some ratio of their diameters. For mixtures of two particle sizes, the diameter ratio is defined as

$$\gamma \equiv \frac{D_2}{D_1} \tag{3-16}$$

where $D_1 \geq D_2$. Since D_1 is always greater than D_2, the diameter ratio varies only between 0 and 1. Another important parameter is the number ratio, defined for mixtures of two particle sizes as

$$\beta \equiv \frac{N_2}{N_1} \tag{3-17}$$

where N_i is the number of particles of diameter D_i present in the bed. The volume fraction of i^{th} size particles is defined as

$$x_i \equiv \frac{V_i}{\sum_{\ell=1}^{N} V_\ell} \tag{3-18}$$

The volume fraction is a useful parameter because it can easily be measured experimentally. The number ratio for mixtures of two particle sizes can be determined from the volume fraction and the diameter ratio as

$$\beta = \frac{x_2}{x_1} \left(\frac{1}{\gamma}\right)^3 \tag{3-19}$$

Let us first assume that the particulate bed is in a perfectly cubic array and that a volume of smaller particles is present which is just sufficient to fit into the pores of the cubic array of larger particles. Now if the smaller particles can be transported into the pores of the array without disturbing the larger particles, a point will eventually be reached when all the pores of the cubic array are filled with smaller particles. At this point the bed is said to be "saturated". If we were to add more of the smaller particles, they could not fit into the pores of the array and would stratify in the bed. The saturation point in the scenario discribed earlier would obviously occur at β equal to one. Had we added particles much smaller than those making up the cubic array, we could have fit more than one particle in each pore and the saturation point would have occured at β greater than one. If β_{sat} is used to denote the number ratio at which saturation occurs then for $\beta > \beta_{sat}$, the smaller particles would separate out of the mixture, and for $\beta < \beta_{sat}$, the larger particles would separate out of the mixture. Here the separation means that some of the particles will form a mixture and some will not. A "mixture" here is defined as a lattice of a given particle size with smaller particles contained within its pores.

In some cases, a certain particle size may separate out of the mixture before the saturation point is reached. One example of this effect is seen in segregated beds, where the smaller particles form a layer above the larger particles without mixing. Uncertainty caused by imperfect mixing can cause significant error in porosity data. Even in vigorously mixed beds there is a tendency for the smaller particles to move through the pores of the larger particles and gather at the bottom of the bed, thus causing mixing error. No effort has been made here to account for mixing error in the porosity correlation for mixtures of two particle sizes. It has been found by experience, however, that the mixing error is nearly zero when $x_2 \geq x_1$.

For each saturated mixture, there exists a saturated porosity, ϵ_{sat}, which is a function of γ and β_{sat}. Since the saturated number ratio, β_{sat}, is a function of γ only, the saturated porosity may be determined by γ alone. A further discussion of ϵ_{sat} and β_{sat} is given later in this section.

The porosity of a perfectly mixed bed of spherical particles can be obtained by averaging the volumes occupied by the separated and mixed particles for two cases as follows:

Case 1

$$\beta \geq \beta_{sat}; \qquad \epsilon = \frac{V_{sep,2}}{V_t}(0.40) + \frac{V_{sat}}{V_t}\epsilon_{sat} \qquad (3\text{-}20)$$

Case 2

$$\beta \leq \beta_{sat}; \qquad \epsilon = \frac{V_{sep,1}}{V_t}(0.40) + \frac{V_{sat}}{V_t}\epsilon_{sat} \qquad (3\text{-}21)$$

The volume of the saturated mixture, the volume of separated particles of diameter D_1, and the volume of separated particles of diameter D_2 are denoted by V_{sat}, $V_{sep,1}$, and $V_{sep,2}$, respectively, and are given by

$$V_{sat} = \left(\frac{1}{1-\epsilon_{sat}}\right)\frac{\pi}{6}\left(N_{2,sat}D_2^{\,3} + N_{1,sat}D_1^{\,3}\right) \qquad (3\text{-}22)$$

$$V_{sep,1} = \frac{1}{0.60} \frac{\pi}{6} (N_1 - N_{1,sat}) D_1^3 \tag{3-23}$$

$$V_{sep,2} = \frac{1}{0.60} \frac{\pi}{6} (N_2 - N_{2,sat}) D_2^3 \tag{3-24}$$

The total volume, V_t, is given simply by $V_{sat} + V_{sep,2}$ in equation (3-20) and by $V_{sat} + V_{sep,1}$ in equation (3-21). It should also be noted that $N_1 = N_{1,sat}$ in equation (3-20) and $N_2 = N_{2,sat}$ in equation (3-21). Dividing equations (3-22), (3-23), and (3-24) by V_t and substituting into equations (3-20) and (3-21), we have the following relation:

$$\varepsilon = \frac{2(1-\varepsilon_{sat}) S + 3\varepsilon_{sat}}{5(1-\varepsilon_{sat}) S + 3} \tag{3-25}$$

where the weighting factor S is defined as follows:

Case 1

$$\beta \geq \beta_{sat}; \qquad S = \frac{(\beta-\beta_{sat})\gamma^3}{1+\beta_{sat}\gamma^3} \tag{3-26}$$

Case 2

$$\beta \leq \beta_{sat}; \qquad S = \frac{(\beta_{sat}/\beta)-1}{1+\beta_{sat}\gamma^3} \tag{3-27}$$

The values of γ, β, and ε are known from experimental data, and it is desired to solve for β_{sat} and ε_{sat}. Equation (3-25) provides one equation relating β_{sat} and ε_{sat}, and since there are two unknowns, one additional equation is needed. For $\gamma > 0.48$, it is known from simple geometrical models that β_{sat} equals one. For $\gamma \leq 0.48$, a cubic geometry can be assumed to obtain a second equation relating

ϵ_{sat} and β_{sat} as

$$\epsilon_{sat} = 0.40 - \frac{\pi}{6}\beta_{sat}\gamma^3 \tag{3-28}$$

Porosity was determined experimentally for various values of the diameter ratio. Experiments were performed with equal volume fractions of the constituent particles to minimize mixing error. Using equations (3-25) and (3-28), the values of ϵ_{sat} and β_{sat} were obtained from the porosity data for various γ and are plotted in Figures 3.3 and 3.4, respectively.

The solid line in Figure 3.3 represents the mean of the data and can be written algebraically as

$$\epsilon_{sat} = 0.40 - 0.24(\gamma-1)^2 \tag{3-29}$$

Substituting equation (3-29) into (3-28), an algebraic correlation for β_{sat} can be written as

$$\beta_{sat} = 0.458\,\frac{(\gamma-1)^2}{\gamma^3} \tag{3-30}$$

Equation (3-30) is plotted in Figure 3.4 and is seen to fit the data well. The endpoints of the curve in Figure 3.3 may also be predicted theoretically. As γ approaches one, D_2 approaches D_1 and the porosity must go to that of a bed composed of uniform size spherical particles, or 0.40. Alternatively, as D_2 approaches zero, or γ approaches zero, the surface of the larger particles will have a negligible effect upon the smaller particles and the saturated porosity should

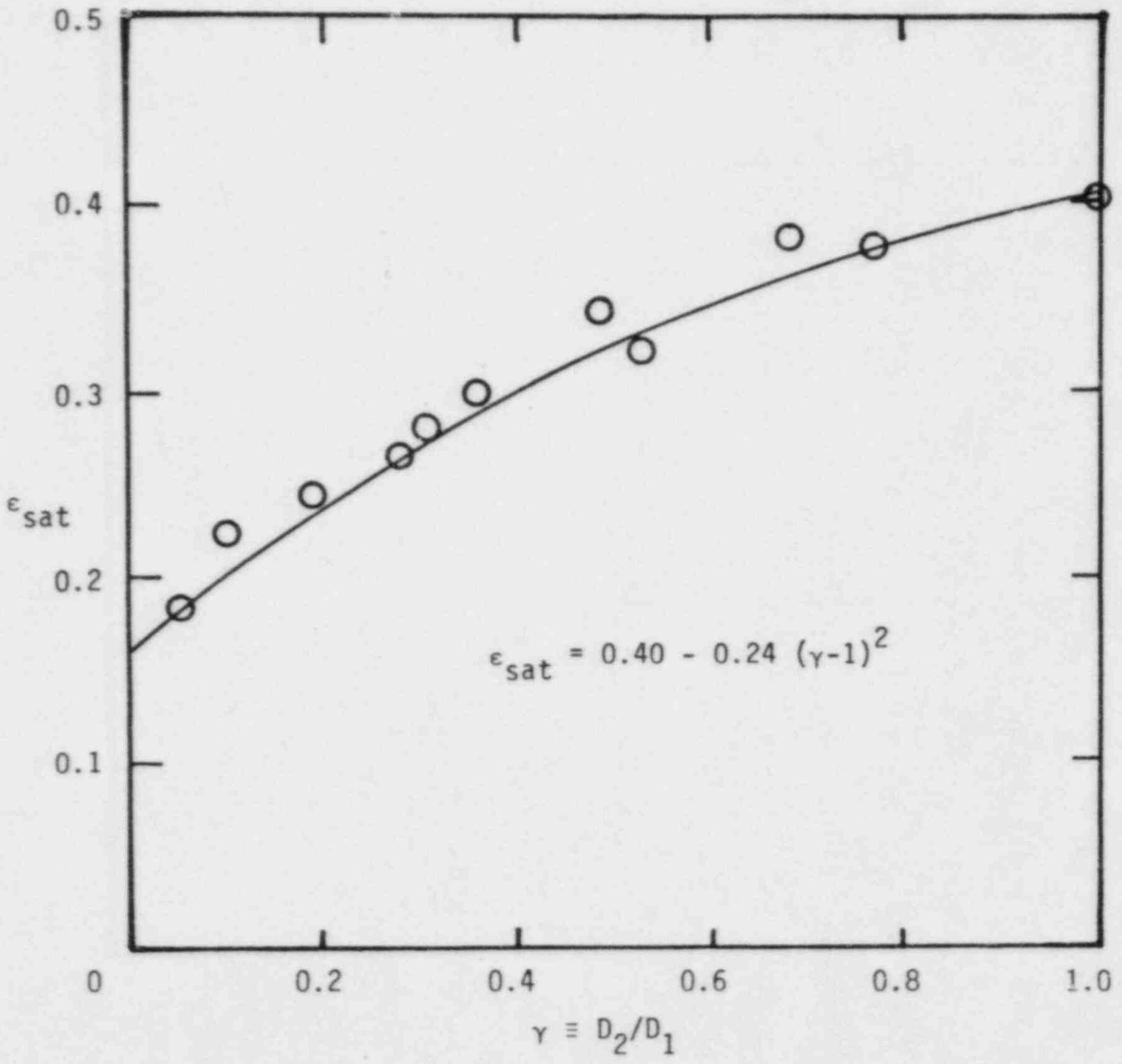

Figure 3.3 Saturated Porosity as a Function of Diameter Ratio

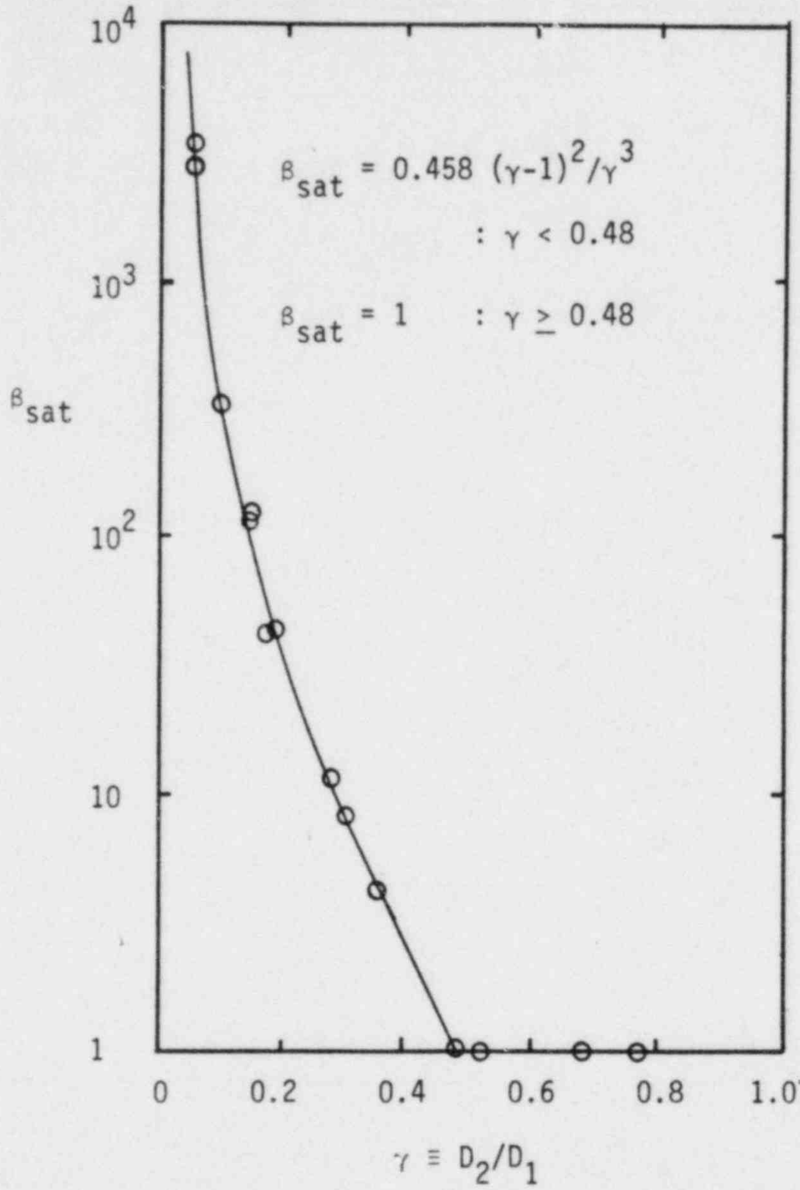

Figure 3.4 Saturated Number Ratio as a Function of Diameter Ratio

Table 3.3 Comparison Between Observed and Predicted Porosities for Beds Composed of Mixtures of Two Size Particles

Diameters of Constituent Particles (mm)	Volume Fractions of Constituent Particles	Observed Porosity	Predicted Porosity
3,19	0.50,0.50	0.262	0.294
10,19	0.50,0.50	0.350	0.370
15,19	0.31,0.69	0.378	0.387
10,15	0.24,0.76	0.380	0.375
1,3	0.50,0.50	0.343	0.345
3,6	0.50,0.50	0.367	0.366
1,19	0.34,0.66	0.209	0.204

approach (0.40)x(0.40), or 0.16. The data for ϵ_{sat} in Figure 3.3 is seen to fall on a parabolic curve between these limits.

It is noted that this analysis should also be applicable to non-spherical particles if the curves in Figures 3.3 and 3.4 are altered to account for shape factor. From a set of curves of ϵ_{sat} versus γ, where the shape factor is held constant on each curve, one may correlate ϵ_{sat} and β_{sat} as functions of diameter ratio and shape factor. These expressions can then be substituted into equation (3-25) to obtain the porosity.

A comparison between the predicted and observed porosities is given in Table 3.3 for several mixtures of two particle sizes. The predicted porosities are within ± 12% of the observed porosities for the data given in Table 3.3. The experimental repeatability of the data is also approximately ± 12%.

3.2.3 Porosity of Beds Composed of Mixtures of Three or More Size Particles

Before evaluating porosity of mixtures of three or more size particles, it is necessary to form a model to approximate β_{sat} for each constituent particle size. One such model is formed by assuming a simple lattice geometry and classifying the pores occupied by various size particles. Assuming a cubic array with structuring particles of a given diameter D_1, the largest particle to fit into the intersticial region would obviously occupy the pore volume in the center of the cubic lattice. This center located pore will be referred to as a "first level" pore. The diameter ratio of the largest particle that can barely fit into a given pore level of the cubic array is referred to as the "critical ratio" of the pore level and is denoted by γ_{crit}. Simple geometrical arguments yield a value of one for β_{sat} and 0.732 for γ_{crit} for first level pores.

If the first level pore spaces of the cubic array are filled, the next smallest particles to fit into the array will have diameters of 0.414 D_1 and will fit into the pore volume in the center of each face of the cube. These pore spaces are called "second level" pores. Each cube in the array has six faces; however, each face is shared by two cubes. The β_{sat} of second level pores is, therefore, one half of six, or three. The critical ratio of second level pores is 0.414. If the first and second level pores are filled, the next smallest particles that can fit into the array will have diameters of 0.138 D_1. These particles fit into the pore volumes between each two adjacent particles of the cubic lattice and the central particle occupying the first level pore. This pore space is referred to as a "third level" pore. Third level pores have a value of 12 for β_{sat} and a critical ratio of 0.138. Notice that third level pores have no meaning if the first level pore is not filled. Obviously an infinite number of pore levels exist, each with increasing β_{sat} and decreasing γ_{crit}. Due to the increasing complexity of higher pore levels, this study will be limited to distributions with $\gamma \geq 0.05$. In this region, only three pore levels exist. This model is constrained in the sense that it does not allow smaller particles to fill voids in larger pores when larger particles are present. This constraint will later be relaxed by defining an empirical relaxation coefficient which is obtained by comparing predictions with the data.

The fundamental idea in evaluating porosity of mixtures of three or more particle sizes is to divide the particle distribution up into four regions, determined by the range of γ with respect to pore level. The regions are ordered such that region 1 corresponds to the structuring particles of the array and regions 2, 3, and 4 correspond to particles filling the first, second, and third pore levels, respectively. Each region is then treated as a single particle size of diameter equal to the mean diameter within the region. The volume fraction of each region is taken to be the sum of the volume fractions of the particles contained within that region. By this method, any mixture of n particle sizes can be treated as a mixture of only four particle sizes. Furthermore, the value of β_{sat} is known for each of the four regions of this reduced mixture.

To facilitate the determination of the porosity of the reduced mixture, it can be imagined that a mixture involving all of the initially given particles forms as a bottom layer in the bed. When eventually all of the particles in a certain region are used up, a new mixture will form in the layer immediately above the previous layer. For this new mixture, we must again calculate the reduced particle diameters and volume fractions to determine the layer porosity. This procedure can be repeated until all of the particles are used up. The porosity of such a bed would simply be the sum of the porosity of each layer times the fraction of the total bed volume which the layer occupies. A similar type of volumetric weighting was used to calculate porosity for mixtures of two particle sizes in the previous section. For mixtures of three or more particle sizes, volumetric weighting by the layer volume within the bed becomes extremely complicated since the definitions of β and β_{sat} are based upon the largest diameter particle in the reduced mixture, which changes for the various layers. If the layer porosities are weighted instead by the total initial volume of the particles composing each layer, a much simplified weighting equation can be obtained. The validity of this approximation can be confirmed by calculations using simple geometrical models. An example of such calculations is given in Appendix D.

The procedure for determining porosity of mixtures of three or more particle sizes is outlined as follows:

I. Divide Particle Distribution into Regions

A. Order diameters from largest to smallest. Also rearrange the volume fractions to correspond with the diameters.

B. Determine the largest particle diameter with a non-zero volume fraction and label this diameter D_{max}.

C. Mark boundaries of the regions as follows:†

$$D_{1,2} = 0.732\ D_{max} \quad (3\text{-}31)$$

$$D_{2,3} = 0.414\ D_{max} \quad (3\text{-}32)$$

$$D_{3,4} = 0.138\ D_{max} \quad (3\text{-}33)$$

† Details in Appendix A

II. Determine Mean Diameter, Volume Fraction, and Number Ratio of Each Region

A. The mean diameter of region j can be calculated by the equation

$$d_j = \frac{\sum_{i=n_{j-1}+1}^{n_j} x_i D_i}{\sum_{i=n_{j-1}+1}^{n_j} x_i} \qquad \text{where } j=1,2,3,4 \qquad (3\text{-}34)$$

The variable n_j is simply a counter in the particle diameter array, with the difference between n_j and n_{j-1} being the number of particle sizes present in the region j. This notation is equivalent to stating that the summation should only be carried out in the specified region j.

B. The volume fraction of region j can be calculated from the equation

$$x_j = \sum_{i=n_{j-1}+1}^{n_j} x_i \qquad \text{where } j=1,2,3,4 \qquad (3\text{-}35)$$

C. The number ratio of each region can be calculated as

$$\beta_j = \frac{x_j}{x_1} \left(\frac{d_1}{d_j}\right)^3 \qquad (3\text{-}36)$$

III. Determine the Mixture Set and the Layer Porosity

A. Set values of β_{sat} for each region as follows:

$$\beta_{sat,1} = 1 \qquad \text{(structuring particles)}$$
$$\beta_{sat,2} = 1 \qquad \text{(first level pores)} \qquad (3\text{-}37)$$

$\beta_{sat,3} = 3$ (second level pores)

$\beta_{sat,4} = 12$ (third level pores)

B. Calculate the ratio $\beta_j/\beta_{sat,j}$ for each region. Determine the minimum $\beta_j/\beta_{sat,j}$ ratio which is greater than zero and label it $\beta_{r,min}$.

C. Define a mixture set array M such that

$$\text{If } \beta_j/\beta_{sat,j} \neq 0, \quad \text{then } M_j = 2 \qquad \text{else } M_j = 1 \tag{3-38}$$

This array indiates which regions compose the mixture set and will be used in calculating the saturated layer porosity.

D. If the mixture set is not full (i.e. M_j is not equal to 2 for all j), then the values of $\beta_{sat,j}$ given in III.A may be incorrect. Corrections should be made for the mixture sets given in Table 3.4. The diameter ratio in Table 3.4 is defined as

$$\gamma_{ij} = \frac{d_j}{d_i} \tag{3-39}$$

The corrections for β_{sat} are seen to come directly from the equations for mixtures of two particle sizes. Further details on the derivation of these equations is given in Appendix B. If any correction in β_{sat} was made in this step, one must return to III.B and recalculate the $\beta_j/\beta_{sat,j}$ ratios. If no correction was made, one can proceed to the next step.

E. Determine the fraction of the remaining particles, by volume, that has been used in the mixture set and label this fraction

Table 3.4 β_{sat} Corrections for Non-Full Mixture Sets[†]

Regions Present	Correction
14	$\beta_{sat,4} = 0.458 \dfrac{(\gamma_{14}-1)^2}{\gamma_{14}^3}$
13	$\beta_{sat,3} = 0.458 \dfrac{(\gamma_{13}-1)^2}{\gamma_{13}^3}$
134	$\beta_{sat,3} = 0.458 \dfrac{(\gamma_{13}-1)^2}{\gamma_{13}^3}$
	$\beta_{sat,4} = 0.458 \; \beta_{sat,3} \dfrac{(\gamma_{34}-1)^2}{\gamma_{34}^3}$
124	$\beta_{sat,4} = 0.458 \; \beta_{sat,3} \dfrac{(\gamma_{24}-1)^2}{\gamma_{24}^3}$
	$= 1.374 \dfrac{(\gamma_{24}-1)^2}{\gamma_{24}^3}$ since $\beta_{sat,3} = 3$

† Details are given in Appendix B

XUT. This fraction can be determined from the equation

$$XUT = \sum_{\substack{j=1 \\ M_j \neq 1}}^{4} [\beta_{r,min}/(\beta_j/\beta_{sat,j})] \; x_j \qquad (3\text{-}40)$$

In equation (3-40), the summation is not performed for any j such that M_j=1, as indicated, because when M_j=1 the region was empty originally. Obviously no particles could have been used from a region which was originally empty.

F. The layer porosity, ε_{sat}, can be obtained from Table 3.5 for the given mixture set. The total bed porosity is initially set to zero and then incremented for each layer by the equation

$$\varepsilon = \varepsilon + XUT(1-XUTT)\varepsilon_{sat} \qquad (3\text{-}41)$$

where XUTT represents the total volume fraction of particles used by all of the previous mixture sets.

G. Update XUTT using the following equation

$$XUTT = XUTT + XUT(1-XUTT) \qquad (3\text{-}42)$$

IV. Update Volume Fractions

A. The volume fractions of the true constituent particles can be updated by the equation

$$x_i = x_i - \frac{x_i - XU_j}{x_j} \qquad (3\text{-}43)$$

In equation (3-43), the index i indicates the true particle

Table 3.5 Saturated Porosity†

Mixture Set	Saturated Porosity
1,2,3,4 (single size porosity)	$\varepsilon_{sat} = 0.40$
12	$\varepsilon_{sat} = 0.40 - 0.24\ (\gamma_{12}-1)^2$
13	$\varepsilon_{sat} = 0.40 - 0.24\ (\gamma_{13}-1)^2$
14	$\varepsilon_{sat} = 0.40 - 0.24\ (\gamma_{14}-1)^2$
123	$\varepsilon_{sat} = 0.40 - 0.24\ (\gamma_{12}-1)^2 - \frac{\pi}{2}\gamma_{13}^{3}$
124	$\varepsilon_{sat} = 0.40 - 0.24\ (\gamma_{12}-1)^2 - 0.719\ \gamma_{12}^{3}(\gamma_{24}-1)^2$
134	$\varepsilon_{sat} = 2.5\ [0.40 - 0.24\ (\gamma_{13}-1)^2]\ [0.40 - 0.24\ (\gamma_{34}-1)^2]$
1234	$\varepsilon_{sat} = 0.40 - 0.24\ (\gamma_{12}-1)^2 - \frac{\pi}{2}\gamma_{13}^{3} - 2\pi\ \gamma_{14}^{3}$

† Details are given in Appendix C

size and the index j represents the region to which particles of size D_i belong. The variable XU_j is the volume fraction of the remaining particles of those used in the mixture set belonging to region j. The value of XU_j can be obtained from equation (3-40) for any j.

B. Normalize the updated volume fractions of the i^{th} particle size by the equation

$$x_i = \frac{x_i}{\sum_{\ell=1}^{N} x_\ell} \tag{3-44}$$

where N is the total number of particles present and x_ℓ is the volume fraction of unused particles of size ℓ.

C. If 99% of the original particles, by volume, have been used, then stop the iteration. If less than this have been used, then go to I.B and repeat the procedure. This step can also be stated as follows:

If XUTT > 99%, then stop

else go to I.B

For a perfectly continuous particle distribution, the procedure would repeat indefinitely had we demanded that 100% of the particles be used before stopping. For this reason, a cutoff ratio of 99% was used in this study. For discrete particle distributions, this value can be changed to 100% if the user desires.

The results of this procedure for several particle distributions are given in Table 3.6 in comparison with experimental results. The predicted porosities from this procedure tend to be slightly higher than the experimental data. This trend is due to separation of the smaller particles of regions 3 and 4 from the larger particles of region 2. It is visually observed that for an array formed of a given structuring particle size, some fraction ω of the pores are occupied by only small particles and a fraction $(1-\omega)$ of the pores are occupied by a mixture of large and small particles. In the model, ω is assumed to be zero such that small particles are not allowed to fill the large pores when the large particles are present. "Large" particles here refer to those belonging to region 2 and not the structuring particles of region 1. Altering the procedure to account for such imperfect mixing and varying the value of ω, it was found that a value for ω of 0.6 gives excellent agreement with the experimental results, as shown in Table 3.6. This value of 0.6 for ω also agrees with estimates made from visual observations of the surfaces of various particulate beds.

A FORTRAN computer code using the previously discribed procedure and a value of 0.6 for ω is given in Appendix E. The program has been used to predict porosities to within ± 12% of the available data. This program is applicable to any distribution of spherical particles where the "spread" (i.e. the minimum particle diameter divided by the maximum particle diameter) is not less than 0.05 and where no more than about 15% of the particles have

Table 3.6 Comparison Between Observed and Predicted Porosities for Beds Composed of Three or More Size Particles

Constituent Particle Diameters (mm)	Constituent Particle Volume Fractions	Experimental Porosity	Predicted Porosity (ω = 0)	Predicted Porosity (ω = 0.6)
6,10,15,19	0.20,0.30,0.30,0.20	0.336	0.319	0.322
3,6,10,15,19	0.16,0.21,0.21,0.21,0.21	0.280	0.339	0.310
1,3,6,10,15,19	0.10,0.15,0.25,0.25, 0.15,0.10	0.270	0.326	0.261

diameters less than 1 mm. These two conditions avoid complications brought about by additional pore levels and bridging of the particles.

3.3 Flooding Limit

The flooding point is defined as the limit of upward gas and downward liquid superficial velocities which can exist in a particular bed. Sherwood, Shipley, and Holloway (11) performed a very early study of flooding in porous media using large diameter Raschig rings. Upon comparison with data of other investigators for particles of various geometries, Sherwood et al. (11) found that flooding data can be collapsed onto one curve by a plot of $(j_g^2 a/g\varepsilon^3)(\rho_g/\rho_\ell)\mu^{0.2}$ versus $(j_\ell/j_g)(\rho_\ell/\rho_g)^{1/2}$. This plot clearly shows that the effect of varying particle geometry upon the flooding limit can be correlated by the surface area per unit volume, a.

Dell and Pratt (12), in a study of flooding limits of immiscible liquids, found that flooding velocities can be correlated by the equation

$$j_1^{1/2} + j_2^{1/2} = C \tag{3-45}$$

where the constant C is a function of porosity, surface area, and phase densities and 1 and 2 represent the two phases or immiscible fluids present. The value of C was found to be negligibly affected by changes in viscosity or surface tension of the phases.

Wallis (13) defined dimensionless superficial velocities as follows:

$$j_\ell^{\star} = j_\ell \left[\rho_\ell \;/\; g(\rho_\ell - \rho_g) \frac{\varepsilon^3}{a} \right]^{\frac{1}{2}} \tag{3-46}$$

$$j_g^{\star} = j_g \left[\rho_g \;/\; g(\rho_\ell - \rho_g) \frac{\varepsilon^3}{a} \right]^{\frac{1}{2}} \tag{3-47}$$

For equations (3-46) and (3-47), a is the surface area of packing per unit volume and is given for spherical particles as

$$a = \frac{6(1-\varepsilon)}{D_p} \tag{3-48}$$

By nondimensionalizing equation (3-45), Wallis (13) determined the following correlation for the flooding limit:

$$j_g^{\star\,\frac{1}{2}} + j_\ell^{\star\,\frac{1}{2}} = C \tag{3-49}$$

where C is a universal constant. Upon comparison with the data of Sherwood et al. (11) and Lobo et al. (14), Wallis (13) obtained a value of 0.775 for C for flow through porous media. When equation (3-49) is used to correlate data for air-water flow in vertical tubes, Wallis (13) found C to vary between 0.88 and 1.0. Upon substitution of equations (3-46), (3-47), and (3-48) into equation (3-49), the flooding limit for beds composed of spherical particles is seen to be a function of porosity, mean particle diameter, and the phase densities.

The flooding data used to derive equation (3-49) were collected from a large number of independent investiagators and are found to scatter widely. This scattering results partially from confusion over the definition and experimental detection of the flooding limit.

In this study, a given liquid flow rate was set and the gas flow rate was increased in increments to the flooding limit. As the gas flow reached approximately 50% of the flooding limit, the overlying liquid height began increasing at a very slow rate, indicating slight liquid accumulation above the bed. Increasing the gas velocity to near the flooding limit, the water height was seen to rise much more rapidly and the discontinuous (gas) phase tended to become continuous in small pockets within the bed.

With increase in the gas flow rate slightly above the flooding point, the flow became annular and gas formed a block in the outlet header and was forced out the water exit rather than through the bed. The flooding limit, therefore, was observed to coincide with the transition to the annular flow regime in the range of liquid and gas superficial velocities studied. From the definition of the flooding limit stated earlier, it is known that the liquid flow through the bed is limited by the gas flow at the flooding point and cannot be further increased. Opening the water drainage valve, which usually increases the water drainage rate until a lower equilibrium height is reached, should have no effect on the water height at the flooding point. The experimental determination of the flooding limit was the gas velicity at which, upon opening the water drainage valve and thus drastically reducing the resistance to water flow downstream of the bed, the water height within the test section was seen to maintain a steady value or increase slightly. Decrease or increase of the water height was indicated very accurately by pressure readings within the overlying layer. This method allowed determination of the flooding point with a minimum accuracy of ± 15%.

A plot of $j_\ell^{*^{1/2}}$ versus $j_g^{*^{1/2}}$ at the flooding limit is shown in Figure 3.5 for beds composed of uniform size spherical particles with nominal diameters of 3, 6, 10, 15, and 19 mm. Figure 3.6 shows the same plot for various mixtures of these particle sizes where the mean diameter from the Kozeny-Carmen equation (3-1) was used in calculating the dimensionless superficial velocities. It is evident in Figures 3.5 and 3.6 that the flooding limit occurs slightly higher than that predicted by using a value of 0.775 for C in equation (3-49). A mean line drawn through these data is obtained by letting C equal 0.875±0.035. Equation (3-49) can thus be written as

$$j_\ell^{*\,1/2} + j_g^{*\,1/2} = 0.875 \tag{3-50}$$

This value of 0.875 for C corresponds to the lower bound for the constants obtained for air-water flow through vertical tubes. At a fixed j_ℓ, this change in C from 0.775 to 0.875 results in a 27% increase in j_g at the flooding limit. Beds composed of 3 mm nominal diameter particles show a slightly lower flooding limit than that given by equation (3-50). One possible explanation for this observation is that the flow is laminar when flooding occurs for small diameter particles, whereas the dimensionless superficial velocities given in equations (3-46) and (3-47) were derived for turbulent flow. Flooding data for a mixture of non-spherical sharps

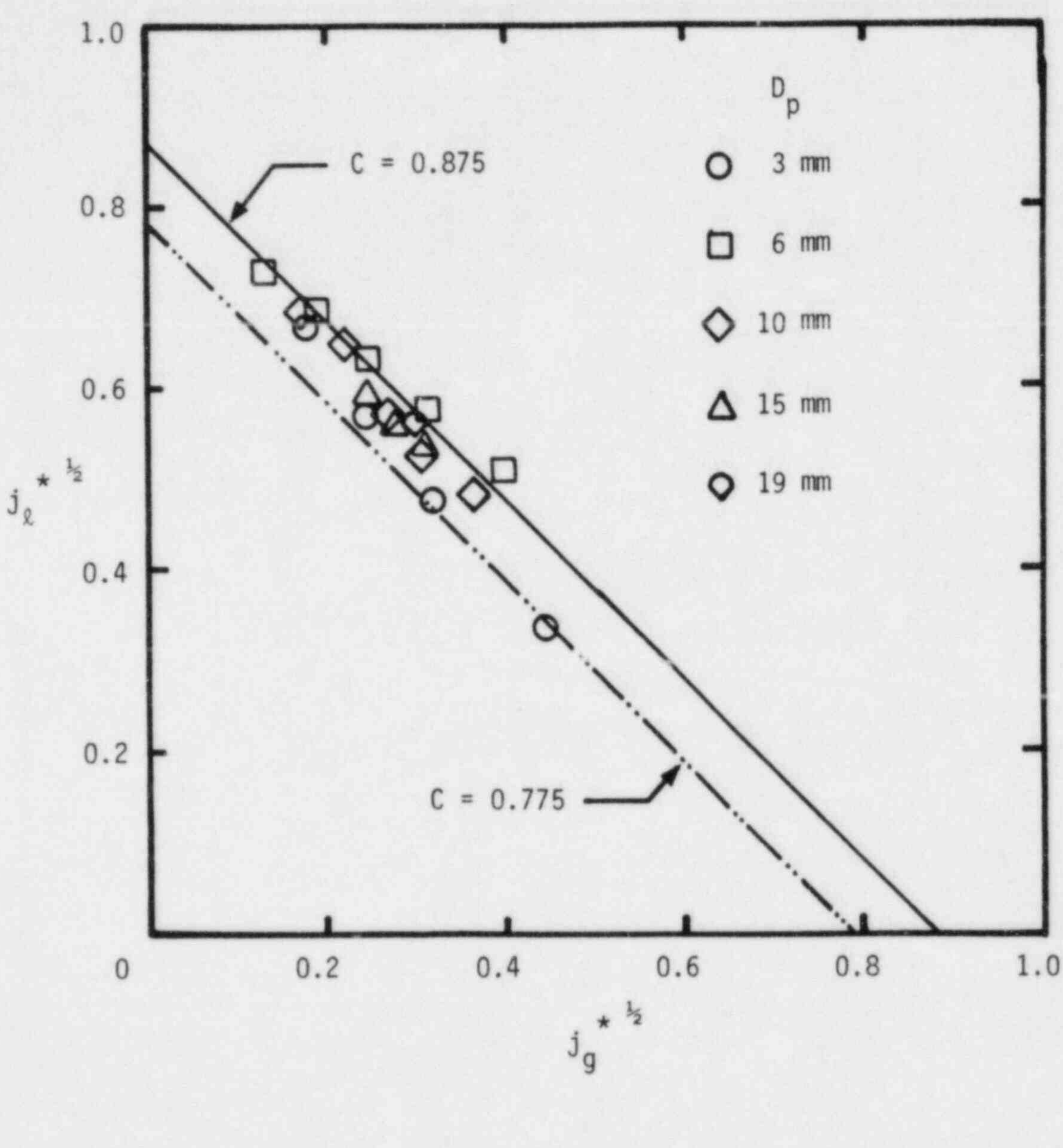

Figure 3.5 Flooding Data for Beds Composed of Uniform Size Spherical Particles

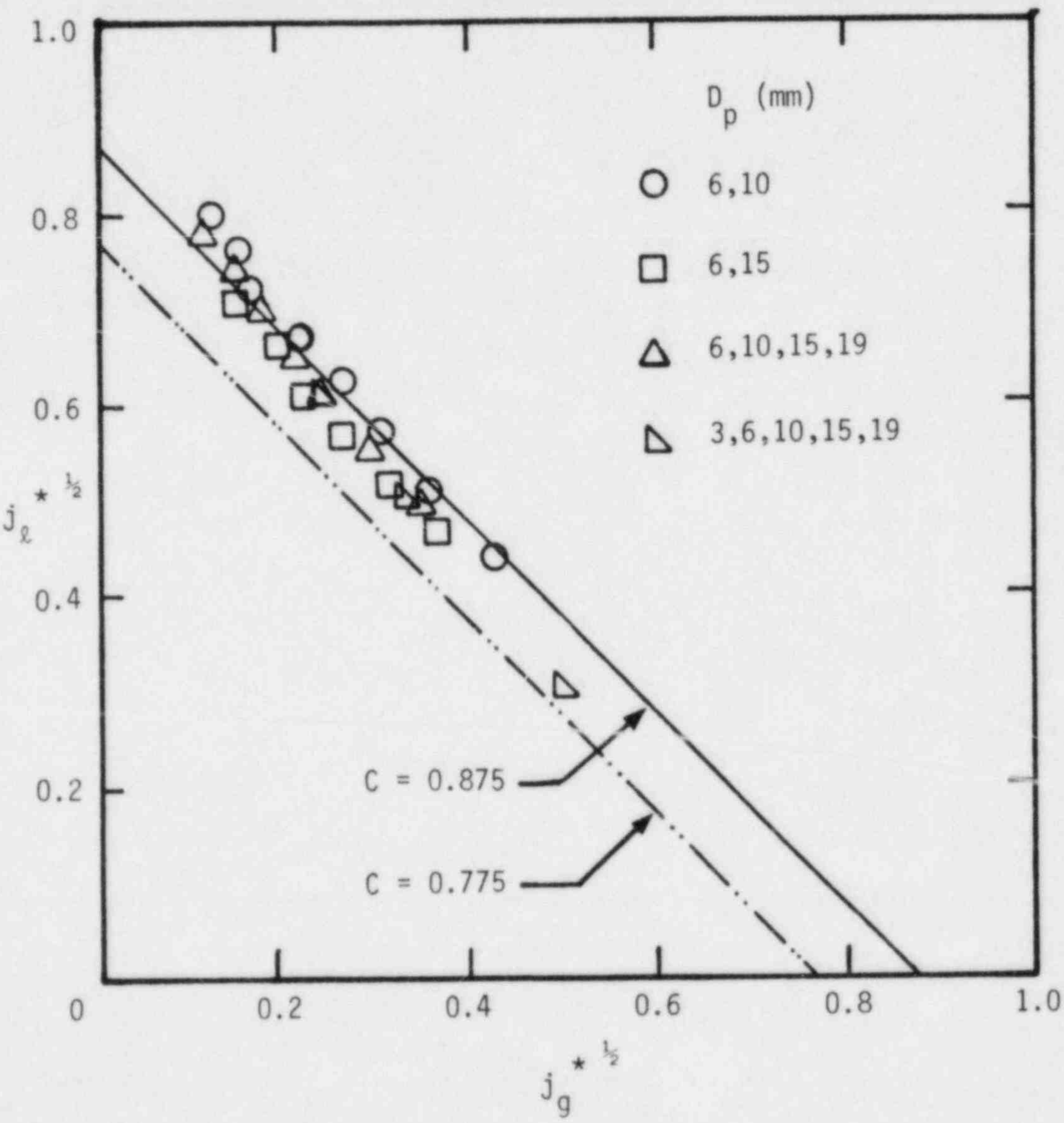

Figure 3.6 Flooding Data for Beds Composed of Mixtures of Various Size Particles

and 6 mm nominal diameter particles are plotted in Figure 3.7 where the mean diameter is obtained from the Kozeny-Carmen equation (3-1). This figure indicates that equation (3-50) can also be used for non-spherical particles if a suitable mean diameter is defined.

Experiments were also performed by injecting gas axially at various locations along the length of the bed. The purpose of these experiments was to determine whether the flooding limit for volume heated beds is different than that for bottom heated beds. Data from these experiments for 10 mm nominal diameter particles plotted as a function of $j_g^{*\frac{1}{2}}$ and $j_\ell^{*\frac{1}{2}}$ are given in Figure 3.8. Upon comparison of Figure 3.8 with Figures 3.5 and 3.6, the flooding limit for axially injected gas flow is seen to be nearly identical to that previously found for bottom injected flow. This result indicates that flooding is a differential effect and therefore does not depend upon bed length or uniformity.

To check this assumption, experiments were performed with a bed composed of 19 mm nominal diameter particles with a stratified 5 cm thick layer of 6 mm nominal diameter particles placed halfway up the bed length. The flooding data from this experiment is plotted in Figure 3.9 where the particle diameter is taken as 6 mm and the porosity is assumed to be 0.40. The data in Figure 3.9 indicate that flooding in the stratified bed occurred at nearly the same velocities as for a bed composed entirely of 6 mm diameter particles. The slight increase in flooding limits for the stratified bed over that predicted using equation (3-50) for a bed composed of 6 mm

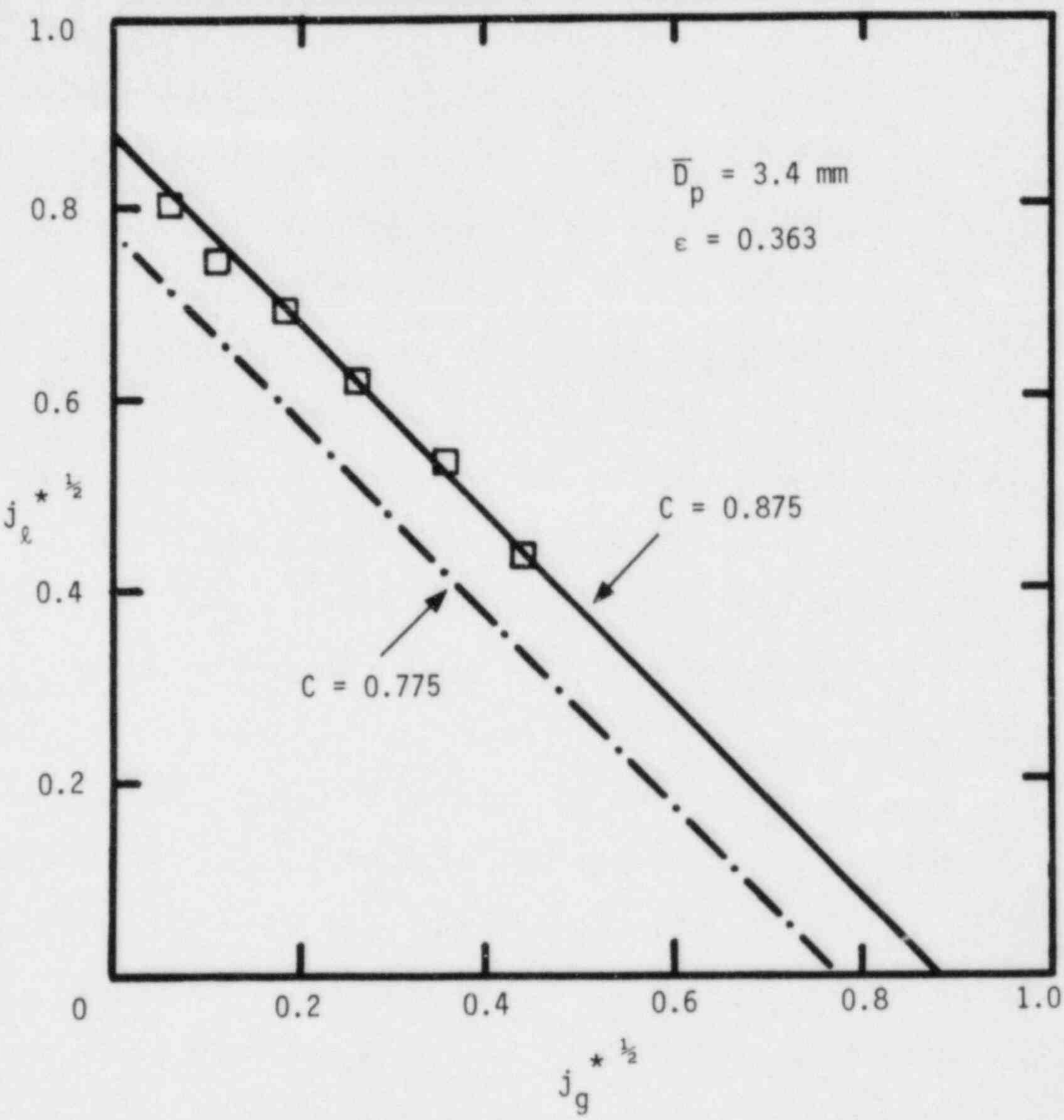

Figure 3.7 Flooding Data for Mixture of Sharps and 6 mm Diameter Spherical Particles

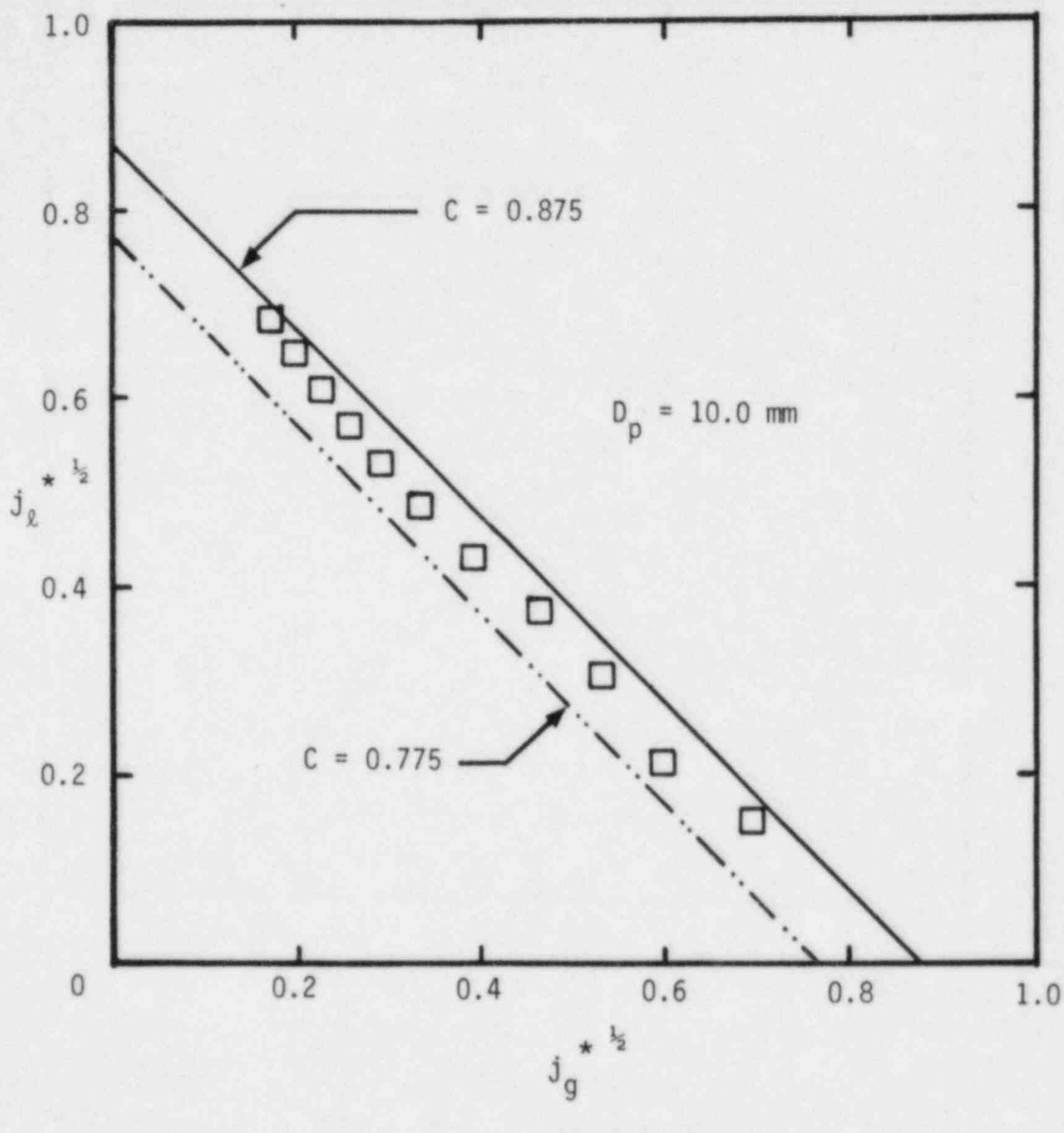

Figure 3.8 Flooding Data for Bed of Uniform Size Spherical Particles with Axially Injected Gas Flow

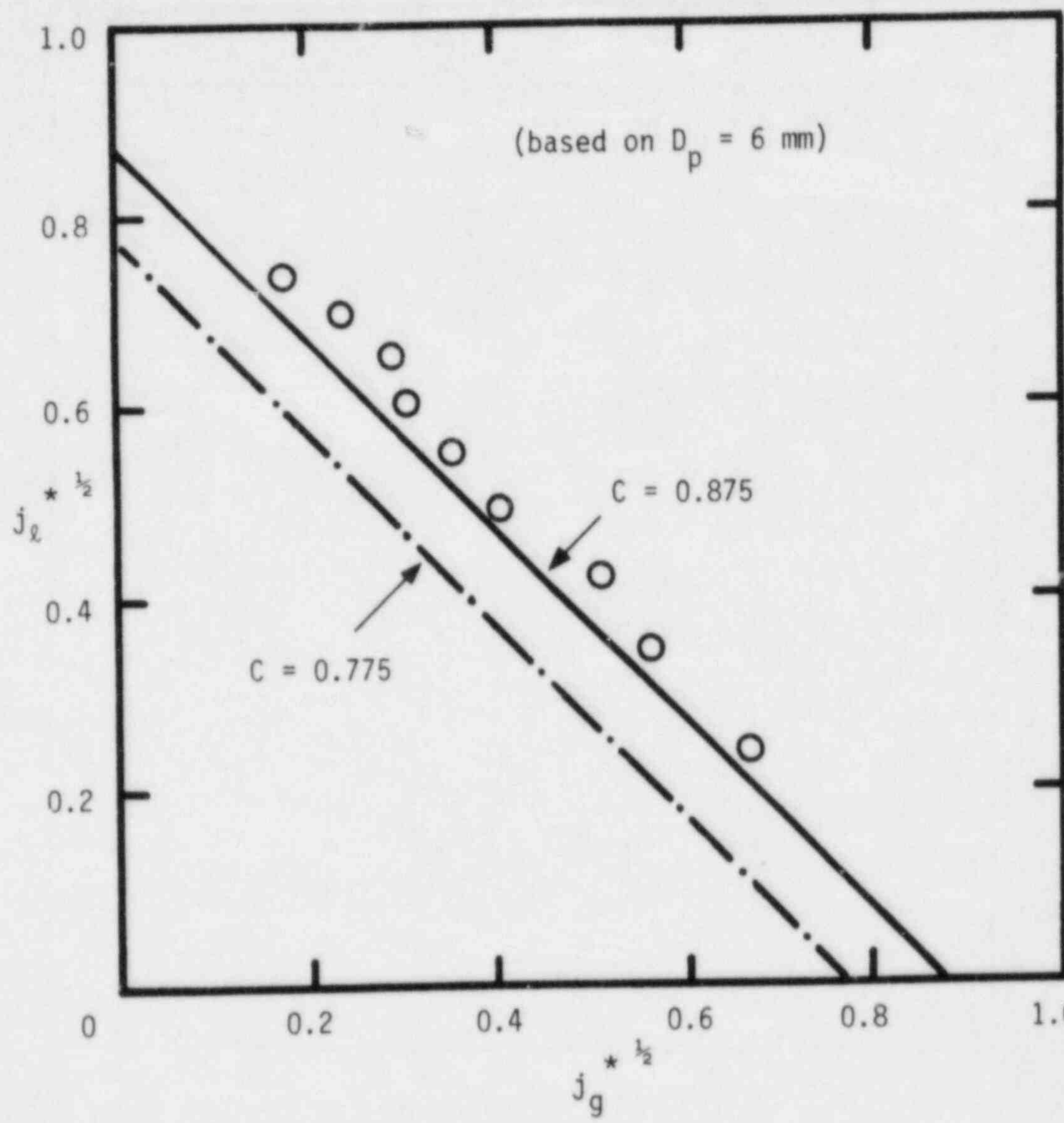

Figure 3.9 Flooding Data for a Bed Composed of 19 mm Diameter Particles with a Stratified 5 cm Thick Layer of 6 mm Diameter Particles Embedded Near the Middle

diameter particles is probably due to coupling between the stratified layers. Such layer coupling will be discussed in more detail in section 3.5 in conjunction with coupling between the overlying liquid layer and the bed.

3.4 Void Fraction and Pressure Gradient at Flooding

Void fraction and total and frictional pressure gradients are given at flooding with various superficial liquid velocities in Table 3.7 for beds composed of a uniform particle size and in Table 3.8 for beds composed of mixtures of particle sizes. The total pressure gradient is also plotted in Figure 3.10 with increasing superficial gas velocity up to the flooding limit for various superficial liquid velocities. Although the plot in Figure 3.10 was made for a bed composed of 6 mm nominal diameter particles, it represents well similar plots for beds composed of other particle sizes. The pressure gradient is defined here as positive if the pressure increases in the downward axial direction. With this definition, it is clear from Figure 3.10 that the total pressure gradient decreases with increase in liquid and gas superficial velocities. The dotted lines in Figure 3.10 represent the observed rapid reduction in total pressure gradient as the superficial gas velocity is increased above the flooding limit.

An interesting experimental result is that the total pressure gradient at flooding seems to have a constant value of about 4.6 kPa/m. This observation can be seen both from the data listed

Table 3.7 Conditions at Flooding for Beds Composed of Uniform Size Particles

$\overline{D}_p$ (mm)	ε	j_g (mm/s)	j_ℓ (mm/s)	$\overline{\alpha}_{ac}$	$\frac{dP_t}{dz}$ (kPa/m)	$\frac{dP_f}{dz}$ (kPa/m)
2.8	0.42	97	1.95	0.27	5.14	-2.00
2.8	0.42	50	3.89	0.18	4.46	-3.55
2.8	0.42	30	5.84	0.13	3.45	-5.05
2.8	0.42	16	7.78	0.08	4.13	-4.86
5.8	0.39	135	7.78	0.34	4.60	-1.85
5.8	0.39	83	9.73	0.26	4.75	-2.48
5.8	0.39	50	11.67	0.20	4.40	-3.46
5.8	0.39	30	13.62	0.19	4.75	-3.15
5.8	0.39	16	15.56	0.13	5.02	-3.50
10.0	0.40	163	9.73	0.46	4.35	-0.98
10.0	0.40	115	11.67	0.39	4.30	-1.67
10.0	0.40	90	13.62	0.34	4.31	-2.15
10.0	0.40	71	15.56	0.30	4.20	-2.64
10.0	0.40	60	17.51	0.27	4.34	-2.78
10.0	0.40	38	19.46	0.23	4.80	-2.73
14.7	0.42	153	15.56	0.46	4.59	-1.47
14.7	0.42	124	17.51	0.37	4.87	-1.26
14.7	0.42	99	19.46	0.33	4.64	-1.95

Table 3.8 Conditions at Flooding for Beds Composed of Mixtures of Various Size Particles

$\overline{D}_p$ (mm)	ε	j_g (mm/s)	j_ℓ (mm/s)	$\overline{\alpha}_{ac}$	$\frac{dP_t}{dz}$ (kPa/m)	$\frac{dP_f}{dz}$ (kPa/m)
3.4	0.37	115	3.89	0.26	6.79	-0.44
3.4	0.37	78	5.84	0.22	6.50	-1.12
3.4	0.37	42	7.78	0.14	5.24	-3.77
3.4	0.37	23	9.73	0.12	4.27	-4.28
5.4	0.28	115	1.95	0.37	5.76	-0.41
5.4	0.27	50	3.89	0.26	5.08	-2.11
5.4	0.27	30	5.84	0.22	2.78	-4.83
5.4	0.27	10	7.78	0.12	4.32	-4.30
7.8	0.36	163	5.84	0.45	4.70	-0.68
7.8	0.36	115	7.78	0.41	4.42	-1.34
7.8	0.36	83	9.73	0.37	4.59	-1.57
7.8	0.36	65	11.67	0.34	4.25	-2.21
7.8	0.36	46	13.62	0.27	4.58	-2.64
7.8	0.36	30	15.56	0.24	4.80	-2.62
7.8	0.36	21	17.51	0.21	4.41	-3.19
7.8	0.36	14	19.46	0.18	4.58	-3.47
9.9	0.34	115	7.78	0.42	4.85	-0.84
9.9	0.34	83	9.73	0.38	4.84	-1.25
9.9	0.34	62	11.67	0.37	4.29	-1.86
9.9	0.34	44	13.62	0.27	4.85	-2.32
9.9	0.34	30	15.56	0.23	4.63	-2.91
9.9	0.34	21	17.51	0.16	4.97	-3.25
9.9	0.34	13	19.46	0.12	5.21	-3.39

Table 3.8 (continued)

$\bar{D}_p$ (mm)	ε	j_g (mm/s)	j_ℓ (mm/s)	$\bar{\alpha}_{ac}$	$\frac{dP_t}{dz}$ (kPa/m)	$\frac{dP_f}{dz}$ (kPa/m)
10.3	0.36	163	5.84	0.43	4.70	-0.87
10.3	0.36	115	7.78	0.41	4.42	-1.34
10.3	0.36	83	9.73	0.37	4.59	-1.57
10.3	0.36	65	11.67	0.34	4.25	-2.21
10.3	0.36	46	13.62	0.27	4.58	-2.64
10.3	0.36	30	15.56	0.24	4.80	-2.62
10.3	0.36	21	17.51	0.21	4.41	-3.19
10.3	0.36	14	19.46	0.18	4.58	-3.47

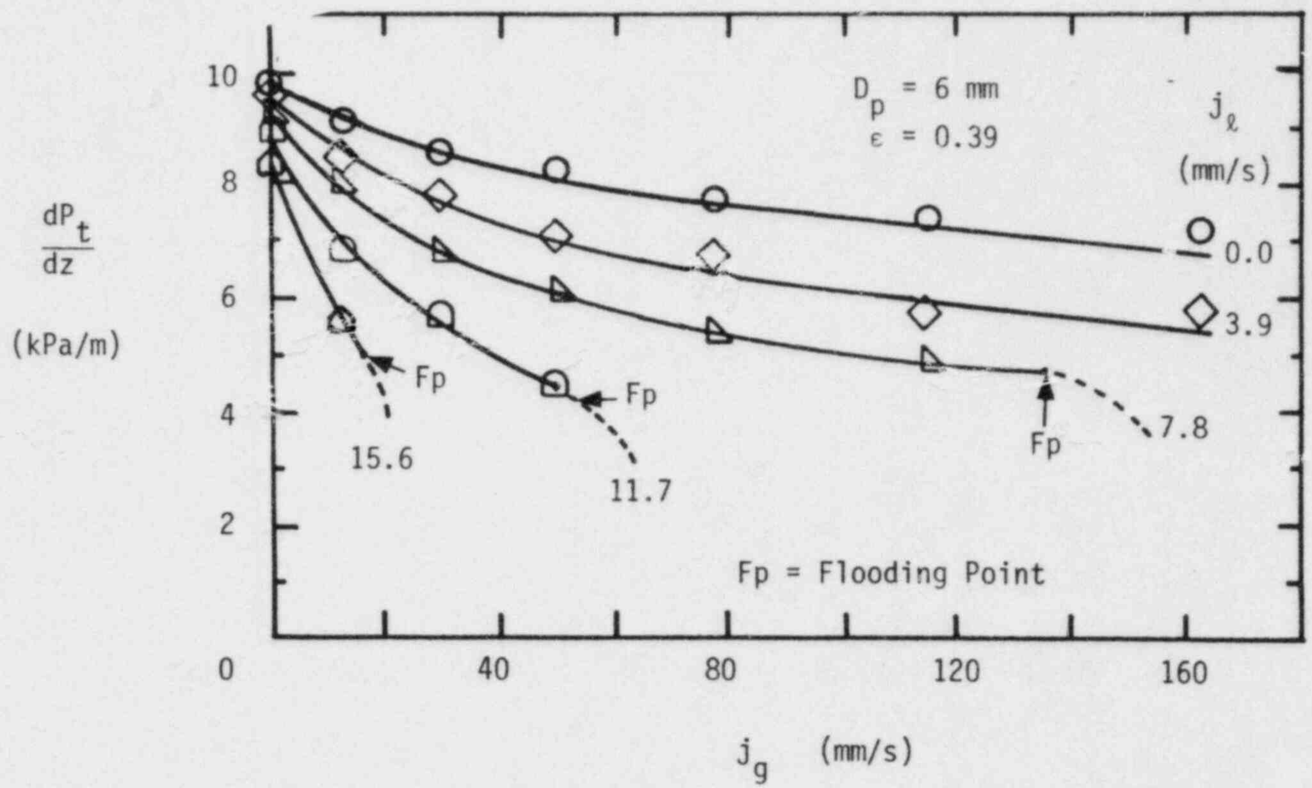

Figure 3.10 Total Pressure Gradient Data up to the Flooding Limit for a Bed Composed of 6 mm Nominal Diameter Particles

in Tables 3.7 and 3.8 and from the curves in Figure 3.10. For the flooding points listed in Tables 3.7 and 3.8, 84% had total pressure gradients within ± 0.5 kPa/m of this mean value. Moreover, the points for which the total pressure gradients at flooding differed appreciably from 4.6 kPa/m were for beds composed of small diameter particles (D_p < 6 mm), for which the pressure gradient changes extremely rapidly near the flooding point. It has not yet been determined whether this result is of some importance or is merely coincidental.

Void fraction is plotted in Figure 3.11 as a function of superficial gas velocity up to the flooding limit for beds composed of 6, 10, and 15 mm nominal diameter particles with a superficial liquid velocity of 15.56 mm/s. No sudden change in void fraction was observed as the flooding limit was approached. The void fraction can be correlated by a drift flux model given in (6) as

$$\bar{\alpha}_{ac} = \frac{j_g}{C_o(j_g \pm j_\ell) + C_1\left(\frac{\varepsilon^3}{1-\varepsilon}\right)^{\frac{1}{2}} \sqrt{\frac{D_p g(\rho_\ell - \rho_g)}{\rho_\ell}} \; \frac{\sqrt{\sigma/g(\rho_\ell - \rho_g)}}{D_p}} \qquad (3\text{-}51)$$

In equation (3-51), the positive sign in the denominator is for co-current flow and the negative sign is for counter-current flow. The liquid superficial velocity is always taken as positive here. The values of C_o and C_1 were found from data with zero superficial liquid velocity to be 2 and 3.44, respectively, for $\bar{\alpha}_{ac} \leq 0.30$ and $\sqrt{2}$ and 5.24, respectively, for $0.30 \leq \bar{\alpha}_{ac} \leq 0.60$.

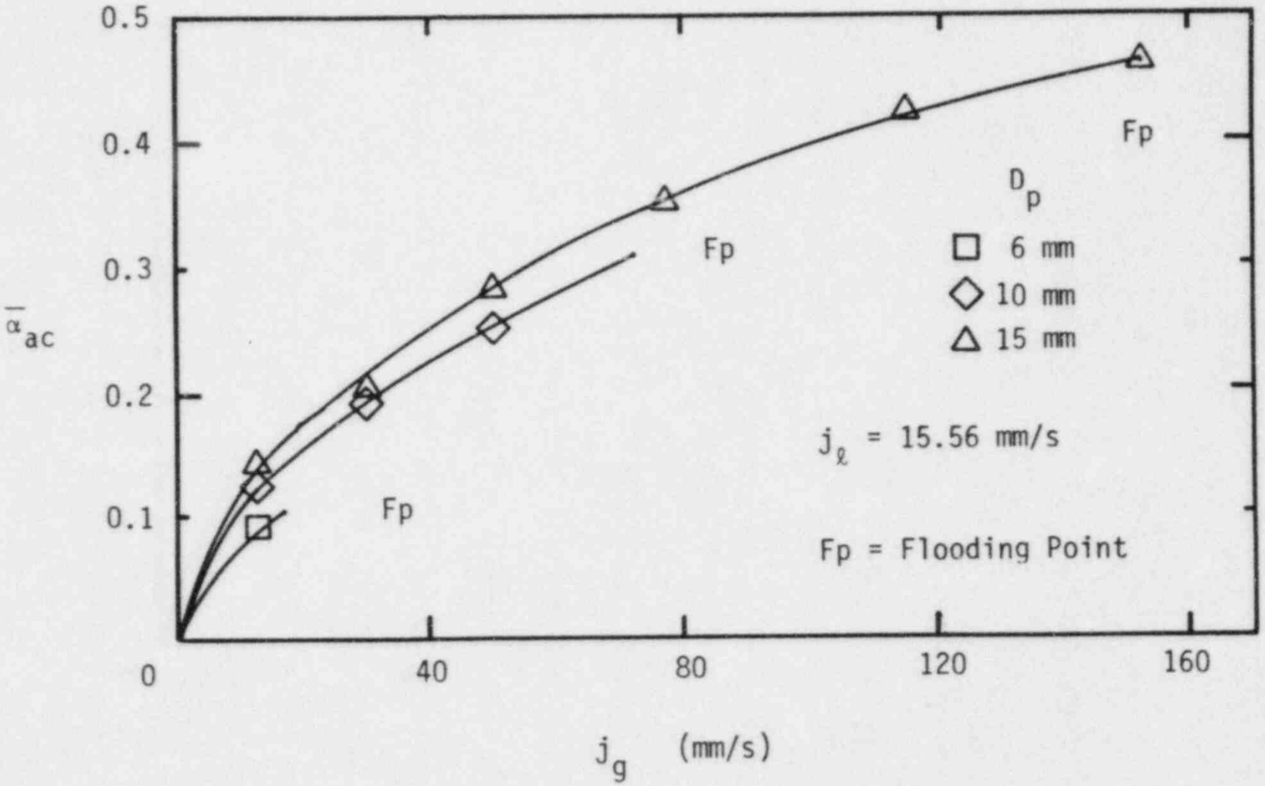

Figure 3.11 Void Fraction Data up to the Flooding Limit for a Set Superficial Liquid Velocity of 15.56 mm/s

According to equation (3-51), the void fraction should increase with increase in the liquid superficial velocity for counter-current flow. In this study, however, the void fraction data taken with increasing j_ℓ were found to scatter around that taken with j_ℓ equal to zero in a band of width ± 0.02. For most of the range of j_ℓ studied, the change in void fraction with superficial liquid velocity is very small; however, for large particle diameters and high j_ℓ the predictions obtained from equation (3-51) are significantly higher than the data. If the value of j_ℓ in equation (3-51) is set to zero, the void fraction predictions are found to match the data to within ± 15% for all superficial liquid and gas velocities studied. Additional void fraction and pressure drop data for liquid and gas superficial velocities at and below the flooding limit are given in Appendices F and G.

3.5 Coupling of the Overlying Liquid Layer with the Bed

The flooding limit given by equation (3-50) cannot be applied near the upper surface of the bed due to coupling of the bed with the overlying layer. This coupling is incurred because the absolute value of the total pressure gradient cannot change instantaneously from the low value within the bed to the relatively high value within the overlying layer. A diagram illustrating this effect is given in Figure 3.12. Pressure data at various locations along the length of the bed and the overlying layer are plotted as a function of axial distance in Figure 3.13. The variation of pressure near the top of the bed was plotted for the same flow rates in Figure 3.14 using an enlarged scale. The data given in Figures 3.13 and 3.14 were taken for 10 mm nominal diameter particles at the flooding limit,

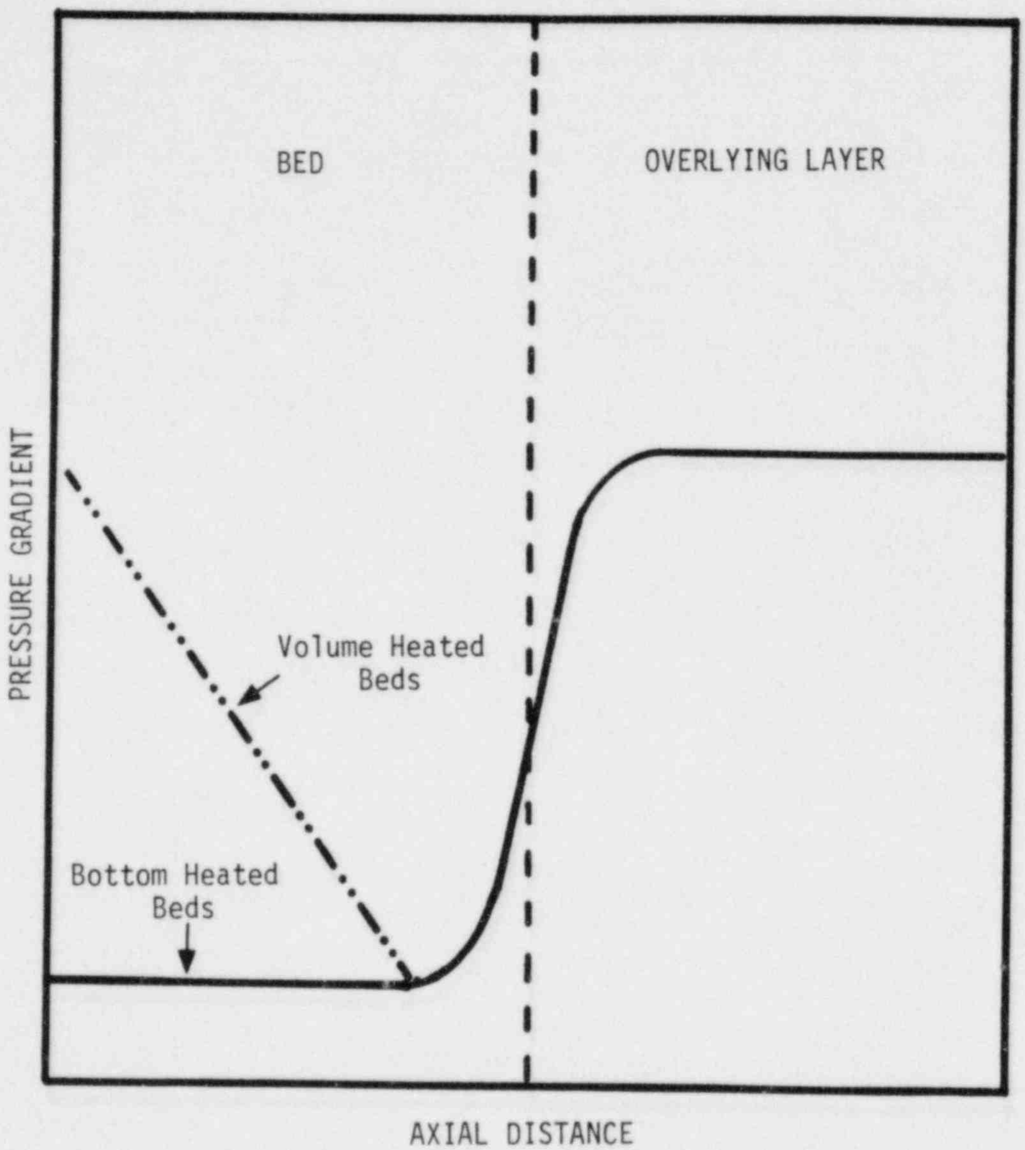

Figure 3.12 Diagram of the Pressure Gradient Through the Bed and Overlying Liquid Layer

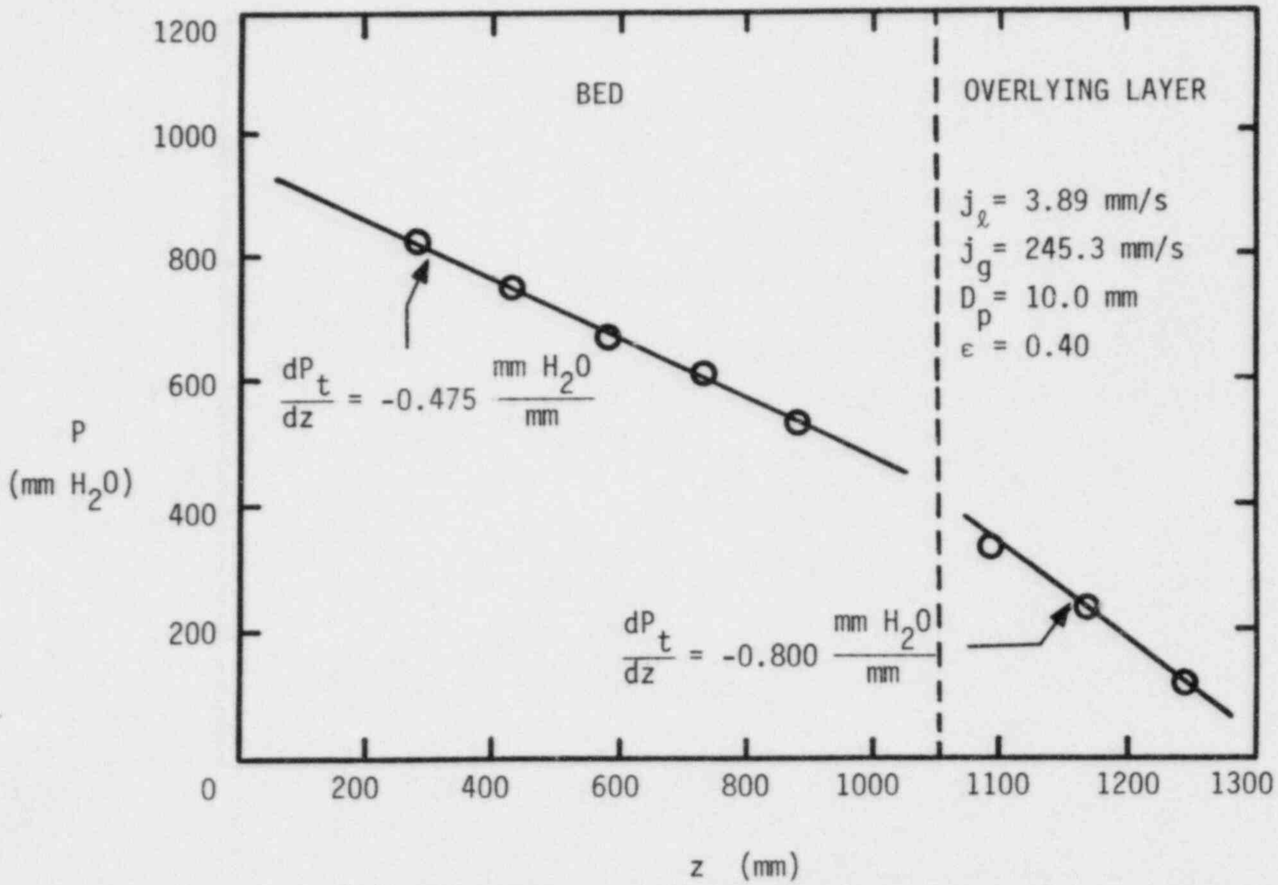

Figure 3.13 Variation of Pressure Through the Bed at the Flooding Limit (j_{ℓ} = 3.89 mm/s)

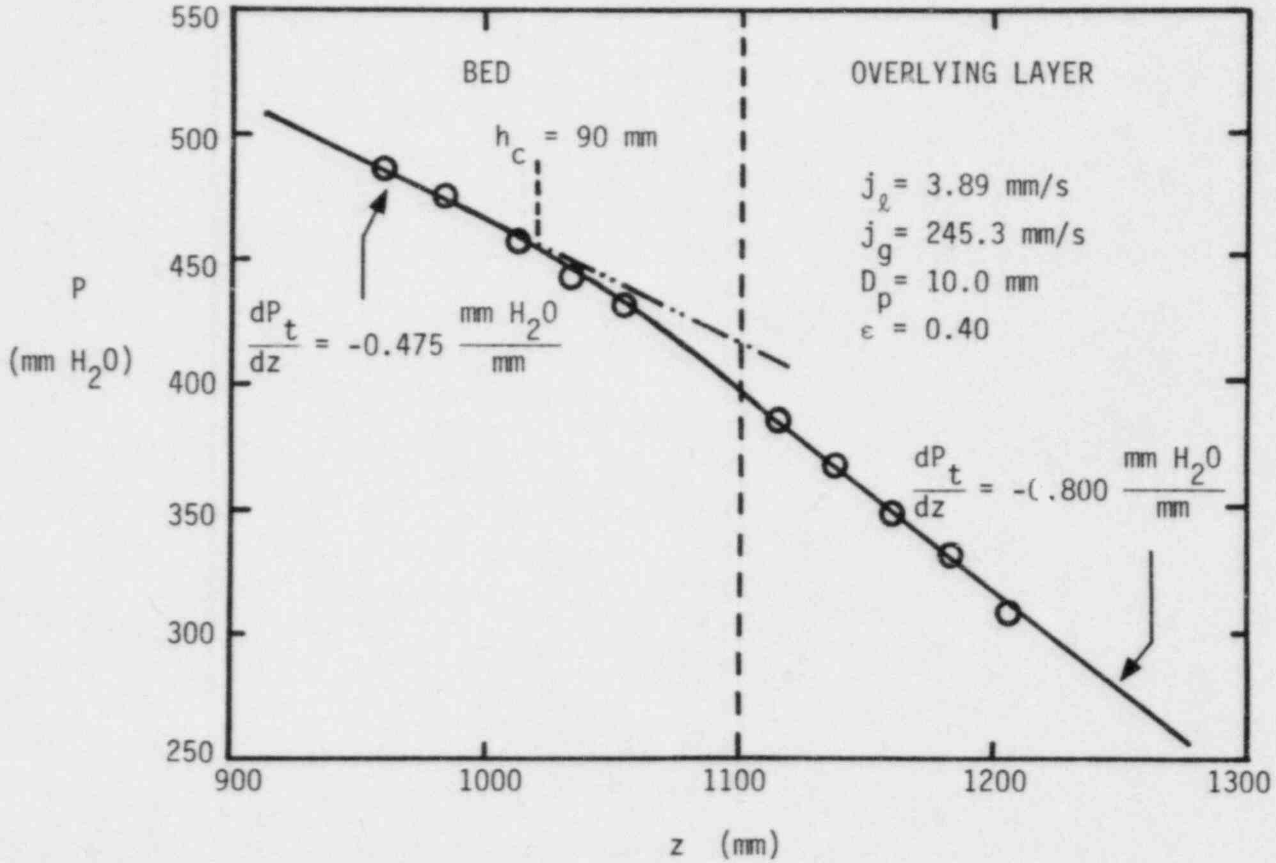

Figure 3.14 Variation of Pressure Near the Top of the Bed at the Flooding Limit (j_ℓ = 3.89 mm/s)

with gas and liquid superficial velocities of 245.3 mm/s and 3.89 mm/s, respectively. The coupling height, defined as the distance from the top of the bed at which the pressure gradient first deviates from a constant value, is seen in Figure 3.14 to be about 90 mm. Similar plots for other liquid and gas superficial velocities, given in Figures 3.15 through 3.18, show a variation in the coupling height of between 65 mm and 90 mm for beds composed of 10 mm diameter particles.

Physically, the increase in pressure gradient induced by overlying layer coupling is caused by an acceleration of the gas phase, and therefore a decrease in void fraction and liquid-particle drag, in the coupling layer. As the pressure gradient is increased the downward liquid flow will experience a greater driving force, thus increasing the flooding limit over that given by equation (3-50) near the top of the bed. If vapor is produced within the bed, as in volume heated beds, this increase of the flooding limit within the coupling layer will increase the dryout heat flux of the bed.

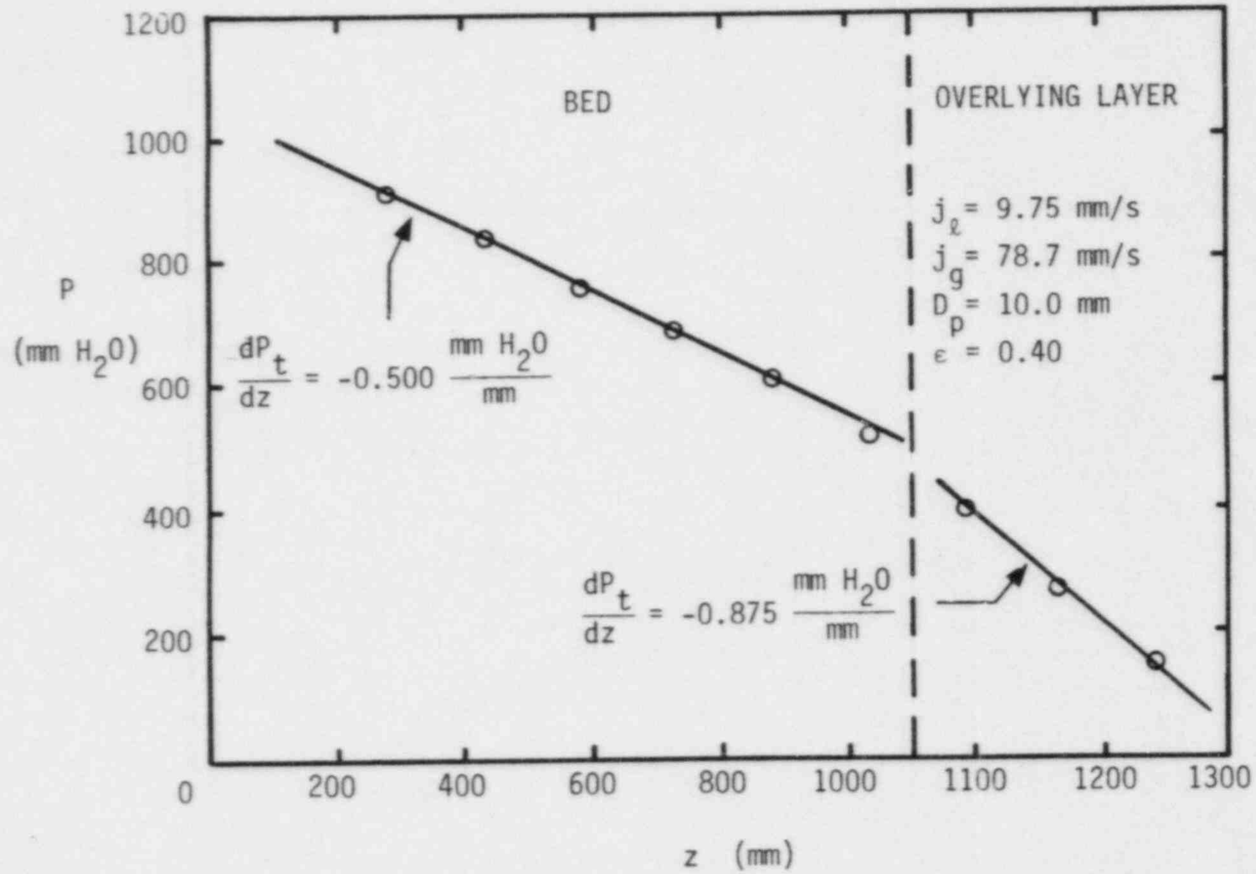

Figure 3.15 Variation of Pressure Through the Bed at the Flooding Limit (j_ℓ = 9.75 mm/s)

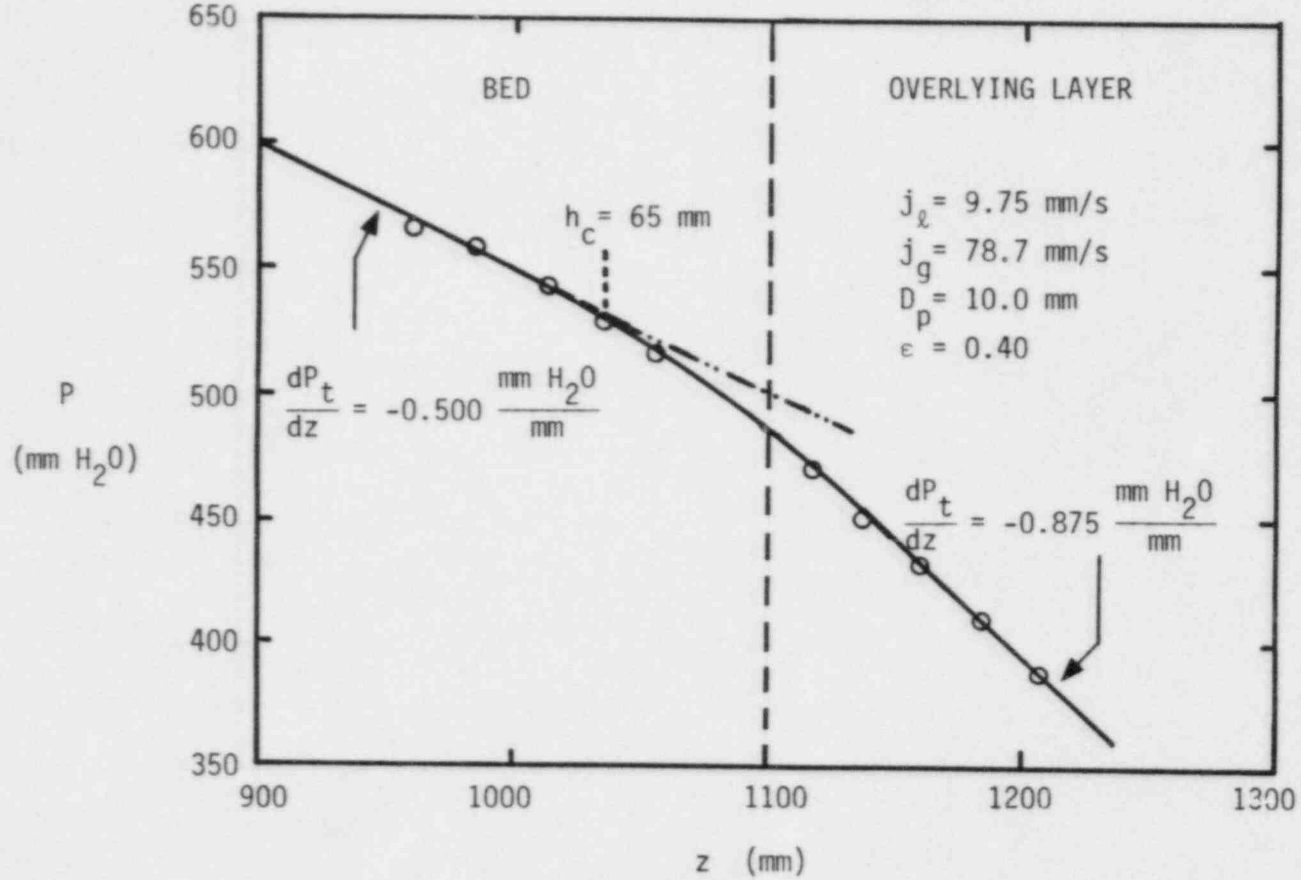

Figure 3.16 Variation of Pressure Near the Top of the Bed at the Flooding Limit (j_ℓ = 9.75 mm/s)

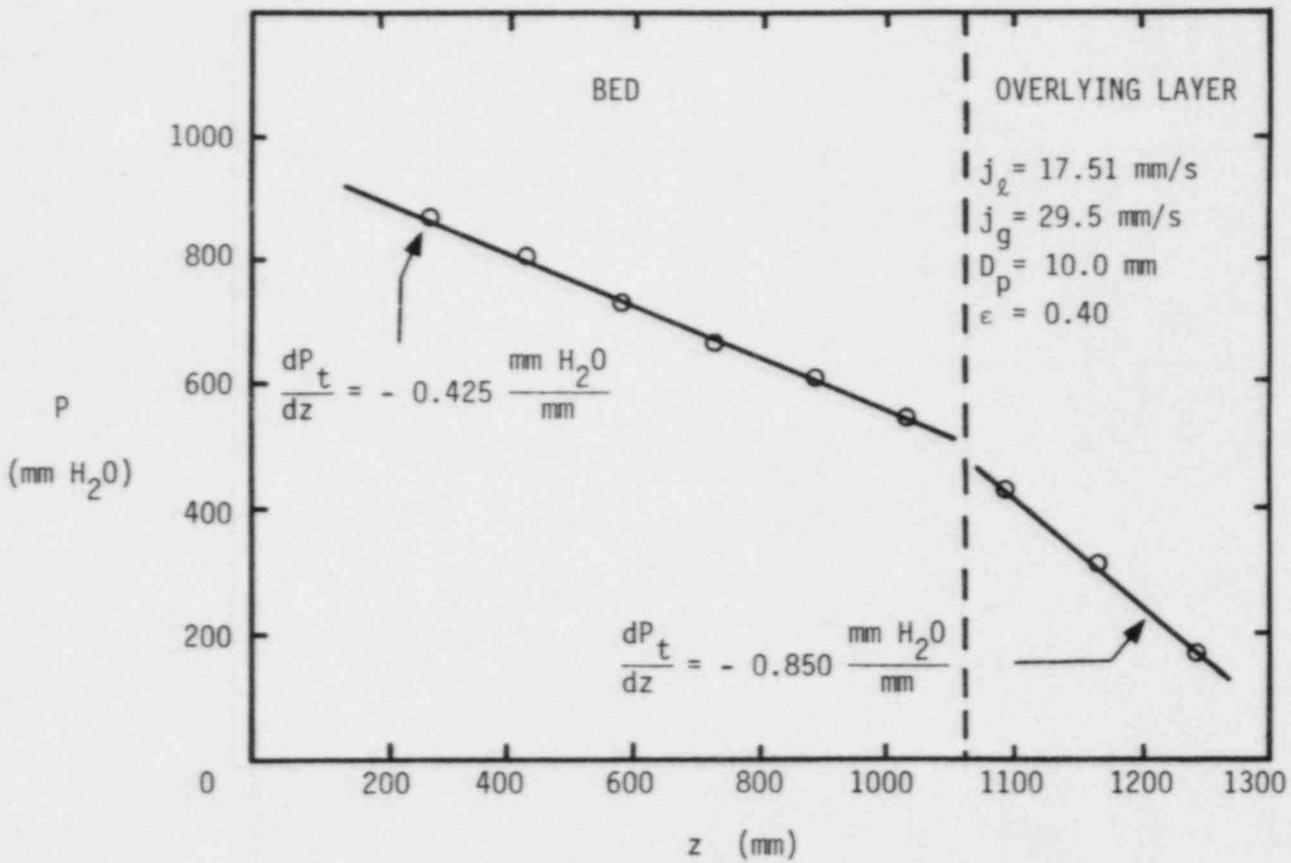

Figure 3.17 Variation of Pressure Through the Bed at the Flooding Limit (j_ℓ = 17.51 mm/s)

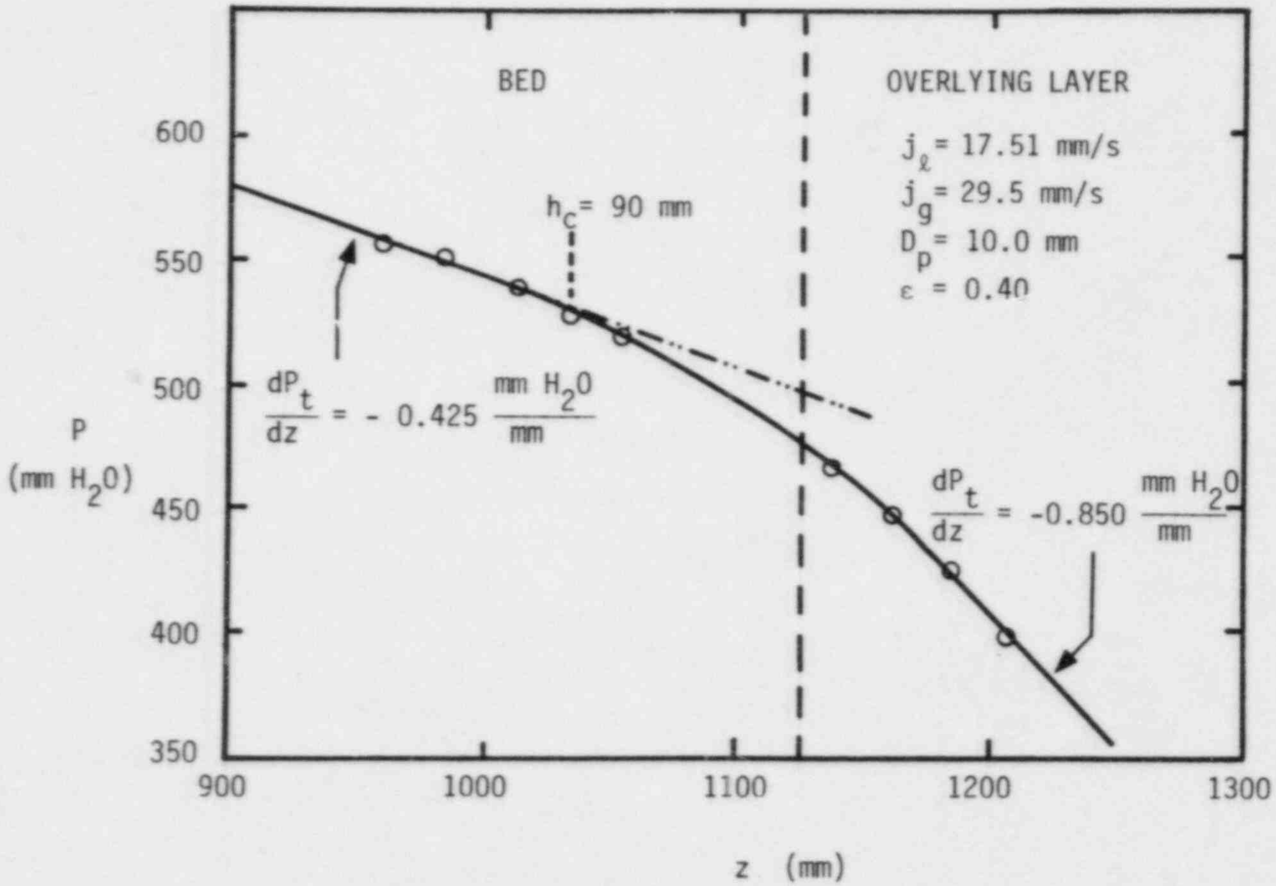

Figure 3.18 Variation of Pressure Near the Top of the Bed at the Flooding Limit (j_ℓ = 17.51 mm/s)

Chapter 4

APPLICATION TO TOP FLOODING OF A DEGRADED CORE

In the event of nuclear reactor core degradation, several scenarios can be envisioned in which the flow path of liquid coolant supplied at the bottom of the bed is blocked and cooling of the core material can only be accomplished by liquid supplied at the top of the debris bed. Such a situation would occur if an impervious blockage were to form at the core inlet, as shown in Figure 4-1a, or if the core debris were to drop down into the lower plenum, as shown in Figure 4-1b (1). If liquid coolant is supplied onto the top of a debris bed, a downward liquid and upward vapor flow would exist within the bed. The superficial velocities of the downward liquid flow and upward flow of vapor would be constrained by the flooding limit of two phase flow through the debris bed.

4.1 Dryout Heat Flux of a Liquid Saturated Bottom Heated Bed

Assuming that the debris bed forms in a pool of liquid so that the bed is initially saturated, the core material can readily be cooled provided that the energy generation rate is less than the maximum possible energy removal rate. The maximum energy removal rate is given simply by the dryout heat flux times the cross-sectional area of the bed. The dryout heat flux can be written as

$$q = \rho_g \, j_g \, h_{fg} \tag{4-1}$$

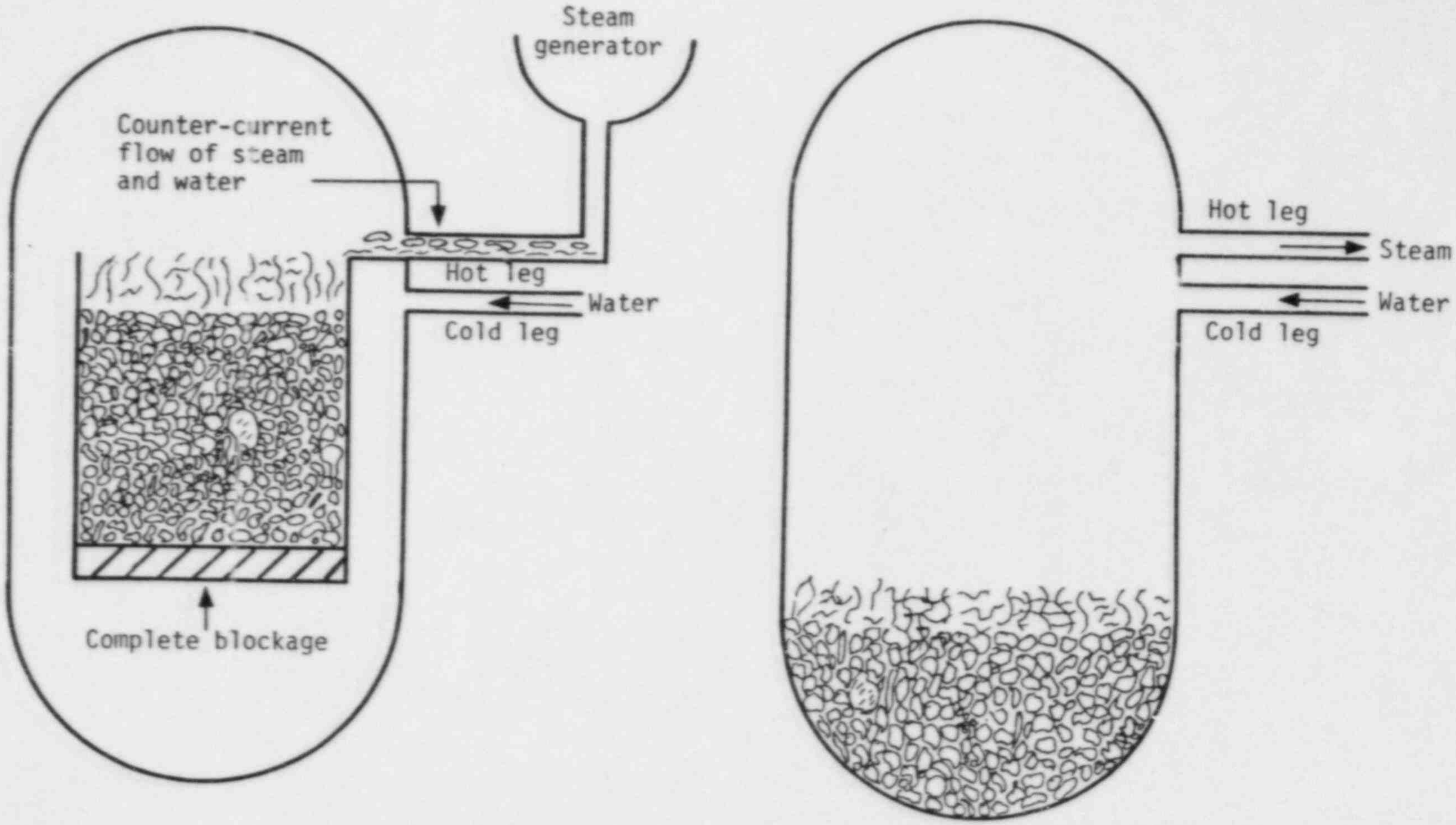

a. Counter-Current Flow Configuration for In-Place Cooling of Degraded Core

b. Core Debris Bed Formed in Lower Plenum

Figure 4.1

The amount of downward liquid and upward vapor flow through the bed is restricted by the flooding limit. For bottom heated beds, the flooding limit is given by equation (3-50). Conservation of mass provides a third equation, written as

$$\rho_\ell \, j_\ell = \rho_g \, j_g \tag{4-2}$$

Solving equations (3-50), (4-1), and (4-2) simultaneously for q, j_g, and j_ℓ, a relation for dryout heat flux of bottom heated beds composed of arbitrarily shaped particles can be determined as

$$q = \frac{0.766 \, h_{fg} \, \rho_\ell}{\left[1+(\rho_\ell/\rho_g)^{1/4}\right]^2} \left\{ \frac{g(\rho_\ell-\rho_g)\varepsilon^3}{\rho_\ell \, a} \right\}^{1/2} \tag{4-3}$$

For spherical particles, the surface area of packing per unit volume is given by equation (3-48). Equation (4-3) can be written for spherical particles as

$$q = \frac{0.313 \, h_{fg} \, \rho_\ell}{\left[1+(\rho_\ell/\rho_g)^{1/4}\right]^2} \left\{ \frac{g(\rho_\ell-\rho_g)\varepsilon^3 \overline{D}_p}{\rho_\ell (1-\varepsilon)} \right\}^{1/2} \tag{4-4}$$

The flooding data for the mixture of sharps and 6 mm nominal diameter spherical particles indicates that equation (4-4) can also be used for non-spherical particles if a suitable mean diameter is defined. The dryout heat flux is seen to depend upon the bed parameters ε and $\overline{D}_p$ and the flow parameters ρ_ℓ, ρ_g, and h_{fg}. For beds composed of mixtures of spherical particles, expressions for mean particle diameter and porosity obtained previously can be used to determine dryout heat flux at a given system pressure.

Figure 4.2 shows a plot of dryout heat flux versus spherical particle diameter for both water and Freon-113 systems at atmospheric pressure and with an assumed porosity of 0.40. The constant 0.875 was used in equation (3-49) for the solid lines in Figure 4.2 and the constant 0.775 was used for the dotted lines. The data given in Figure 4.2 was obtained by Barleon and Werle (5). For water systems, the predictions obtained using the constant 0.875 very nearly represent the mean of the data, whereas predictions obtained using the constant 0.775 underpredict the data by about 22%. For Freon-113 systems, predictions made using the constants 0.875 and 0.775 in equation (3-49) underpredict the data by 17% and 34%, respectively. The data given in Figure 4.2 has an average uncertainty of 14%, which may account for some of the differences between the predicted and experimental results.

The dryout heat flux can also be plotted as a function of system pressure at a fixed particle diameter. Figure 4.3 shows plots of the maximum energy removal rate (dryout heat flux times cross-sectional area) and the steam generation rate as functions of system pressure for water cooled beds composed of various diameter spherical particles. An assumed cross-sectional area of 15 m^2 and porosity of 0.40 were used to obtain the results in Figure 4.3. The maximum energy removal rate is seen to obtain a peak value at system pressures of 6 MPa for all particle diameters. It can be seen from Figure 4.3 that for water cooling with a system pressure of 6 MPa and average heat generation rate of 30 MW, beds with a mean particle diameter

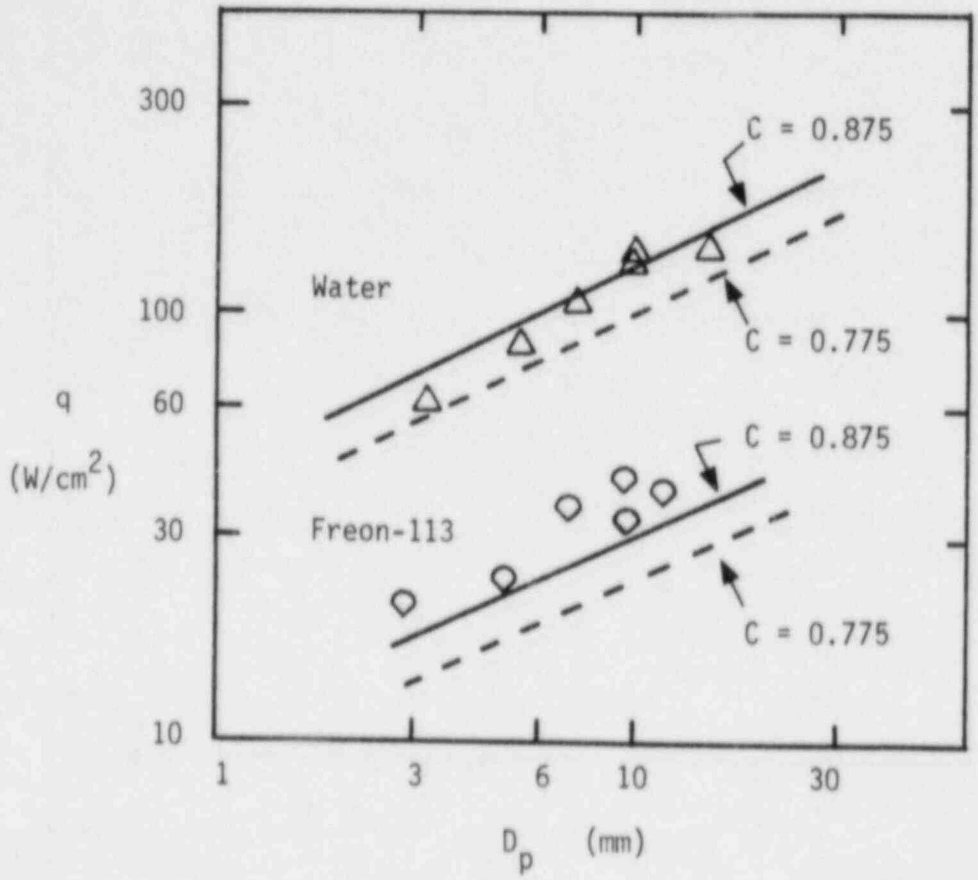

Figure 4.2 Dryout Heat Flux Plotted as a Function of Particle Diameter

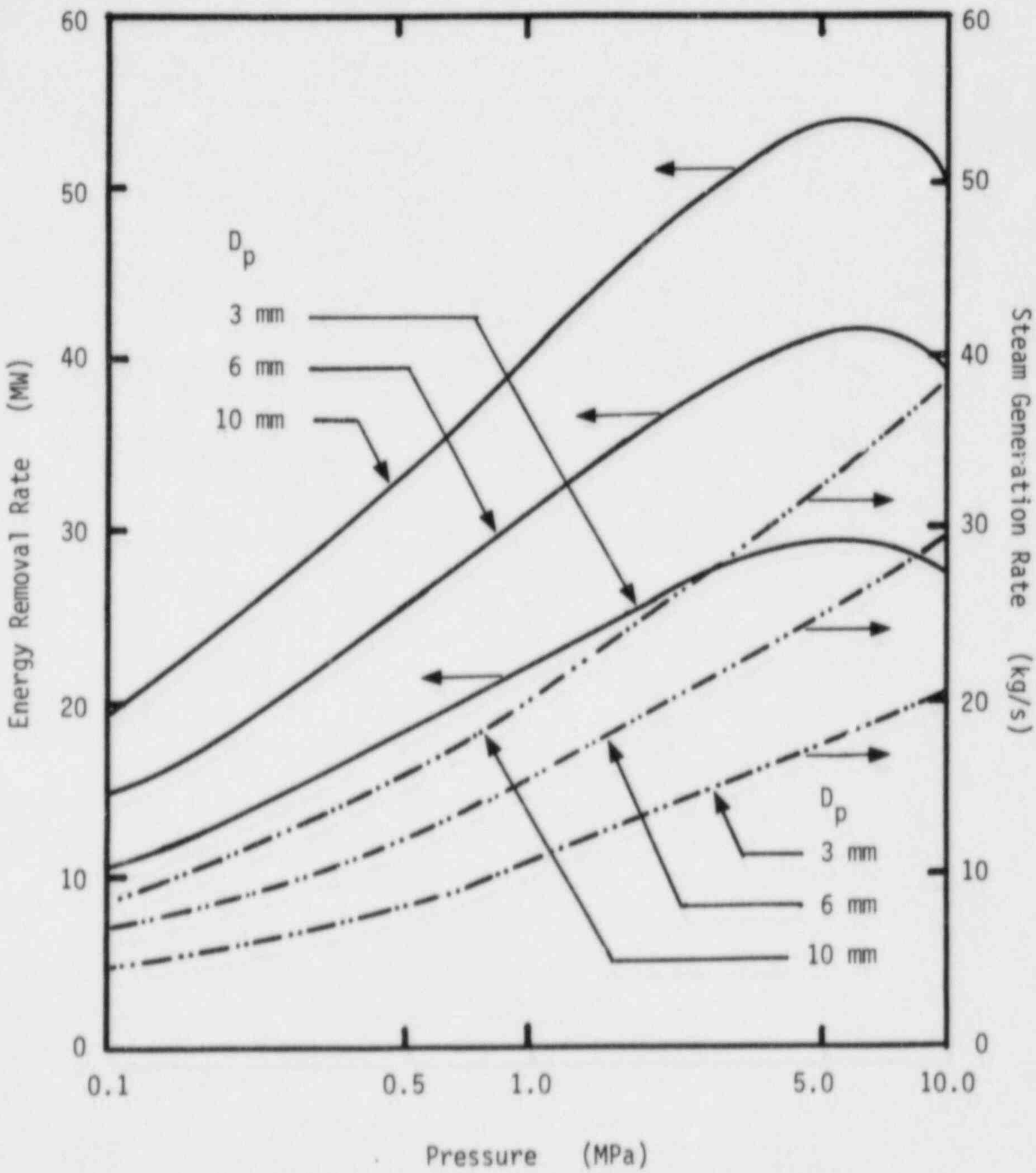

Figure 4.3 Variation of Maximum Energy Removal Rate with System Pressure

of 4 mm or greater and a porosity of 0.40 can be cooled assuming they are initially saturated with liquid. These conditions are typical for a degraded nuclear reactor core.

4.2 Dryout Heat Flux of a Liquid Saturated Volume Heated Bed

It was shown in section 3.5 that the flooding is increased markedly in the top portion of the bed due to coupling of the bed with the overlying liquid layer. Since for bottom heated beds no vapor is generated within the bed, the increase in flooding limit near the top of the bed has no effect upon the dryout heat flux. For volume heated beds, however, the overlying layer coupling will increase the rate of vapor production within the bed, and thus the dryout heat flux, above that predicted by applying the flooding limit given in equation (3-50) at the top of the bed. A diagram illustrating the increase in vapor generation rate due to overlying layer coupling is given in Figure 4.4.

A more qualitative analysis can be made by defining $\dot{Q}_v$ as the maximum rate of energy removal per unit volume and q as the maximum rate of energy removal per unit area, or the dryout heat flux. Furthermore, for a bed of height L, let $\dot{Q}_v$ have a value $\dot{Q}_{v1}$ in the main portion of the bed of height $L - h_c$ and a value $\dot{Q}_{v2}$ in the coupling layer of height h_c at the top of the bed. At a height $L - h_c$, the vapor and liquid superficial velocities are limited by the flooding limit. If the superficial vapor velocity obtained by solving the flooding limit equation (3-50) and the

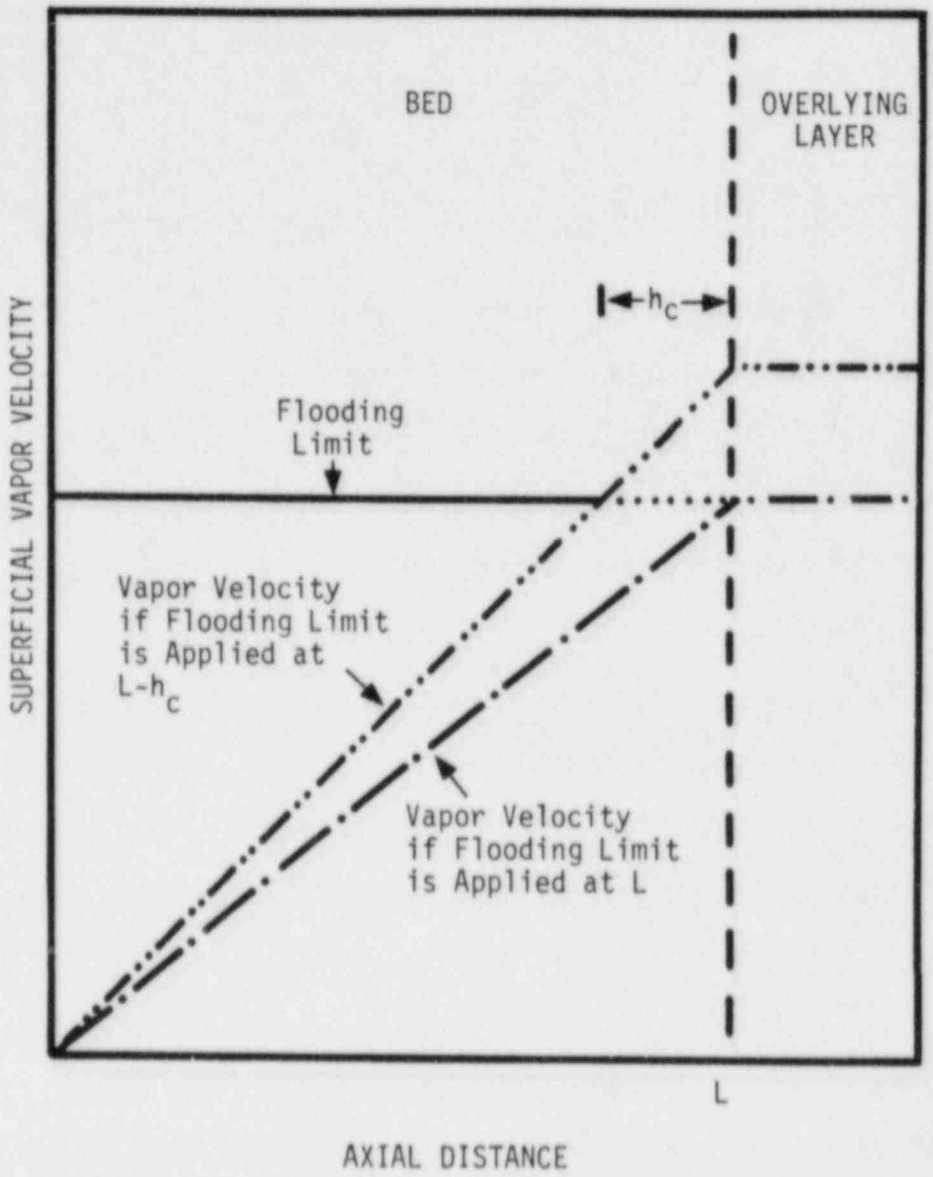

Figure 4.4 Vapor Generation Rate for Volume Heated Beds

conservation of mass equation (4-2) is denoted as $j_{g,fl}$, an expression for $\dot{Q}_{v1}$ can be obtained as

$$\dot{Q}_{v1} = \frac{\rho_g \, j_{g,fl} \, h_{fg}}{L-h_c} \tag{4-5}$$

The average volumetric heat flux is written as

$$\bar{\dot{Q}}_v = \frac{L-h_c}{L} \dot{Q}_{v1} + \frac{h_c}{L} \dot{Q}_{v2} \tag{4-6}$$

At steady state, the energy flow into the bed must equal the energy removal rate. For uniformly heated beds at steady state, we can therefore set $\dot{Q}_{v2}$ equal to $\dot{Q}_{v1}$. Applying this condition, equation (4-6) becomes

$$\bar{\dot{Q}}_v = \dot{Q}_{v1} \tag{4-7}$$

Turning our attention now to dryout heat flux, equation (4-1) gives dryout heat flux of a bottom heated bed as

$$q = h_{fg} \, \rho_g \, j_{g,fl} \tag{4-8}$$

For volume heated beds, an additional term must be added to equation (4-8) to account for the vapor generated in the coupling layer. This additional heat flux is given as

$$q_{add} = h_c \, \bar{\dot{Q}}_v \tag{4-9}$$

Substituting equation (4-5) and (4-7), equation (4-9) can be written as

$$q_{add} = h_{fg} \, \rho_g \, j_{g,fl} \left(\frac{h_c}{L-h_c}\right) \tag{4-10}$$

Adding the additional heat flux (4-10) to equation (4-8), the dryout heat flux for volume heated beds is obtained as

$$q = h_{fg} \rho_g j_{g,fl} \left(1 + \frac{h_c}{L-h_c}\right) \tag{4-11}$$

Sustituting equation (4-3) for dryout heat flux for bottom heated beds into equation (4-11), the dryout heat flux for volume heated beds composed of spherical particles can be written as

$$q = \frac{0.313\, h_{fg}\, \rho_\ell}{[1+(\rho_\ell/\rho_g)^{1/4}]^2} \left\{ \frac{g(\rho_\ell-\rho_g)\varepsilon^3 \bar{D}_p}{\rho_\ell\,(1-\varepsilon)} \right\}^{1/2} \left(1 + \frac{h_c/L}{1-h_c/L}\right) \tag{4-13}$$

Notice that as the bed length L becomes much larger than h_c, the ratio h_c/L becomes very small and the dryout heat flux goes to that for a bottom heated bed.

Chapter 5

CONCLUSIONS

1. For beds composed of mixtures of various size particles, a mean particle diameter can be defined which can be used to predict the flooding limits.
2. A semi-empirical procedure to determine porosity of beds composed of mixtures of various size spherical particles has been developed which can be used to predict the available porosity data to within ± 12%.
3. The flooding limits are found to depend upon the bed porosity, the mean particle diameter, and the fluid densities.
4. The Wallis correlation underpredicts the flooding limit by about 25%. A better correlation is obtained by changing Wallis' constant from 0.775 to 0.875.
5. The pressure gradient near the top of the bed is found to be significantly increased due to coupling of the bed with the overlying layer. This overlying layer coupling causes the flooding limit to increase near the top of the bed.
6. The flooding limits for beds with axially injected gas flow are found to be the same as those for beds with bottom injected gas flow as long as no gas is injected within the coupling layer.
7. The flooding correlation obtained in this study can be used to predict the dryout heat flux for bottom heated particulate beds to within ± 17% of the data in the literature.
8. The dryout heat flux correlation derived for bottom heated beds can be modified to apply to volume heated beds.

REFERENCES

1. Dhir, V.K.,"On the Coolability of Degraded LWR Cores", Nuclear Safety, July-August (1983).

2. Ostensen, R.W. and Lipinski, R.J., "A Particule Bed Dryout Model Based on Flocding", Nuclear Science and Engineering, Vol. 79 (1981).

3. Dhir, V.K. and Barleon, L., "Dryout Heat Flux in a Bottom Heated Porous Layer", ANS Transactions, Vol. 38 (1981).

4. Lipinski, R.J., "A One Dimensional Particle Bed Dryout Model", ANS Transactions, Vol. 38 (1981).

5. Barleon, L. and Werle, H., "Dependence of Dryout Heat Flux on Particle Diameter for Volume and Bottom Heated Beds", KFK 3138 (1981).

6. Chu, W., Dhir, V.K., and Marshall, J.S., "Study of Pressure Drop, Void Fraction, and Relative Permeabilities of Two Phase Flow Through Porous Media", AIChE Symposium Series 225, Vol. 79 (1983).

7. Dhir, V.K., Tung, V.X., Marshall, J.S., Catton, I., Tsai, F.P., and Lee, H., "Heat Transfer and Fluid Dynamics Under Simulated Degraded Core Conditions", Transactions of the Eleventh Water Reactor Safety Research Information Meeting, Gaithersburg, Maryland (1983).

8. Scheidegger, Adrian E., The Physics of Flow Through Porous Media, Macmillan Publishing Comp., New York, N.Y. (1960).

9. Collins, Royal E., Flow of Fluids Through Porous Media, Reinhold Publishing Corp., New York, N.Y. (1961).

10. El-Genk, M.S., Louie, D., Bergeron, E., and Mitchell, D., "Dependence of Porosities and Capillary Pressures in Particle Beds on the Morphology and the Size of Particles", AIChE Symposium Series 225, Vol. 79 (1983).

11. Sherwood, T.K., Shipley, G.H., and Holloway, F.A.L., "Flooding Velocities in Packed Columns", Ind. Eng. Chem., Vol. 30 (1938).

12. Dell, F.R. and Pratt, H.R.C., "Flooding Rates for Packed Columns", Inst. Chem. Eng., Vol. 29 (1951).

13. Wallis, G.B., One Dimensional Two Phase Flow, McGraw-Hill Book Comp., New York, N.Y. (1969).

14. Lobo, W.E., Friend, L., Hashmall, F., and Zenz, F., "Limiting Capacity of Dumped Tower Packings", Am. Inst. Chem. Eng., Vol. 41 (1946).

APPENDIX A: Calculation of Pore Level Sizes

A.1 First Level Pores

The diagonal plane of the cube is shown in Figure A.1. The structuring particle diameter is denoted as D_1, and the diameter of the particle filling the first level pore is denoted as D_2. From the Phythagorian theorem, we known that

$$D_1^2 + 2D_1^2 = (D_1 + D_2)^2$$

$$D_2 = 0.732\ D_1 \qquad \text{(A-1)}$$

A.2 Second Level Pores

A face of the cube is shown in Figure A.2. If D_3 denotes the diameter of a particle filling the second level pore in the center of a face of a cube, we have

$$D_1^2 + D_1^2 = (D_1 + D_3)^2$$

$$D_3 = 0.414\ D_1 \qquad \text{(A-2)}$$

It should be noted that D_3 can also be calculated from Figure A.1, giving a value of only 0.268 D_1 when a particle of diameter 0.732 D_1 is filling the central pore. However, since perfectly cubic arrays rarely form with very large diameter central particles, the characteristic diameter of the second level pore will be governed by the

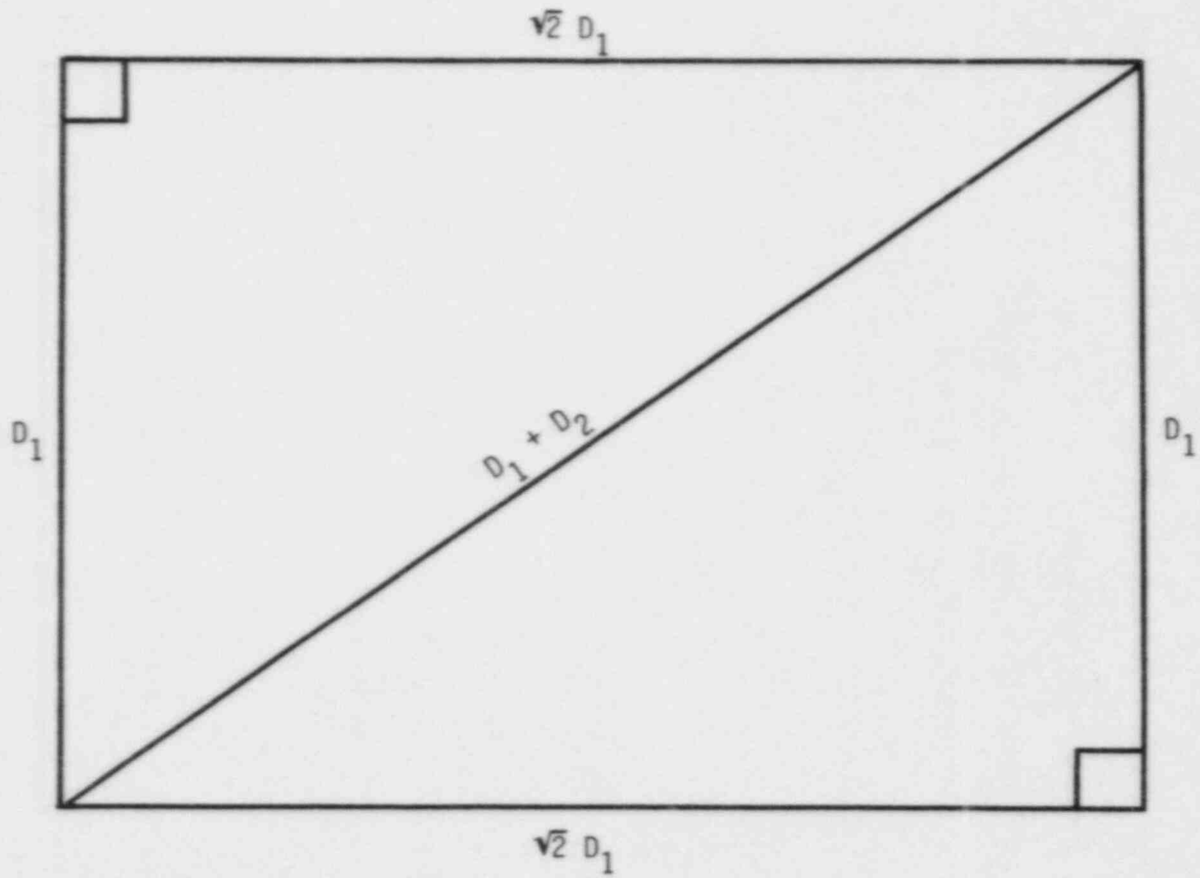

Figure A.1 First Level Pore Located in Diagonal Plane of Cube

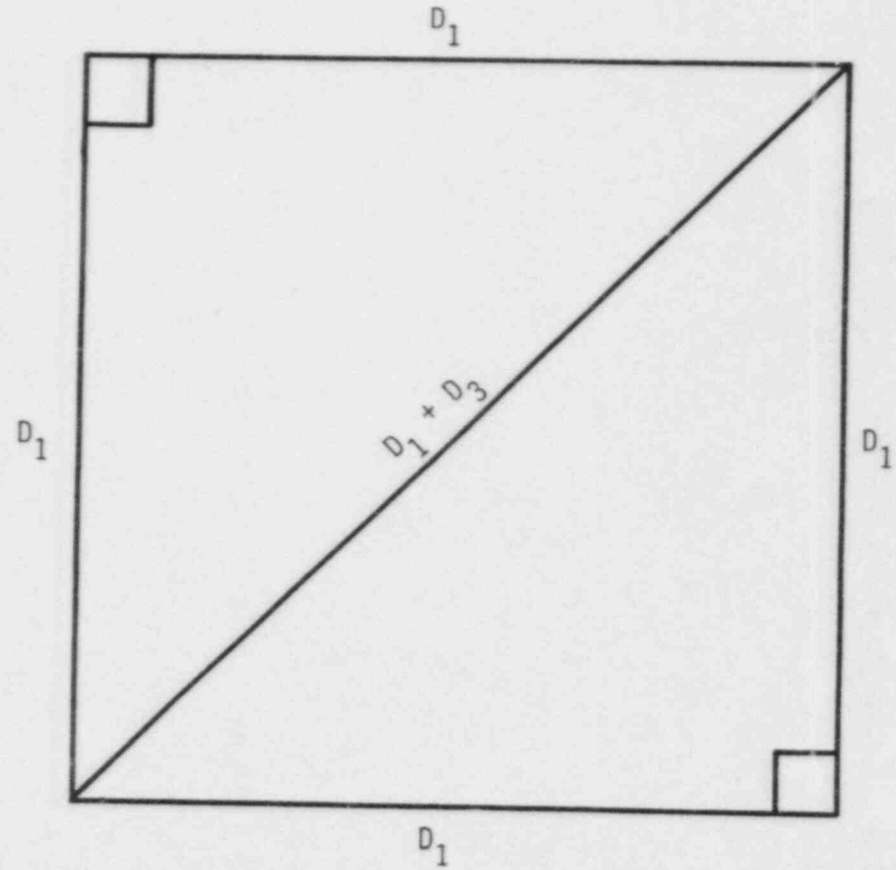

Figure A.2 Second Level Pore Located in Face of Cube structuring particles and not the central particle.

A.3 Third Level Pores

The diagonal plane is again shown in Figure A.3. If D_4 denotes the diameter of a particle filling the third level pore located between any two adjacent structuring particles of the cubic array and the central particle, we can write

$$\left(\frac{\sqrt{2}}{2} D_1 - y\right)^2 + (D_1/2)^2 = x^2$$

where

$$x = \frac{D_1}{2} + \frac{D_4}{2}$$

and

$$y = \frac{D_2}{2} + \frac{D_4}{2}$$

Solving quadratically for D_4 gives

$$D_4 = 0.138\ D_1 \qquad \text{(A-3)}$$

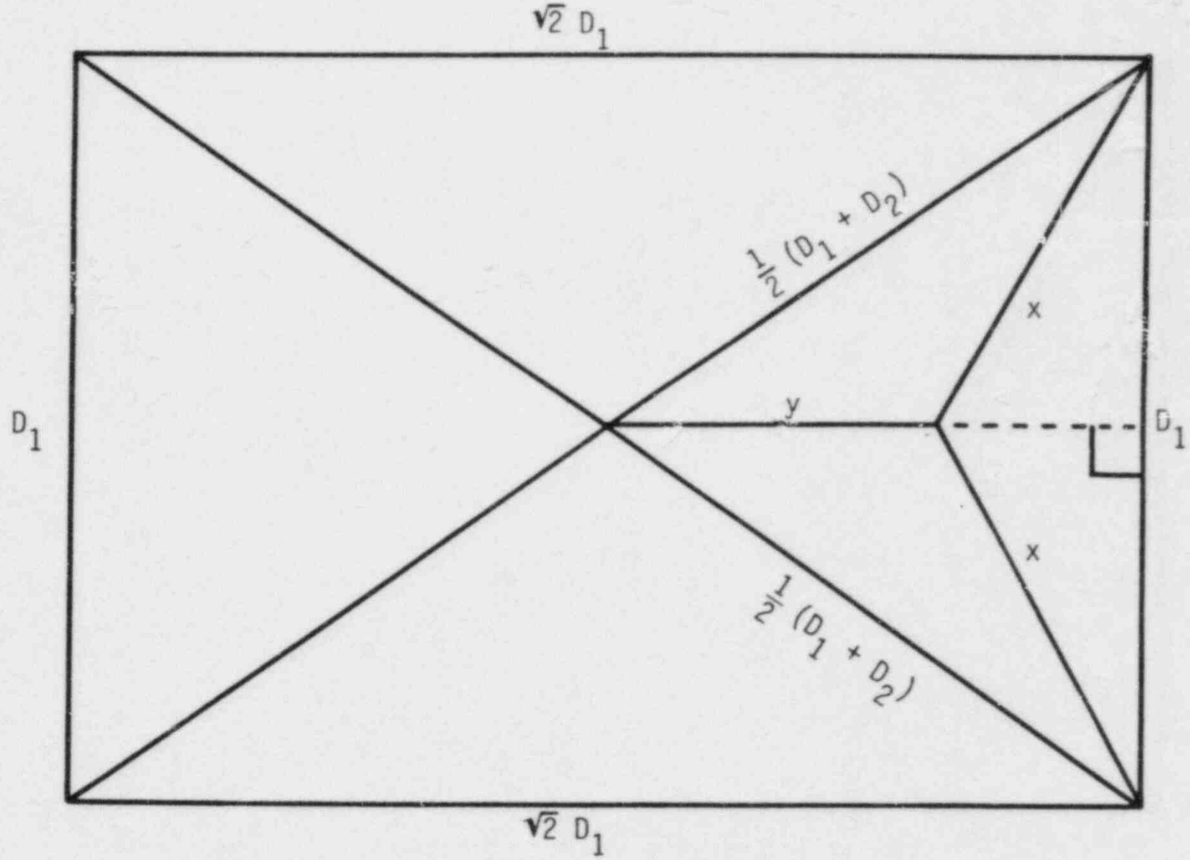

Figure A.3 Third Level Pore Located in Diagonal Plane of Cube

APPENDIX B: Calculation of Saturated Number Ratio for Non-Full Mixture Sets

B.1 Mixtures of Particles from Regions 1 and 3 and Regions 1 and 4

An expression for β_{sat} for mixtures of particles from regions 1 and 3 and regions 1 and 4 can be obtained by using equation (3-30) for mixtures of two particle sizes.

B.2 Mixtures of Particles from Regions 1,2, and 4

Each cubic structure has three second level pores, so $\beta_{sat,3}$ is equal to three. However, since no particles from region 3 are present, the smaller particles of region 4 fit into the second level pore spaces. Because second level pore spaces are approximately equal in size to the pores formed by a uniform bed of particles of region 2, the number of particles from region 4 needed to fit into each second level pore can be taken as

$$\beta_{sat,24} = 0.458 \frac{(\gamma_{24}-1)^2}{\gamma_{24}^3} \qquad \text{(B-1)}$$

Multiplying $\beta_{sat,24}$ by the number of second level pores in each cube gives $\beta_{sat,4}$ as

$$\beta_{sat,4} = 1.374 \frac{(\gamma_{24}-1)^2}{\gamma_{24}^3} \qquad \text{(B-2)}$$

B.3 Mixtures of Particles from Regions 1, 3, and 4

If we assume that the particles of region 4 have no effect upon the number of particles from region 3 that are present, we find from equation (3-30) that $\beta_{sat,3}$ is given by the equation

$$\beta_{sat,3} = 0.458 \frac{(\gamma_{13}-1)^2}{\gamma_{13}^3} \tag{B-3}$$

In the pore of each small cube formed of particles of region 3 there are $\beta_{sat,34}$ particles of region 4 present, where $\beta_{sat,34}$ is given by equation (3-30) as

$$\beta_{sat,34} = 0.458 \frac{(\gamma_{34}-1)^2}{\gamma_{34}^3} \tag{B-4}$$

The total number of particles from region present in each pore of a lattice formed of particles from region 1 can be obtained by multiplying $\beta_{sat,3}$ by $\beta_{sat,34}$, thus

$$\beta_{sat,4} = 0.458\, \beta_{sat,3} \frac{(\gamma_{34}-1)^2}{\gamma_{34}^3} \tag{B-5}$$

APPENDIX C: Calculation of Saturated Porosity

C.1 Mixtures of Two Particle Sizes

An expression for saturated porosity of mixtures of two particle sizes is given by equation (3-29) in section 3.2.2.

C.2 Mixtures of Particles from Regions 1, 2, and 3

The saturated porosity for mixtures of particles from regions 1 and 2 is given by equation (3-29) as

$$\varepsilon_{sat,12} = 0.40 - 0.24\ (\gamma_{12}-1)^2 \qquad \text{(C-1)}$$

The change in saturated porosity when particles from region 3 are added can be calculated by assuming a cubic model as

$$\Delta\varepsilon_{sat,3} = -\frac{\pi}{6}\ \beta_{sat,3}\ \gamma_{13}^{\ 3} \qquad \text{(C-2)}$$

Since $\beta_{sat,3}$ is equal to three, the final saturated porosity is given by

$$\varepsilon_{sat,123} = 0.40 - 0.24\ (\gamma_{12}-1)^2 - \frac{\pi}{2}\ \gamma_{13}^{\ 3} \qquad \text{(C-3)}$$

C.3 Mixtures of Particles from Regions 1, 2, 3, and 4

The change in $\varepsilon_{sat,123}$, given by equation (C-3), when particles from region 4 are added can be calculated by again assuming a cubic model as

$$\Delta\varepsilon_{sat,4} = -\frac{\pi}{6}\ \beta_{sat,4}\ \gamma_{14}^{3} \tag{C-4}$$

Since $\beta_{sat,4}$ is equal to 12, the saturated porosity for this mixture is given by

$$\varepsilon_{sat,1234} = 0.40 - 0.24\ (\gamma_{12}-1)^2 - \frac{\pi}{2}\gamma_{13}^{3} - 2\pi\ \gamma_{14}^{3} \tag{C-5}$$

C.4 Mixtures of Particles from Regions 1, 2, and 4

The change in $\varepsilon_{sat,12}$ when particles from region 4 are added, $\Delta\varepsilon_{sat,4}$, is given by equation (C-4). For this mixture set, an expression for $\beta_{sat,4}$ is given in equation (B-2). Substituting this expression for $\beta_{sat,4}$ into equation (C-1) results in an expression for saturated porosity of this mixture set as

$$\varepsilon_{sat,124} = 0.40 - 0.24\ (\gamma_{12}-1)^2 - 0.719\ \gamma_{12}^{3}\ (\gamma_{24}-1)^2 \tag{C-6}$$

C.5 Mixtures of Particles from Regions 1, 3, and 4

The saturated porosity for mixtures of particles from regions 1 and 3 is given by equation (3-29) as

$$\varepsilon_{sat,13} = 0.40 - 0.24\ (\gamma_{13}-1)^2 \tag{C-7}$$

Since the particles of region 3 are much smaller than those of region 1, the porosity of the small cubes formed of particles from region 3 lying within the larger cubes can be assumed to be 0.40. If we now add particles from region 4 into the mixture, the porosity of the small cubes formed of particles from region 3 becomes

$$\epsilon_{sat,34} = 0.40 - 0.24\ (\gamma_{34}-1)^2 \qquad \text{(C-8)}$$

The porosity of the large cubes formed of particles from region 1 is thus reduced by a factor $\epsilon_{sat,34}/0.40$ upon addition of particles from region 4. Multiplying $\epsilon_{sat,13}$ by this factor, the saturated porosity for this mixture set is obtained as

$$\epsilon_{sat,134} = 2.5\ [0.40 - 0.24(\gamma_{13}-1)^2]\ [0.40 - 0.24(\gamma_{34}-1)^2] \qquad \text{(C-9)}$$

APPENDIX D: Example of Porosity Weighting Methods

In this study, the porosities of the particulate layers were weighted either by the final volume of the layers within the bed or by the sum of the initial volumes of the particles making up each layer. The latter weighting technique was used as an approximation to the former in order to simplify the required equations for mixtures of two particle sizes. The approximation can be validated by assuming a simple geometrical array and comparing the porosity results for the two weighting methods. Assuming a partially filled cubic array consisting of six cubes formed of large particles of diameter D_1 with small particles of diameter D_2 filling the pores of four of the cubes, as shown in Figure D.1, the porosity of the filled and empty cells is given by

$$\varepsilon_{filled} = 1 - \frac{\pi}{6}\frac{D_1^{\,3}}{D_1^{\,3}} - \frac{\pi}{6}\frac{D_2^{\,3}}{D_1^{\,3}} \qquad \text{(D-1)}$$

$$\varepsilon_{empty} = 1 - \frac{\pi}{6}\frac{D_1^{\,3}}{D_1^{\,3}} \qquad \text{(D-2)}$$

The maximum value of the diameter D_2 is 0.732 D_1. Substituting this value for D_2 into equation (D-1), the porosities of the filled and empty cubes are found to be 0.2727 and 0.4764, respectively. These local porosities can be weighted by the volumes within the array to obtain the total array porosity as follows:

$$\varepsilon = \frac{4}{6}\,(0.2727) + \frac{2}{6}\,(0.4764) \qquad \text{(D-3)}$$

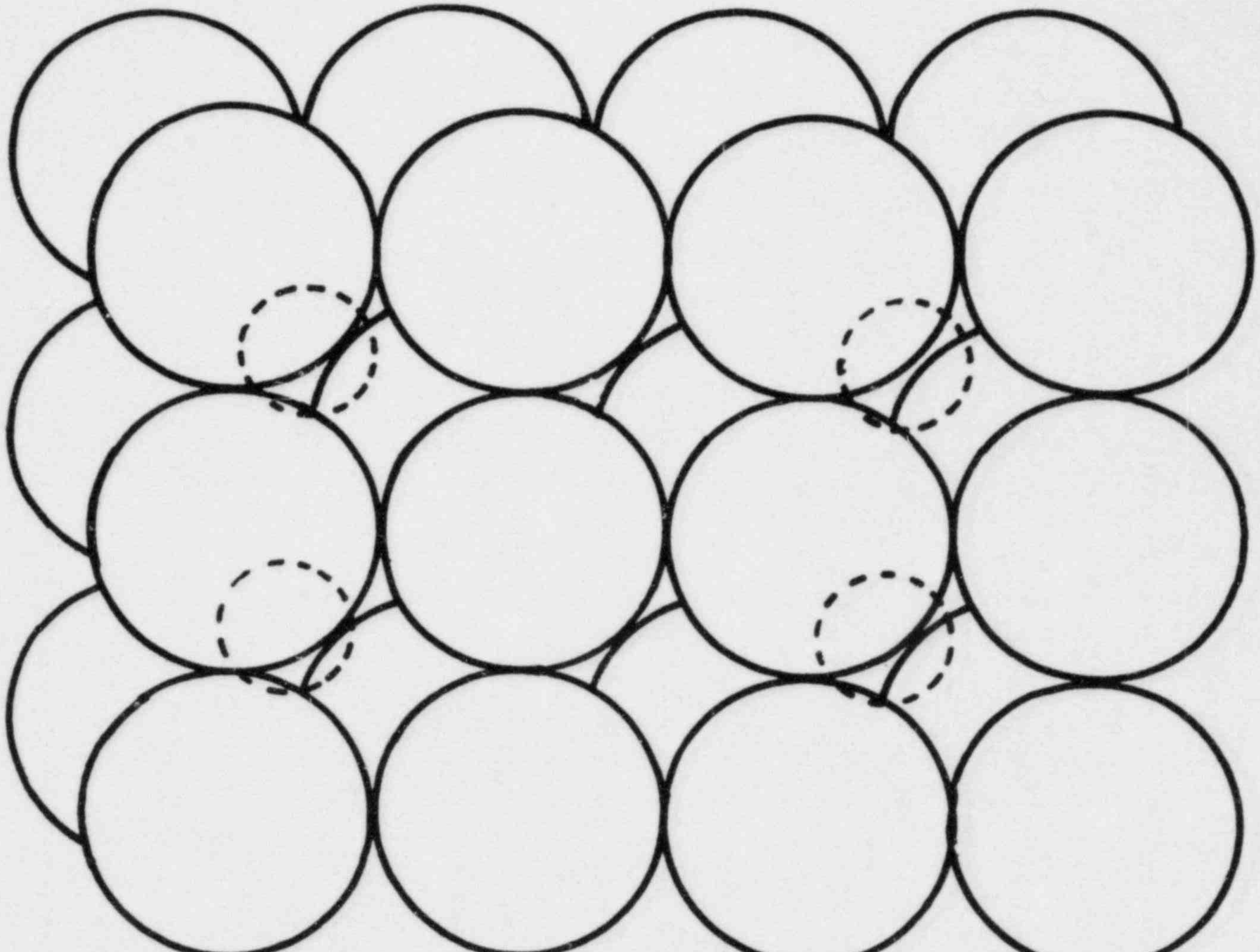

Figure D.1 Cubic Array Partially Filled with Smaller Particles (Dotted) in the Pores

Performing the algebra in equation (D-3), the porosity of the array is found to be 0.3406.

An approximation to this result can also be obtained by weighting the local porosities by the sum of the initial volumes of the constituent particles as follows:

$$\varepsilon = \left(\frac{V_{i,2} + (4/6)\, V_{i,1}}{V_{i,1} + V_{i,2}}\right)(0.2727) + \left(\frac{(2/6)\, V_{i,1}}{V_{i,1} + V_{i,2}}\right)(0.4764)$$

(D-4)

where $V_{i,1}$ and $V_{i,2}$ are the initial volumes of the particles of sizes 1 and 2, respectively. The values of $V_{i,1}$ and $V_{i,2}$ are simply

$$V_{i,1} = 6\,\frac{\pi}{6}\,(D_1/2)^3 = \pi\, D_1^{\,3} \qquad \text{(D-5)}$$

$$V_{i,2} = 4\,\frac{\pi}{6}\,(0.732\, D_1/2)^3 = 0.2593\,\pi\, D_1^{\,3} \qquad \text{(D-6)}$$

Substituting these values into equation (D-4), the approximate porosity obtained by initial volume weighting is found to be 0.3266, which is 4.1% higher than the exact porosity determined earlier. If the diameter D_2 is decreased below 0.732 D_1, the percent weighting error would also decrease. For instance, for a value for D_2 of 0.6 D_1, the error caused by initial volume weighting is only 1.2% when the cubic model in Figure D.1 is assumed. Weighting of the layer porosities by the initial volumes of the constituent particles can therefore be used to predict bed porosities to within 5% of predictions made using the layer volumes within the bed.

APPENDIX E: Porosity Computer Program

A FORTRAN computer program is given in the following pages which can be used to determine the porosity of beds composed of mixtures of various size spherical particles. The computer program is based on the algorithm given in section 3.2.3. Unformatted input statements are used for all data entry. The constituent particle diameters should be listed in the first line of data and the corresponding particle volume fractions in the second. These data can be listed in any order; however, it is important that the particle diameters and volume fractions correspond. The parameter N is simply the number of particle sizes present. The relaxation parameter ω is written as W and is given the value 0.6 in the program. The program is quite general and can be applied to any distribution of spherical particle sizes for which the spread (i.e. D_{min}/D_{max}) is not less than 0.05 and where no more than about 15% of the particles have diameters less than 1 mm.

The program used to calculate porosity is given as follows:

```
*JOB
C        POROSITY CALCULATION FOR MIXTURES OF N PARTICLE SIZES
C
         IMPLICIT REAL*8(A-H,O-Z)
         DIMENSION D(6),X(6)
         N=6
         W=0.6
         E=0.
         READ,(D(I),I=1,N)
         READ,(X(I),I=1,N)
         CALL POR(D,X,N,E,W)
         WRITE(6,998) E
 998     FORMAT(1X,'THE POROSITY IS ',F14.6)
         STOP
         END
C
         SUBROUTINE POR(D,X,N,E,W)
         IMPLICIT REAL*8(A-H,O-Z)
         INTEGER FLAG1,FP1
         DIMENSION D(N),X(N),DM(4),XM(4),XU(4),BSAT(4),BR(4),B(4),M(4)
C
C        ORDER DIAMETERS FROM LARGEST TO SMALLEST
C
         XUTT=0.
         DO 1 I=1,N
              DO 2 J=I,N
                   IF (D(I).GT.D(J)) GO TO 2
                   TEMPD=D(I)
                   TEMPX=X(I)
                   D(I)=D(J)
                   X(I)=X(J)
                   D(J)=TEMPD
                   X(J)=TEMPX
  2           CONTINUE
  1      CONTINUE
C
C        DETERMINE MAXIMUM PARTICLE SIZE, BOUNDARY REGIONS, AND
C                      MEAN DIAMETERS
C
 250     DO 3 I=1,N
              IF (X(I).EQ.0.) GO TO 3
              DMAX=D(I)
              GO TO 111
  3      CONTINUE
 111     D12=0.732*DMAX
         D23=0.414*DMAX
         D34=0.138*DMAX
         DO 4 K=1,4
             DM(K)=0.
             XM(K)=0.
  4      CONTINUE
         DO 5 J=1,N
              IF (D(J).LT.D12) GO TO 162
              DM(1)=DM(1)+X(J)*D(J)
              XM(1)=XM(1)+X(J)
  5      CONTINUE
 162     DM(1)=DM(1)/XM(1)
         FLAG1=4
         IF (J.LE.N) GO TO 161
         FLAG1=1
         GO TO 261
```

```
 161    DO 6 I=J,N
              IF (D(I).LT.D23) GO TO 163
              DM(2)=DM(2)+D(I)*X(I)
              XM(2)=XM(2)+X(I)
 6      CONTINUE
 163    IF (XM(2).EQ.0.) GO TO 170
        DM(2)=DM(2)/XM(2)
 170    IF (I.LE.N) GO TO 164
        FLAG1=2
        GO TO 261
 164    DO 7 J=I,N
              IF (D(J).LT.D34) GO TO 165
              DM(3)=DM(3)+D(J)*X(J)
              XM(3)=XM(3)+X(J)
 7      CONTINUE
 165    IF (XM(3).EQ.0.) GO TO 171
        DM(3)=DM(3)/XM(3)
 171    IF (J.LE.N) GO TO 166
        FLAG1=3
        GO TO 261
 166    DO 8 I=J,N
              DM(4)=DM(4)+D(I)*X(I)
              XM(4)=XM(4)+X(I)
 8      CONTINUE
        IF (XM(4).EQ.0.) GO TO 261
        DM(4)=DM(4)/XM(4)
 261    DO 9 I=1,FLAG1
              IF (DM(I).NE.0.) GO TO 156
              B(I)=0.
              GO TO 9
 156          B(I)=(XM(I)/XM(1))*(DM(1)/DM(I))**3
 9      CONTINUE
        IF (FLAG1.EQ.4) GO TO 262
        FP1=FLAG1+1
        DO 10 I=FP1,4
              B(I)=0.
 10     CONTINUE
C
C       DETERMINE MIXTURE SET AND MIXTURE SET POROSITY
C
 262    FLAG1=0
        R=1.
        BSAT(1)=1.
        BSAT(2)=1.
        BSAT(3)=3.
        BSAT(4)=12.
 123    BR(1)=B(1)/BSAT(1)
        BRMIN=BR(1)
        DO 11 I=2,4
              BR(I)=B(I)/BSAT(I)
              IF (BR(I).EQ.0.) GO TO 11
              IF (BR(I).GE.BRMIN) GO TO 11
              BRMIN=BR(I)
 11     CONTINUE
        DO 12 I=1,4
              M(I)=2
              IF (BR(I).EQ.0.) M(I)=1
 12     CONTINUE
        IF (FLAG1.EQ.1) GO TO 124
        IF (M(2).EQ.2) GO TO 125
        IF (M(3).EQ.2) GO TO 126
        IF (M(4).EQ.1) GO TO 124
```

```
      BSAT(4)=0.458*(DM(4)/DM(1)-1.)**2/(DM(4)/DM(1))**3
      FLAG1=1
      GO TO 123
126   BSAT(3)=0.458*(DM(3)/DM(1)-1.)**2/(DM(3)/DM(1))**3
      IF (M(4).EQ.1) GO TO 127
      BSAT(4)=(0.458*(DM(4)/DM(3)-1.)**2/(DM(4)/DM(3))**3)*BSAT(3)
127   FLAG1=1
      GO TO 123
125   IF (M(3).EQ.2) GO TO 311
      IF (M(4).EQ.1) GO TO 124
      BSAT(4)=3.*0.458*(DM(4)/DM(2)-1.)**2/(DM(4)/DM(2))**3
      FLAG1=1
      GO TO 123
311   R=1.-W
      DR=DM(3)/DM(1)
      BSAT(3)=R*BSAT(3)+(1.-R)*0.458*(DR-1.)**2/DR**3
      BSAT(2)=R*BSAT(2)
      FLAG1=1
      IF (M(4).EQ.2) GO TO 312
      GO TO 123
312   DR=DM(4)/DM(3)
      BSAT(4)=R*BSAT(4)+(1.-R)*BSAT(3)*0.458*(DR-1.)**2/DR**3
      GO TO 123
124   XUT=0.
      DO 13 I=1,4
            IF (M(I).EQ.1) GO TO 13
            XU(I)=(BRMIN/DR(I))*XM(I)
            XUT=XUT+XU(I)
13    CONTINUE
      CALL SATE(ESAT,M,DM)
      ETEMP=ESAT
      M2T=M(2)
      M(2)=1
      CALL SATE(ESAT,M,DM)
      M(2)=M2T
      ESAT=R*ETEMP+(1.-R)*ESAT
C
C     CALCULATE POROSITY
C
      E=E+XUT*(1.-XUTT)*ESAT
      XUTT=XUTT+XUT*(1.-XUTT)
C
C     UPDATE VOLUME FRACTIONS
C
      SUMX=0.
      DO 14 J=1,K
            IF (D(J).LT.D12) GO TO 181
            X(J)=X(J)-XU(1)*X(J)/XM(1)
            SUMX=SUMX+X(J)
            GO TO 184
181         IF (D(J).LT.D23) GO TO 182
            IF (M(2).EQ.1) GO TO 182
            X(J)=X(J)-XU(2)*X(J)/XM(2)
            SUMX=SUMX+X(J)
            GO TO 184
182         IF (D(J).LT.D34) GO TO 183
            IF (M(3).EQ.1) GO TO 183
            X(J)=X(J)-XU(3)*X(J)/XM(3)
```

```
            SUMX=SUMX+X(J)
            GO TO 184
 183        IF (M(4).EQ.1) GO TO 184
            X(J)=X(J)-XU(4)*X(J)/XM(4)
            SUMX=SUMX+X(J)
 184        IF (X(J).GT.0.001) GO TO 14
            XUTT=XUTT+X(J)
            X(J)=0.
 14     CONTINUE
        DO 15 J=1,N
            X(J)=X(J)/SUMX
 15     CONTINUE
        IF (XUTT.GE.0.99) RETURN
        GO TO 250
        END
C
        SUBROUTINE SATE(ESAT,M,DM)
C
C       CALCULATE SATURATED POROSITY
C
        IMPLICIT REAL*8(A-H,O-Z)
        DIMENSION DM(4),M(4)
        J=M(2)
        K=M(3)
        L=M(4)
        GO TO (300,310), J
 300    GO TO (302,303), K
 302    GO TO (304,305), L
 304    ESAT=0.40
        RETURN
 305    ESAT=0.40-0.24*(DM(4)/DM(1)-1.)**2
        RETURN
 303    GO TO (306,307), L
 306    ESAT=0.40-0.24*(DM(3)/DM(1)-1.)**2
        RETURN
 307    ESAT=2.5*(0.4-0.24*(DM(3)/DM(1)-1.)**2)
        ESAT=ESAT*(0.4-0.24*(DM(4)/DM(3)-1.)**2)
        RETURN
 310    GO TO (312,313), K
 312    GO TO (314,315), L
 314    ESAT=0.4-0.24*(DM(2)/DM(1)-1.)**2
        RETURN
 315    ESAT=0.4-0.24*(DM(2)/DM(1)-1.)**2
        ESAT=ESAT-0.719*(DM(4)/DM(2)-1.)**2*(DM(2)/DM(1))**3
        RETURN
 313    GO TO (316,317), L
 316    ESAT= 0.4-0.24*(DM(2)/DM(1)-1.)**2-1.57*(DM(3)/DM(1))**3
        RETURN
 317    ESAT=0.4-0.24*(DM(2)/DM(1)-1.)**2-1.57*(DM(3)/DM(1))**3
        ESAT=ESAT-6.28*(DM(4)/DM(1))**3
        RETURN
        END
*RUN
```

APPENDIX F: Plots of Void Fraction and Pressure Drop Data at and before Flooding

In this section, plots of all the counter-current void fraction and pressure drop data obtained in this study are given. Plots of active void fraction, total pressure gradient, and frictional pressure gradient are given in Figures F.1 through F.15 for beds formed of uniform size particles and in Figures F.16 through F.33 for beds formed of mixtures of various size particles. All data is plotted as a function of the superficial velocity of gas at and before the flooding limit. Different curves are drawn in the plots of total and frictional pressure gradients for various values of the liquid superficial velocity. A common key, given in the following page, is used for all plots. In this key, different symbols are used for different values of the liquid superficial velocity.

Key for Figures F.1 through F.33:

j_ℓ (mm/s)
0.0
1.95
3.89
5.84
7.78
9.73
11.67
13.62
15.56
17.51
19.46

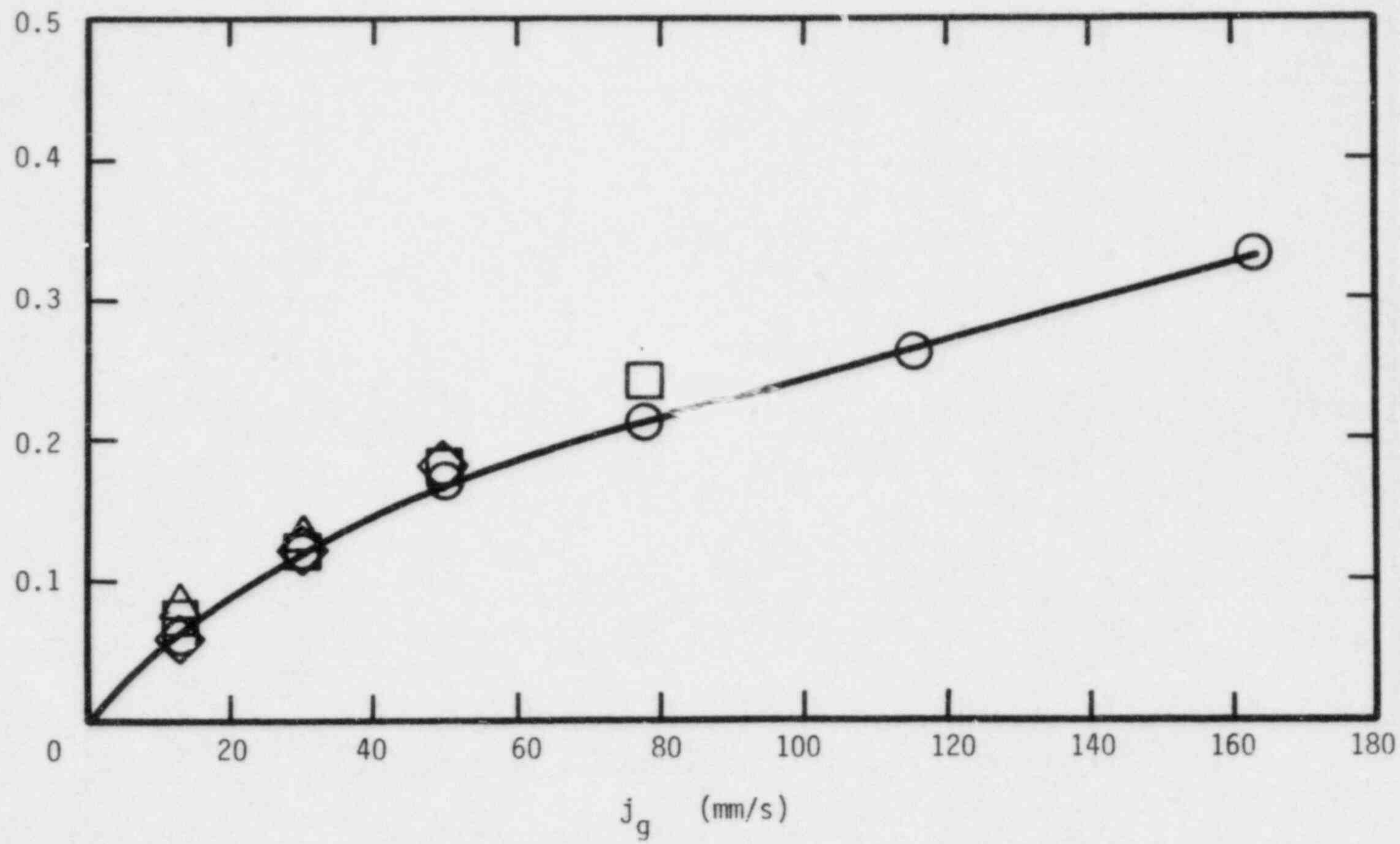

Figure F.1 Active Void Fractions for Beds Composed of 3 mm Nominal Diameter Particles

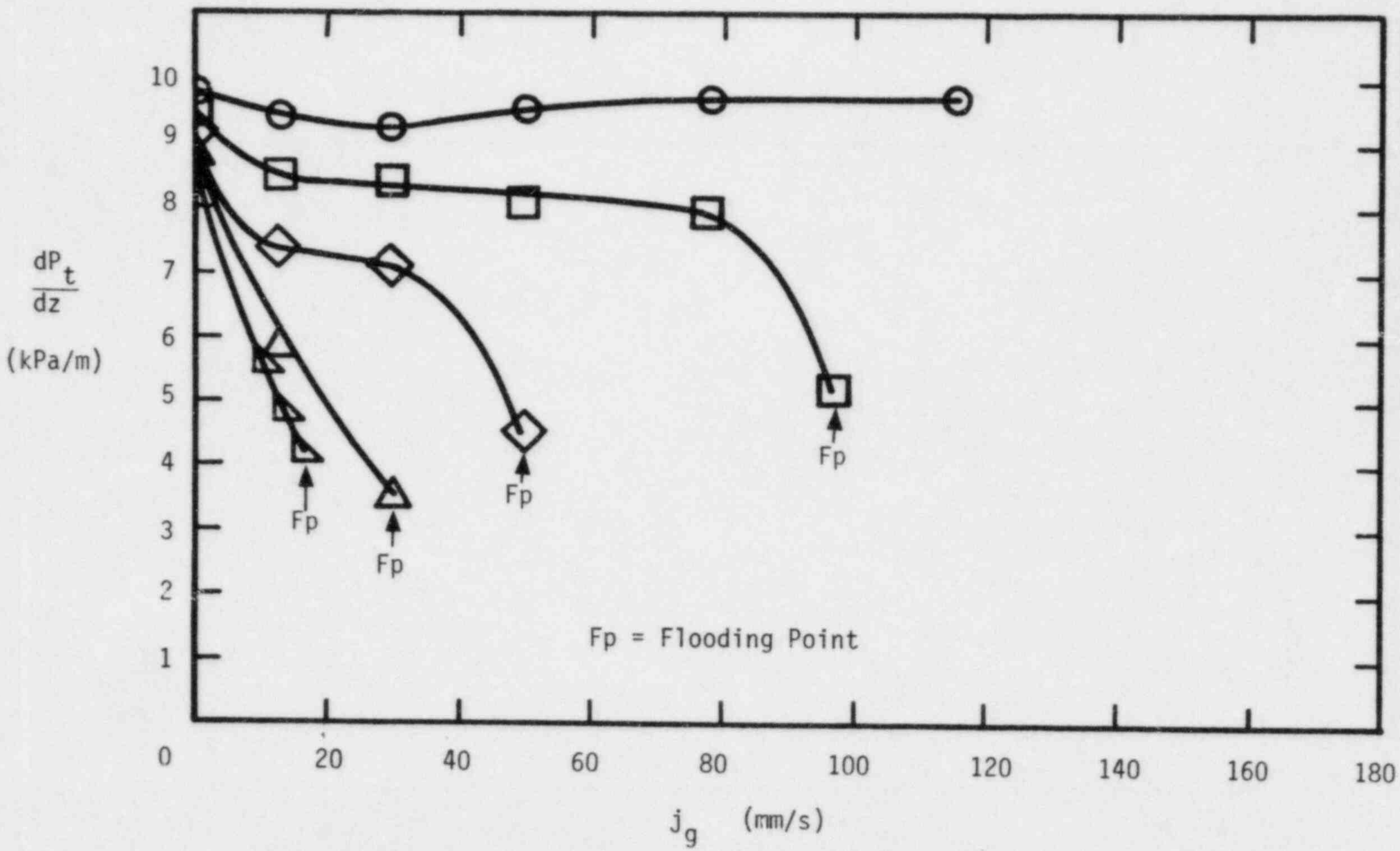

Figure F.2 Total Pressure Gradients for Beds Composed of 3 mm Nominal Diameter Particles

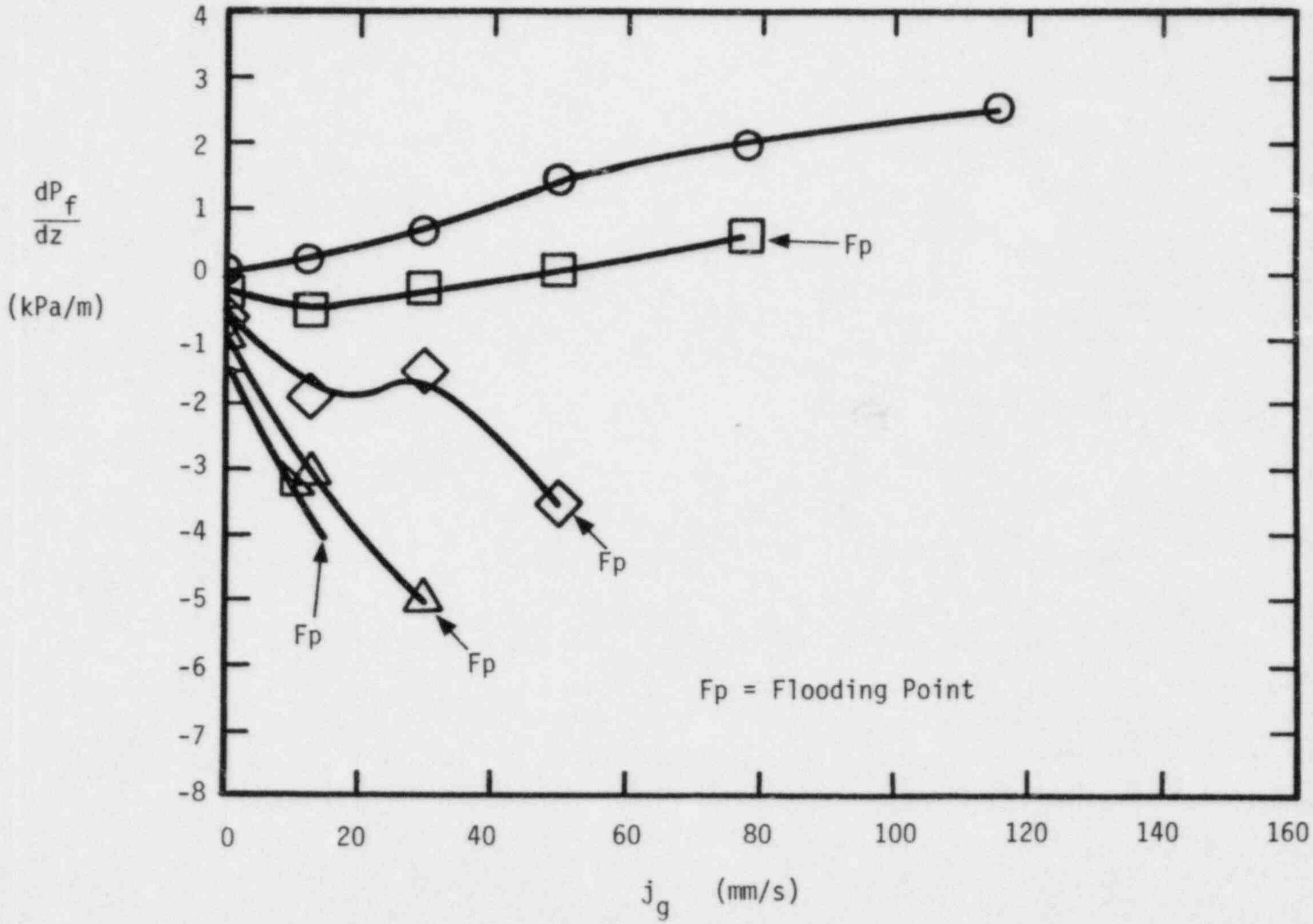

Figure F.3 Frictional Pressure Gradients for Beds Composed of 3 mm Nominal Diameter Particles

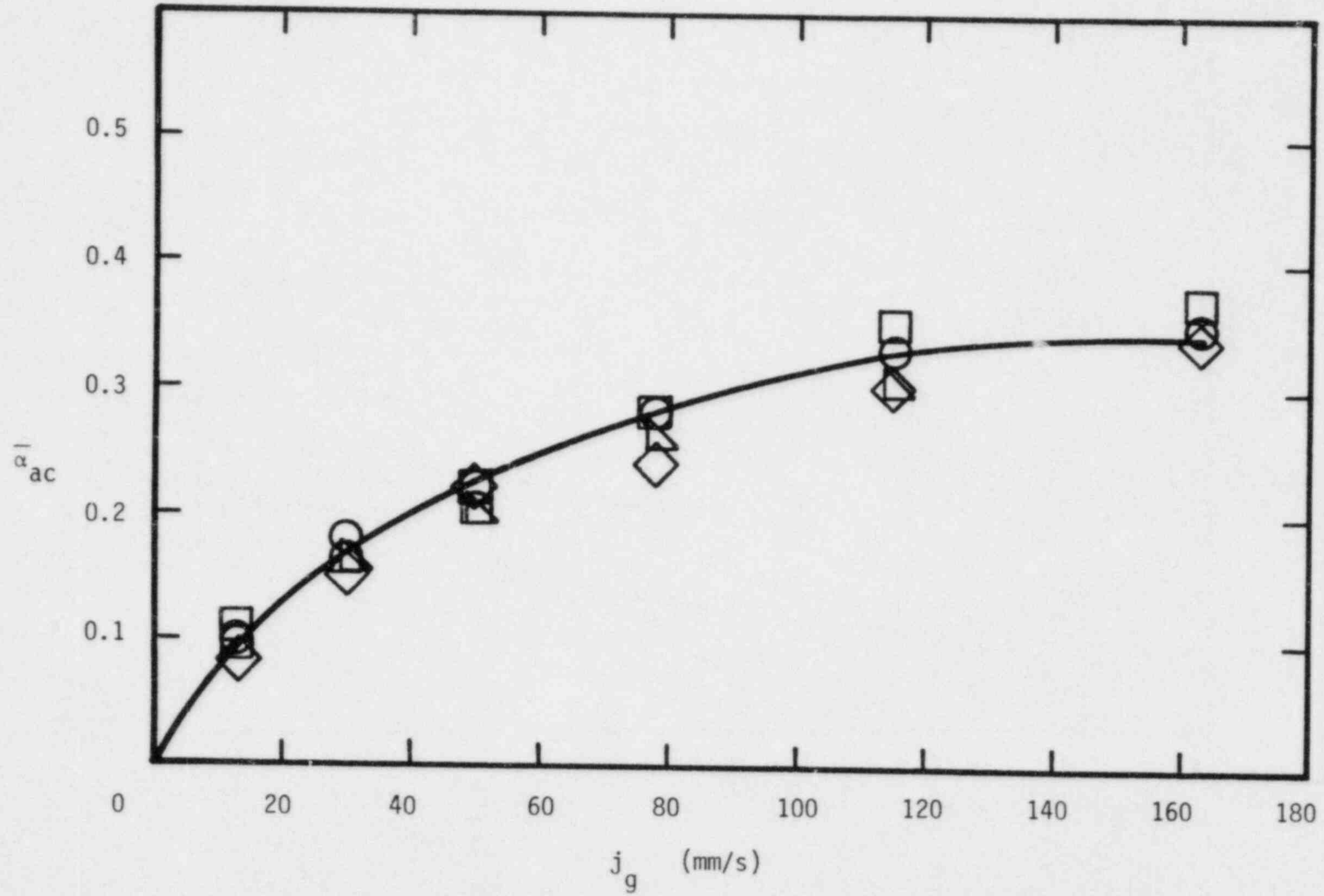

Figure F.4 Active Void Fractions for Beds Composed of 6 mm Nominal Diameter Particles

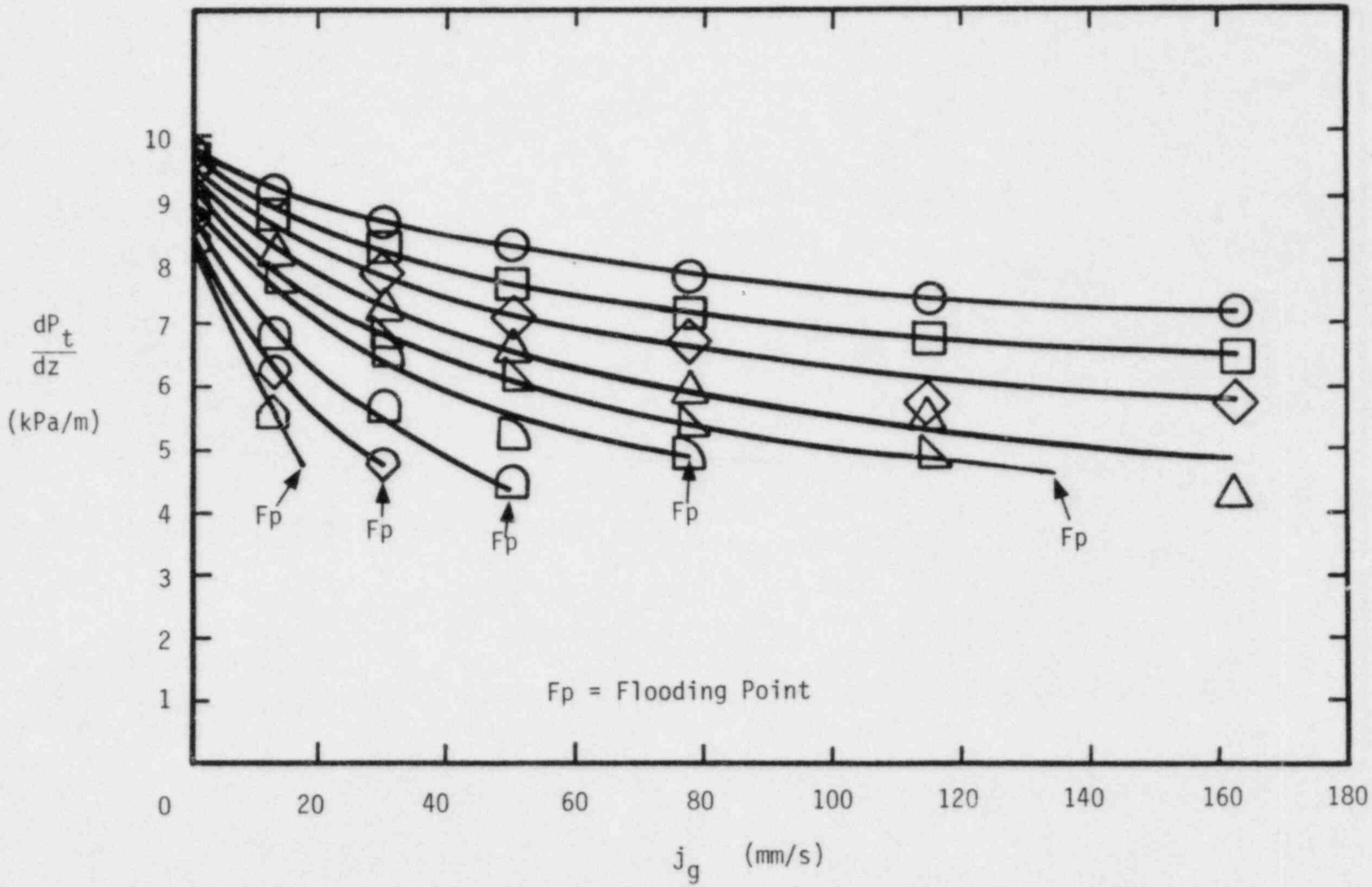

Figure F.5 Total Pressure Gradients for Beds Composed of 6 mm Nominal Diameter Particles

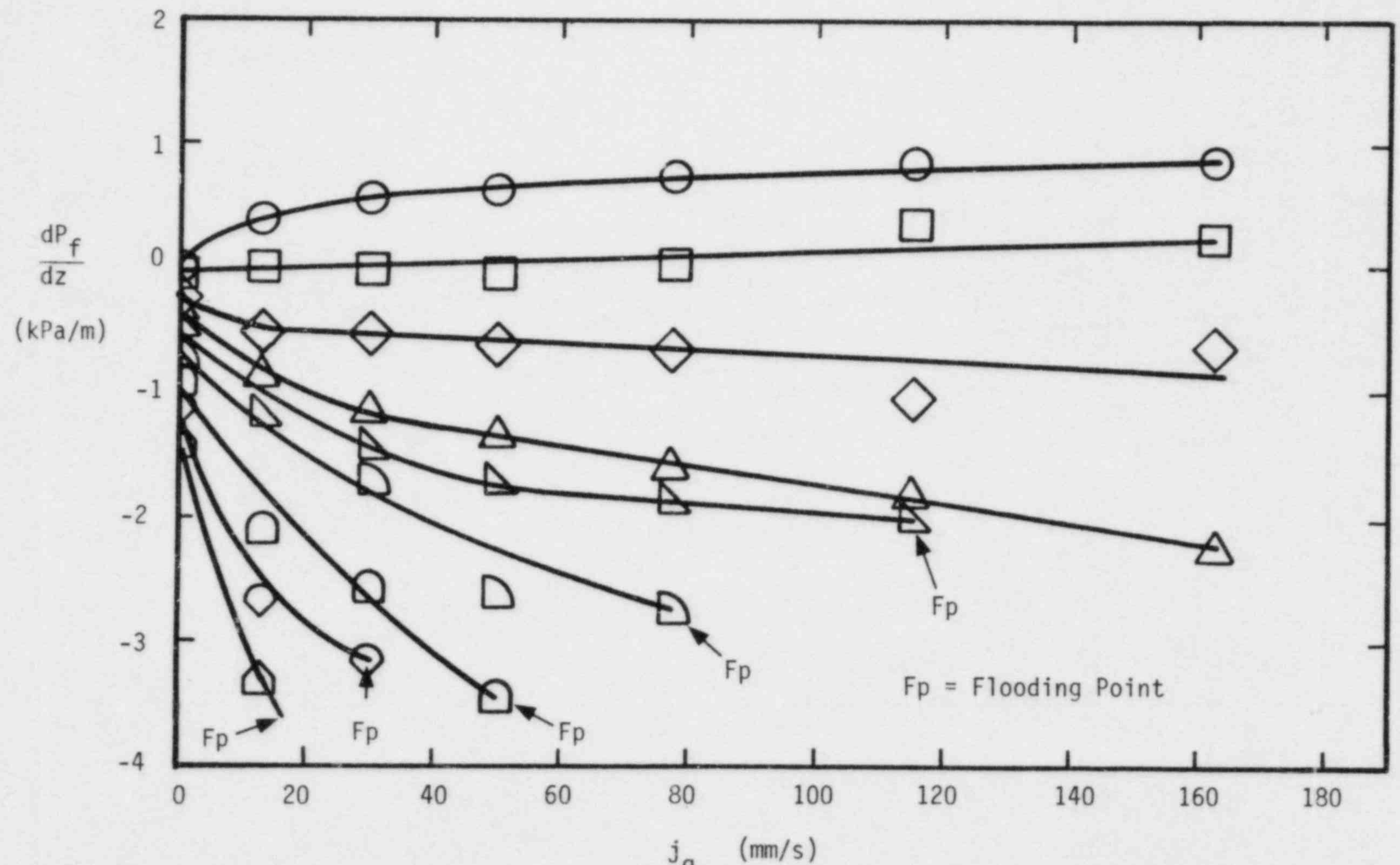

Figure F.6 Frictional Pressure Gradients for Beds Composed of 6 mm Nominal Diameter Particles

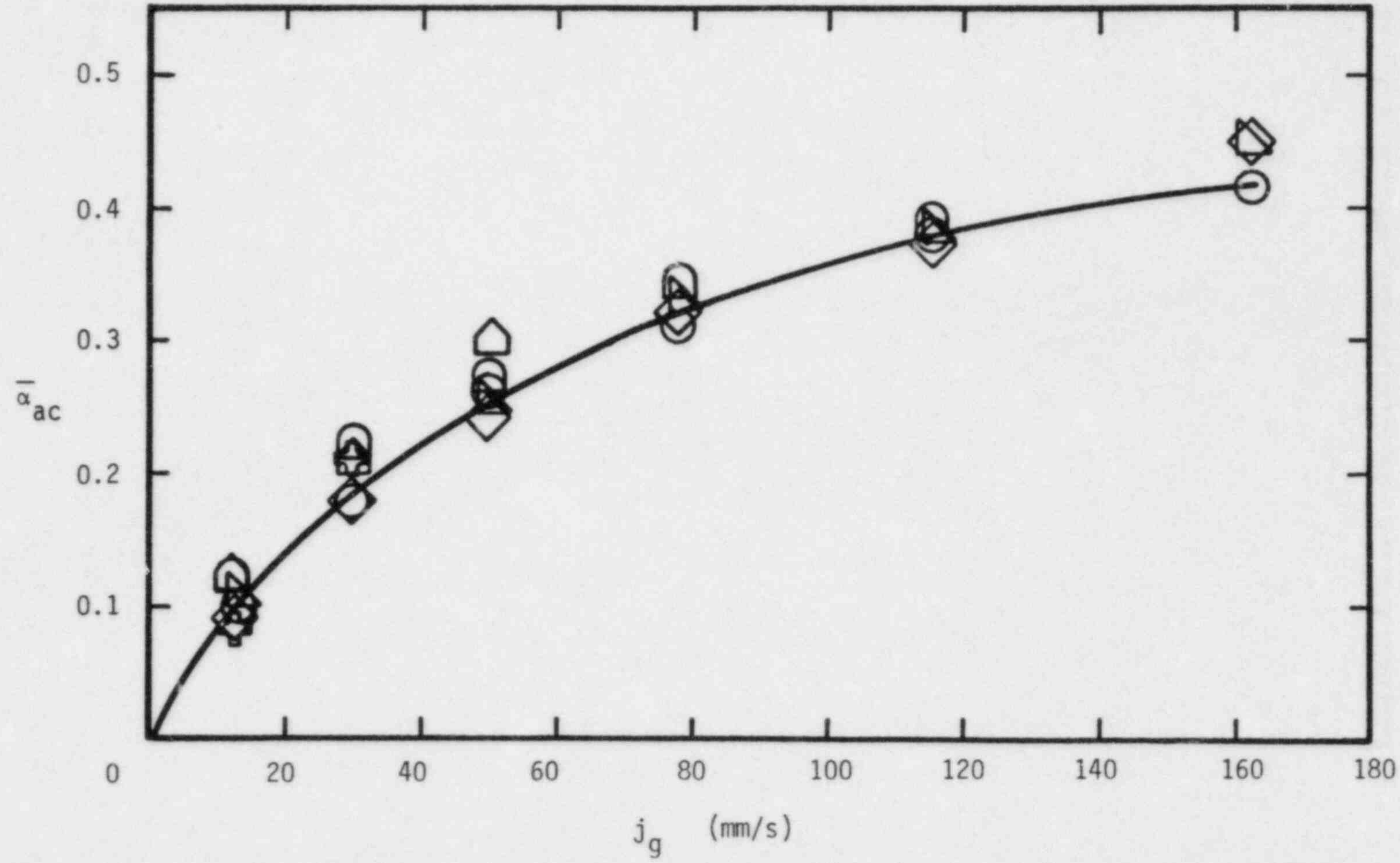

Figure F.7 Active Void Fractions for Beds Composed of 10 mm Nominal Diameter Particles

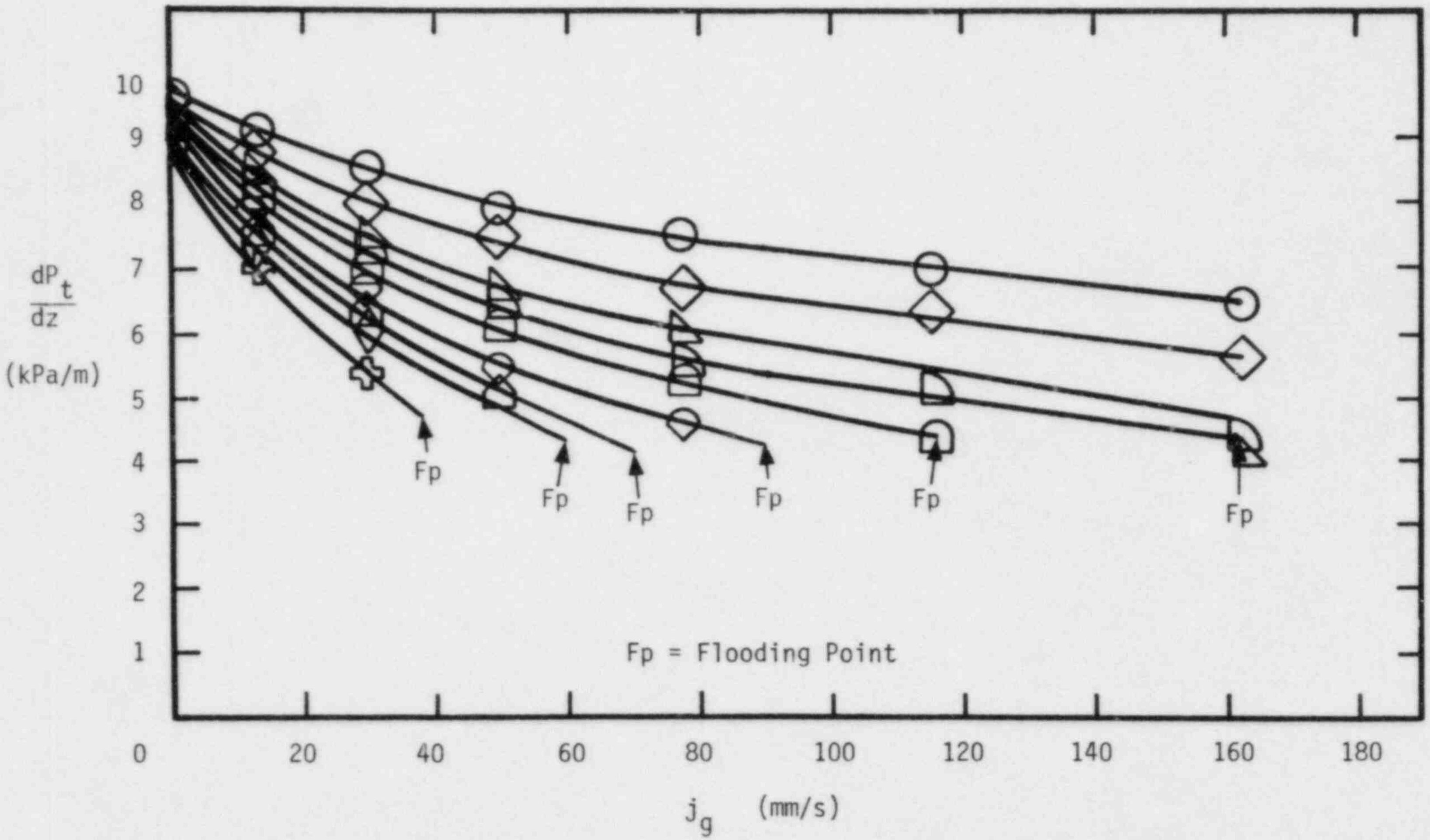

Figure F.8 Total Pressure Gradients for Beds Composed of 10 mm Nominal Diameter Particles

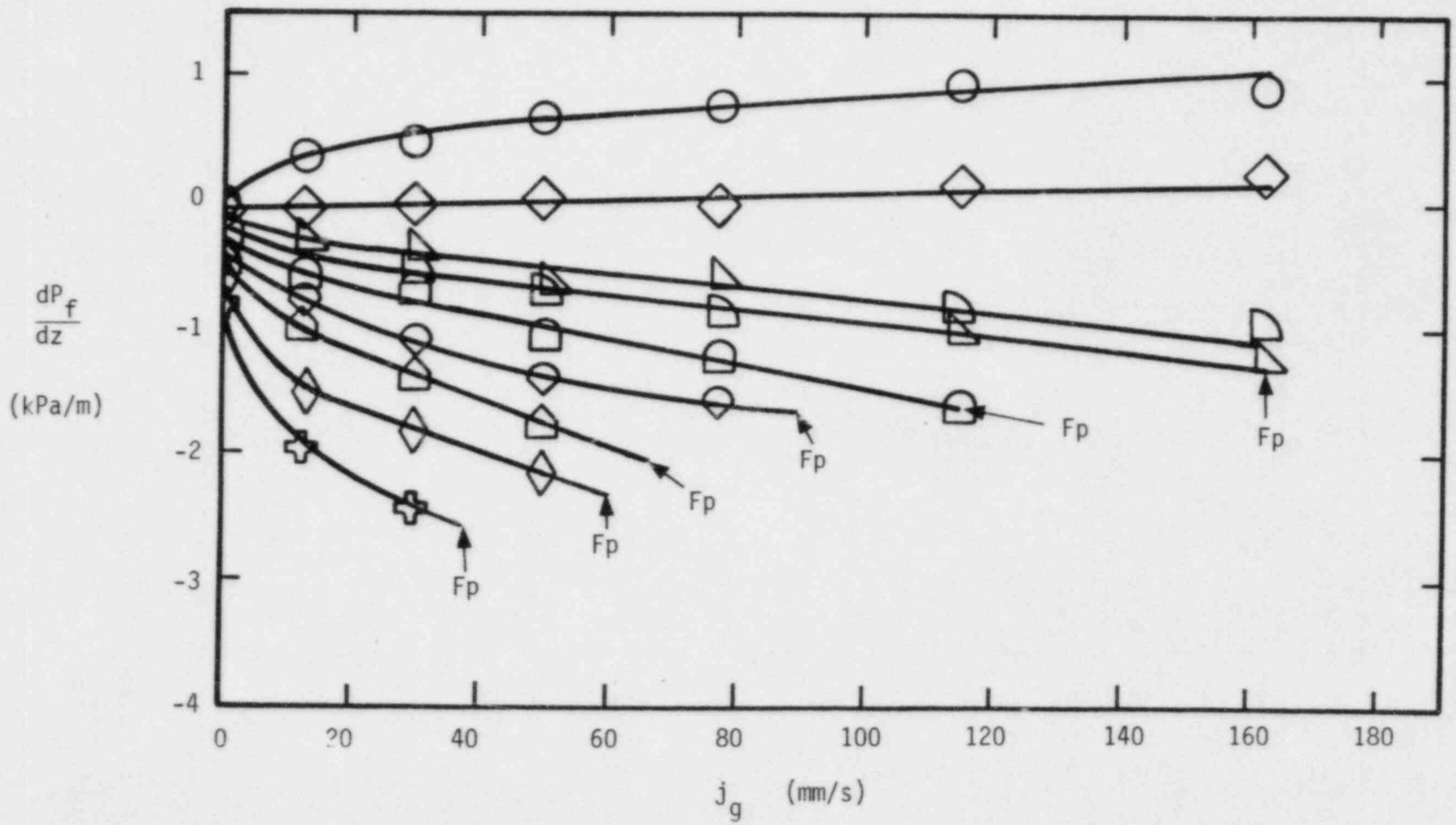

Figure F.9 Frictional Pressure Gradients for Beds Composed of 10 mm Nominal Diameter Particles

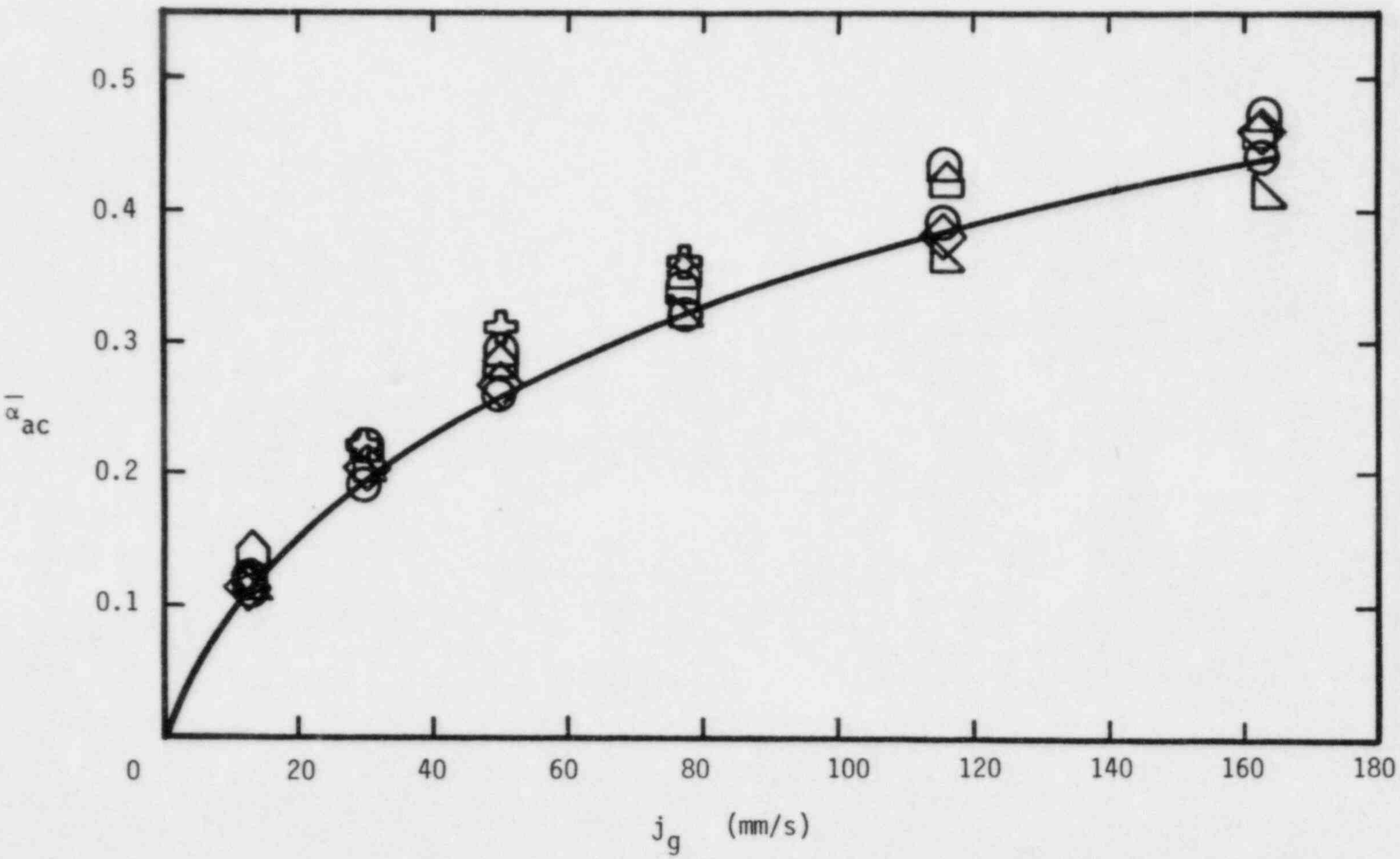

Figure F.10 Active Void Fractions for Beds Composed of 15 mm Nominal Diameter Particles

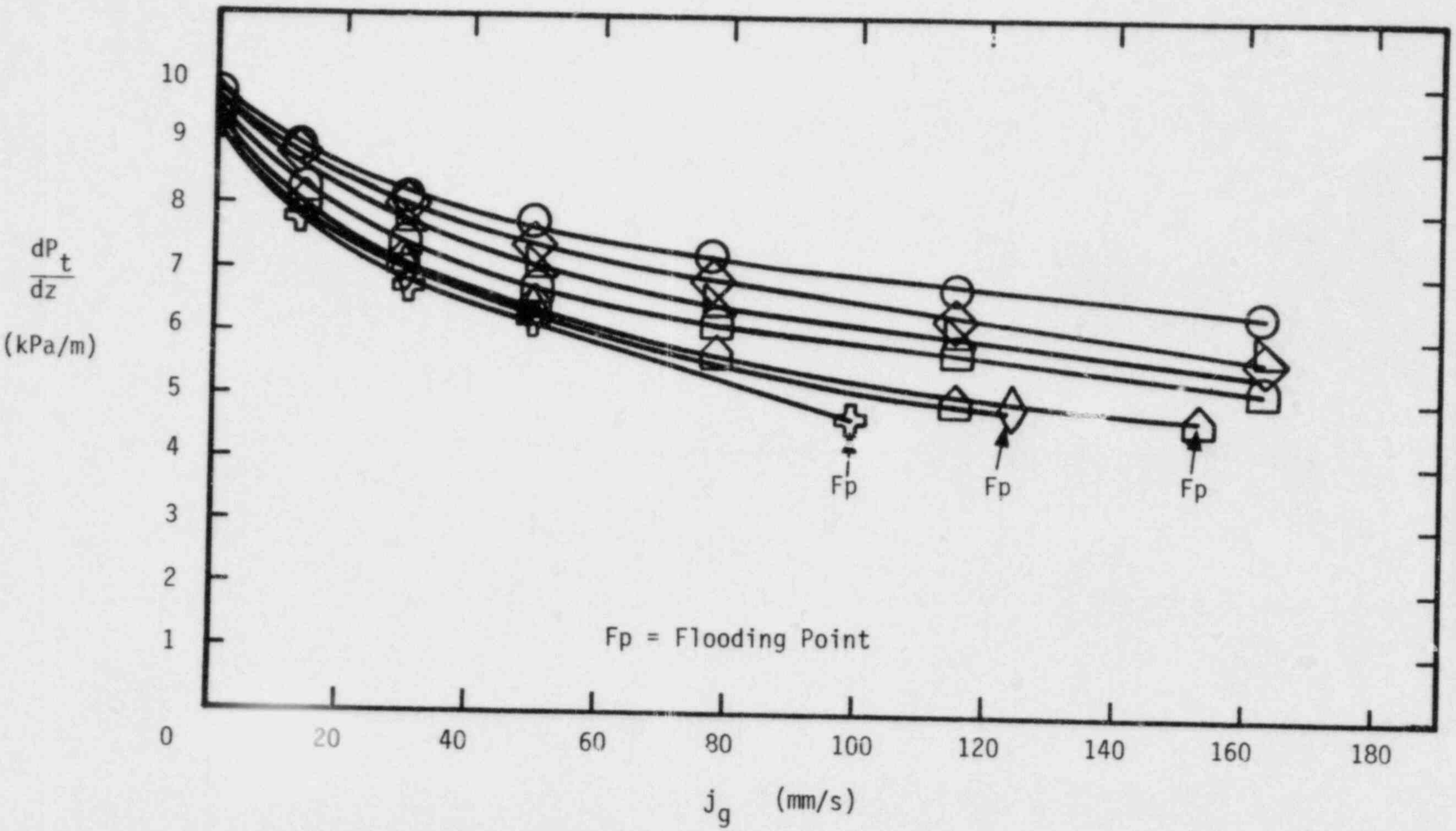

Figure F.11 Total Pressure Gradients for Beds Composed of 15 mm Nominal Diameter Particles

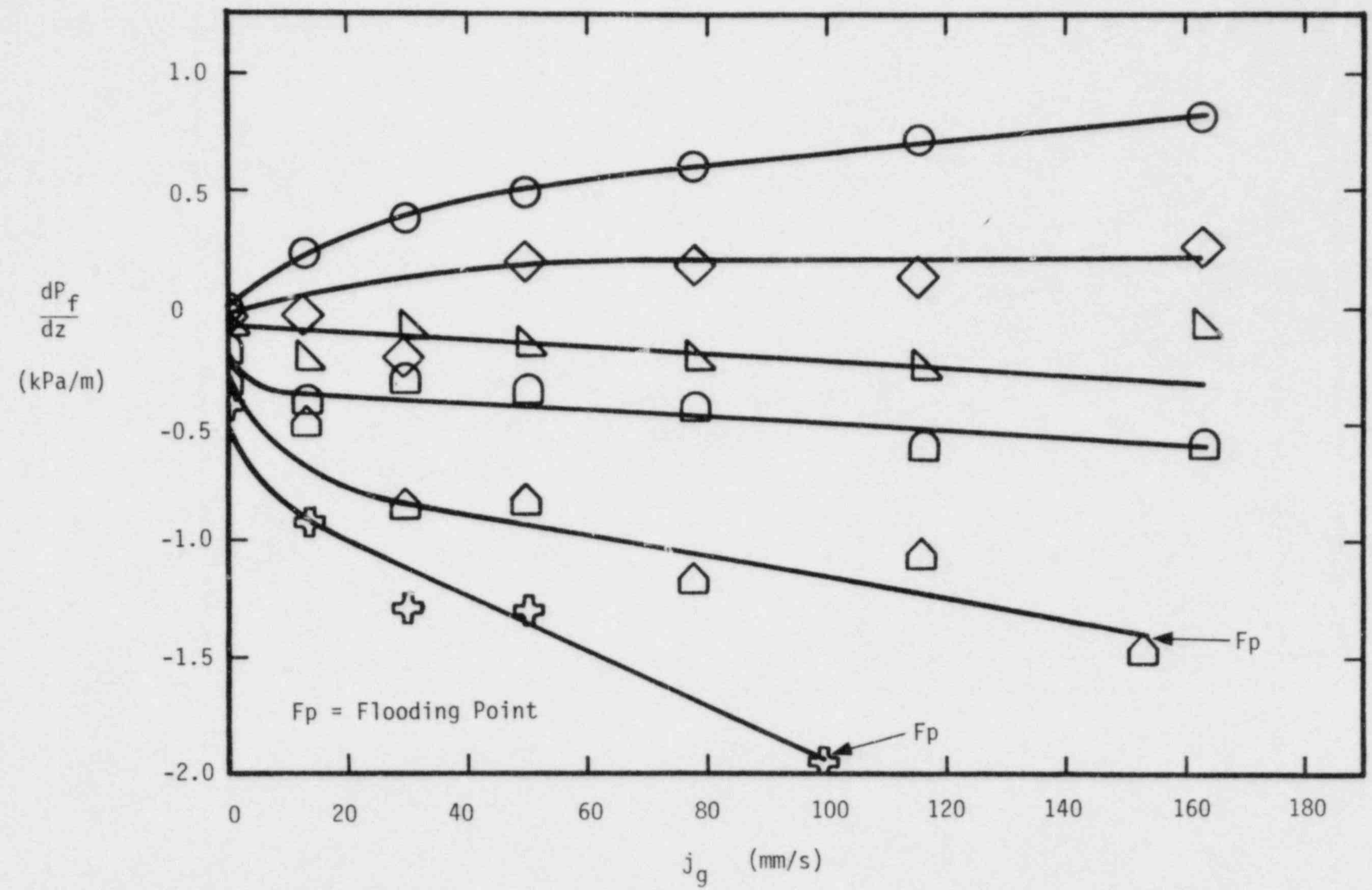

Figure F.12 Frictional Pressure Gradients for Beds Composed of 15 mm Nominal Diameter Particles

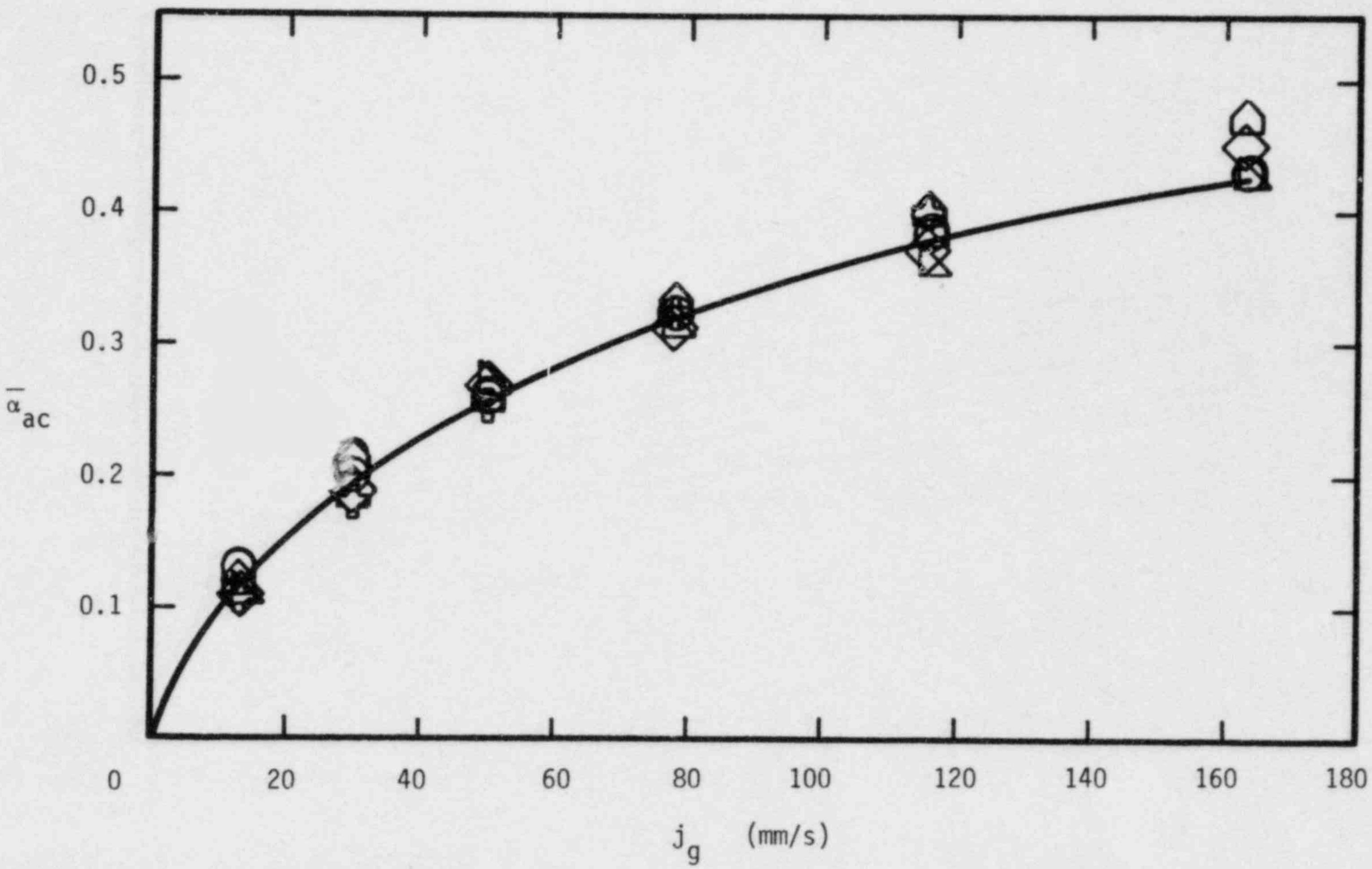

Figure F.13 Active Void Fractions for Beds Composed of 19 mm Nominal Diameter Particles

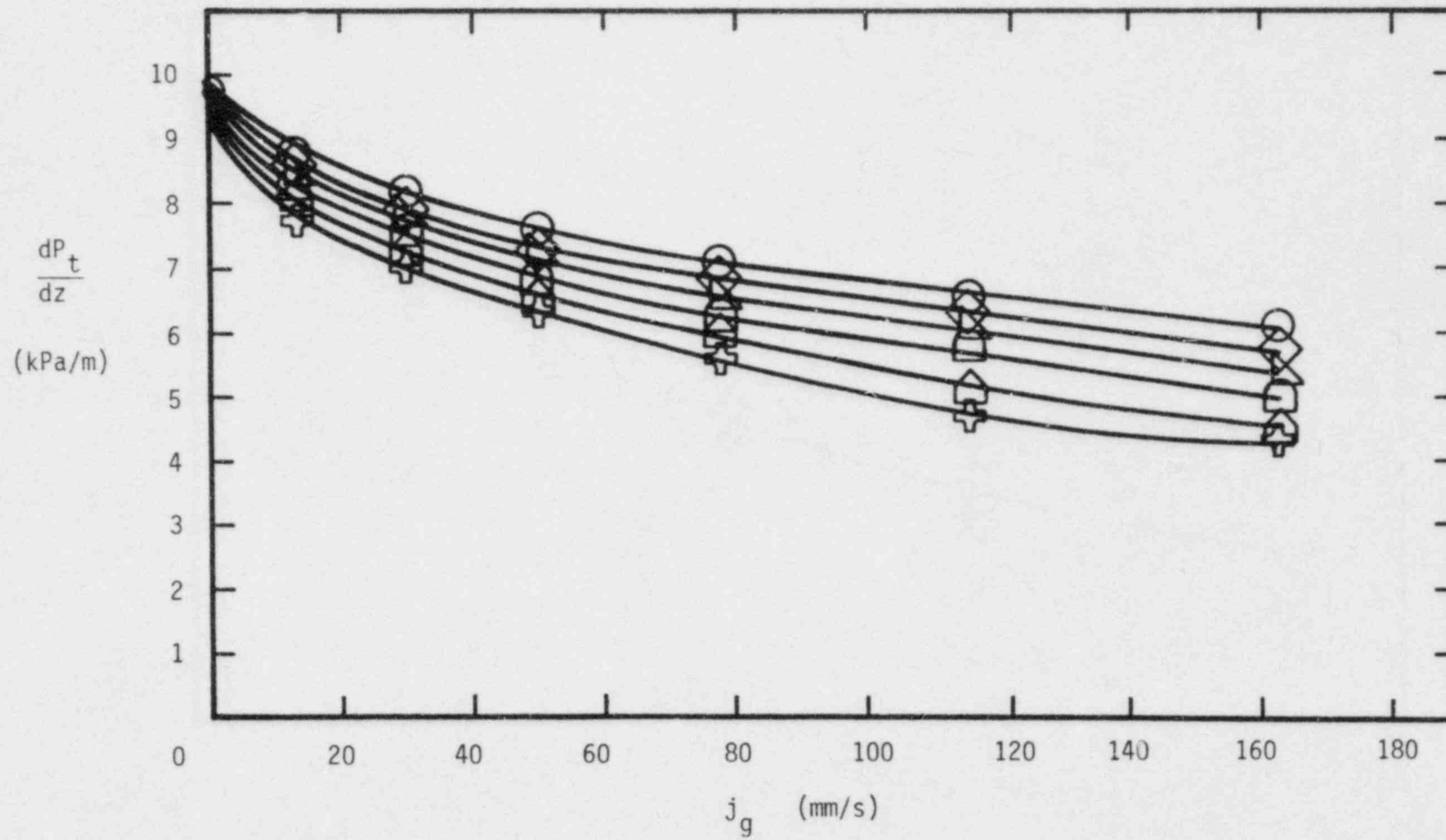

Figure F.14 Total Pressure Gradients for Beds Composed of 19 mm Nominal Diameter Particles

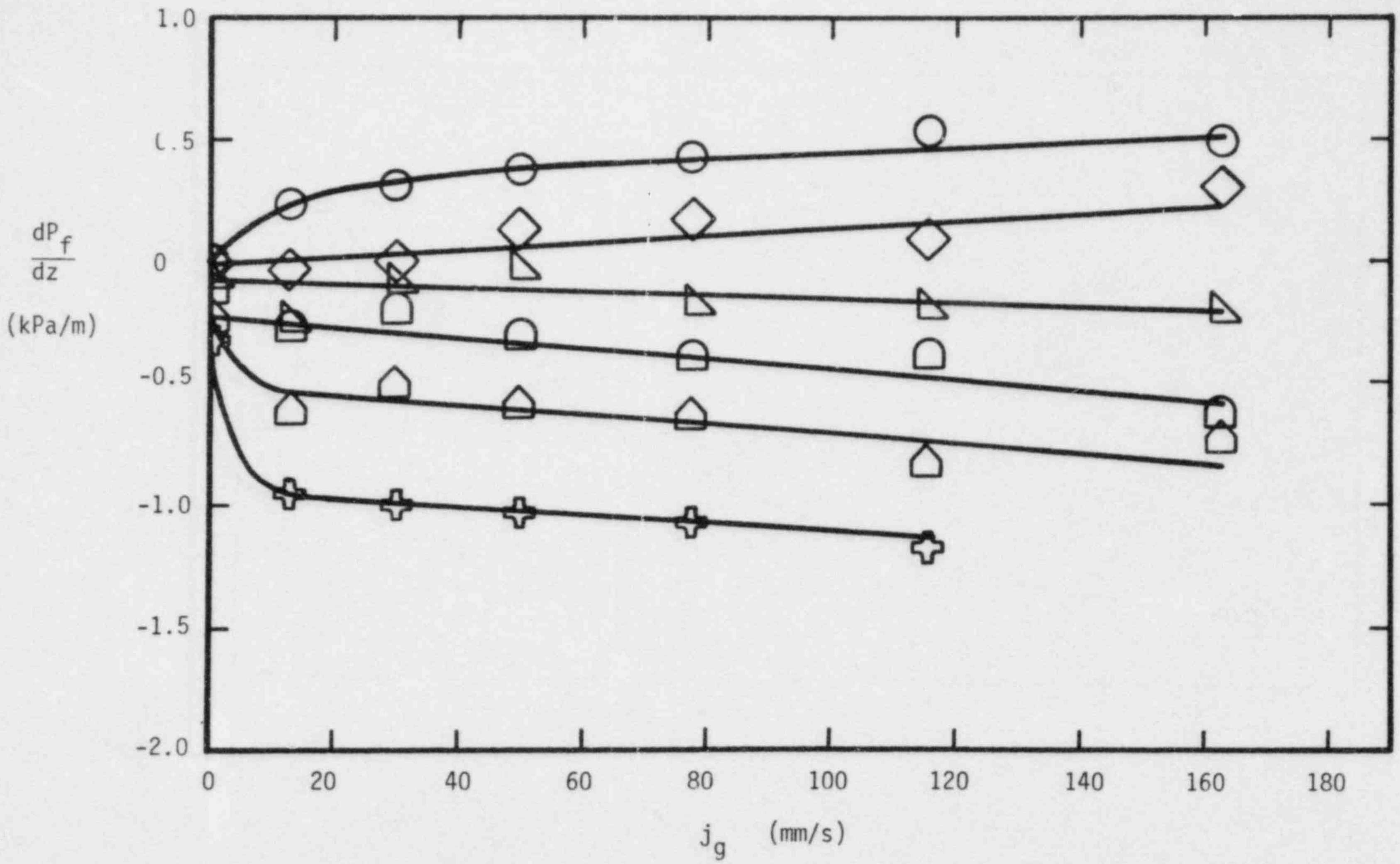

Figure F.15 Frictional Pressure Gradients for Beds Composed of 19 mm Nominal Diameter Particles

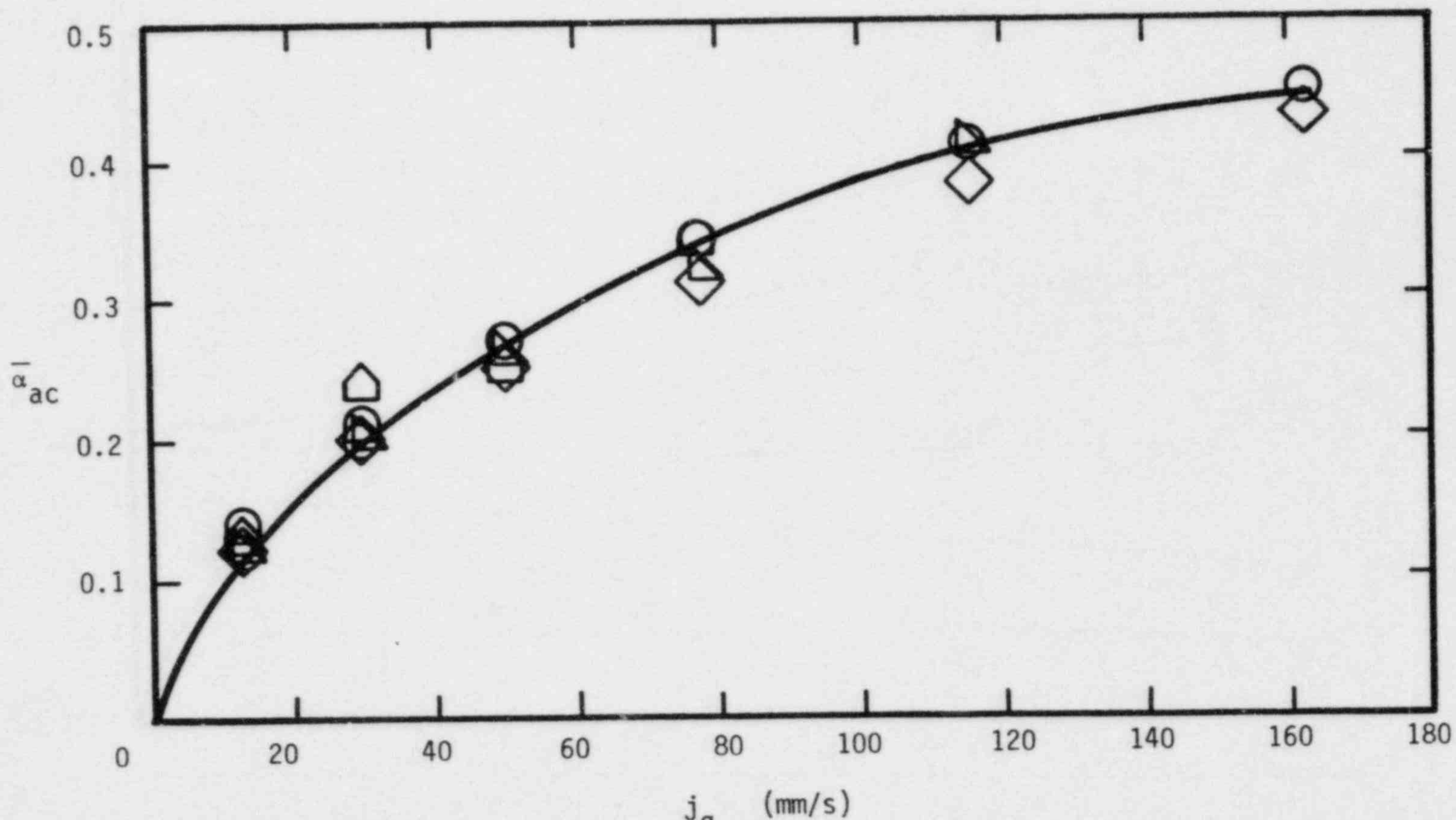

Figure F.16 Active Void Fractions for Mixtures of 10 mm and 6 mm Nominal Diameter Particles

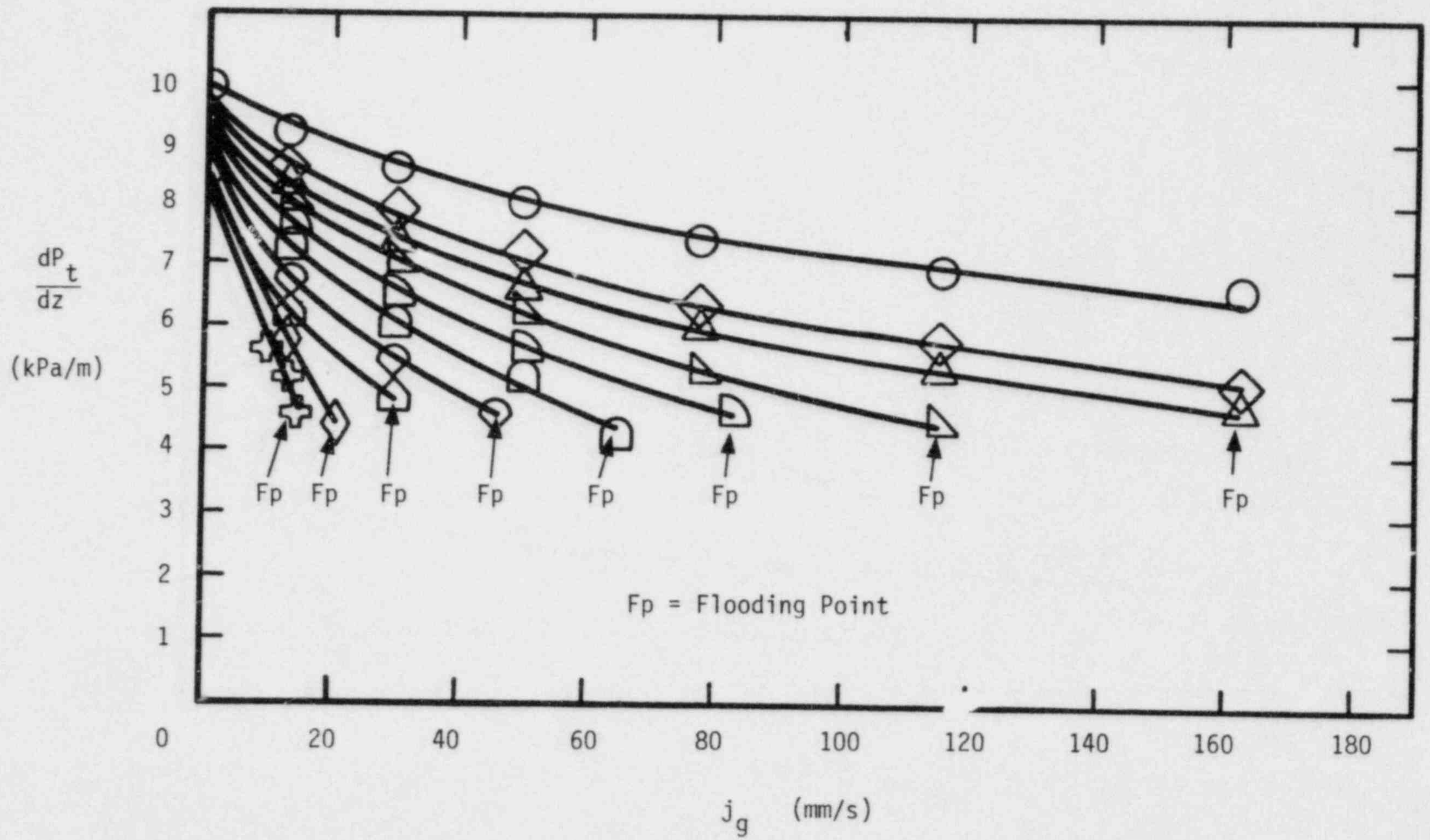

Figure F.17 Total Pressure Gradients for Mixture of 10 mm and 6 mm Nominal Diameter Particles

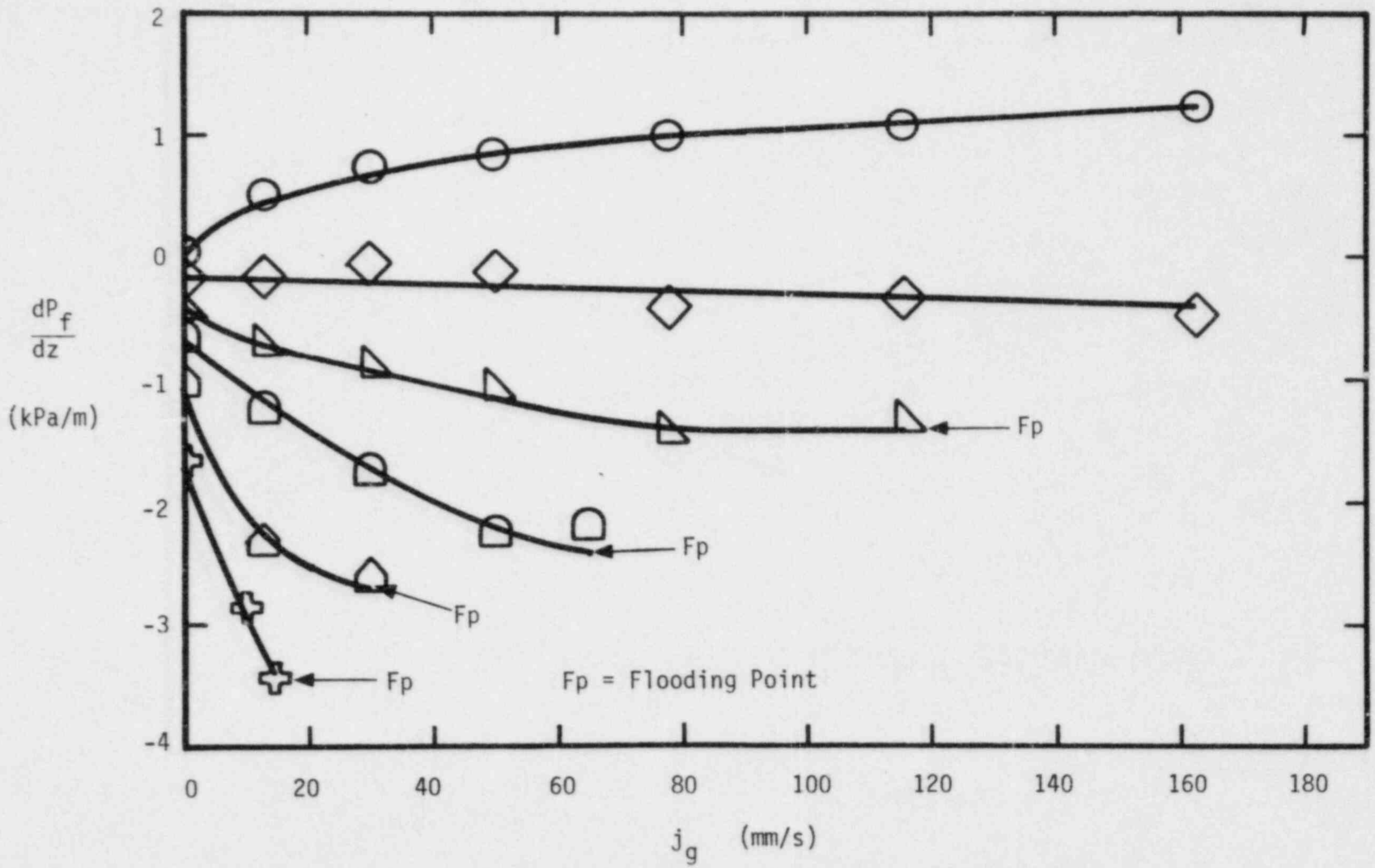

Figure F.18 Frictional Pressure Gradients for Mixture of 10 mm and 6 mm Nominal Diameter Particles

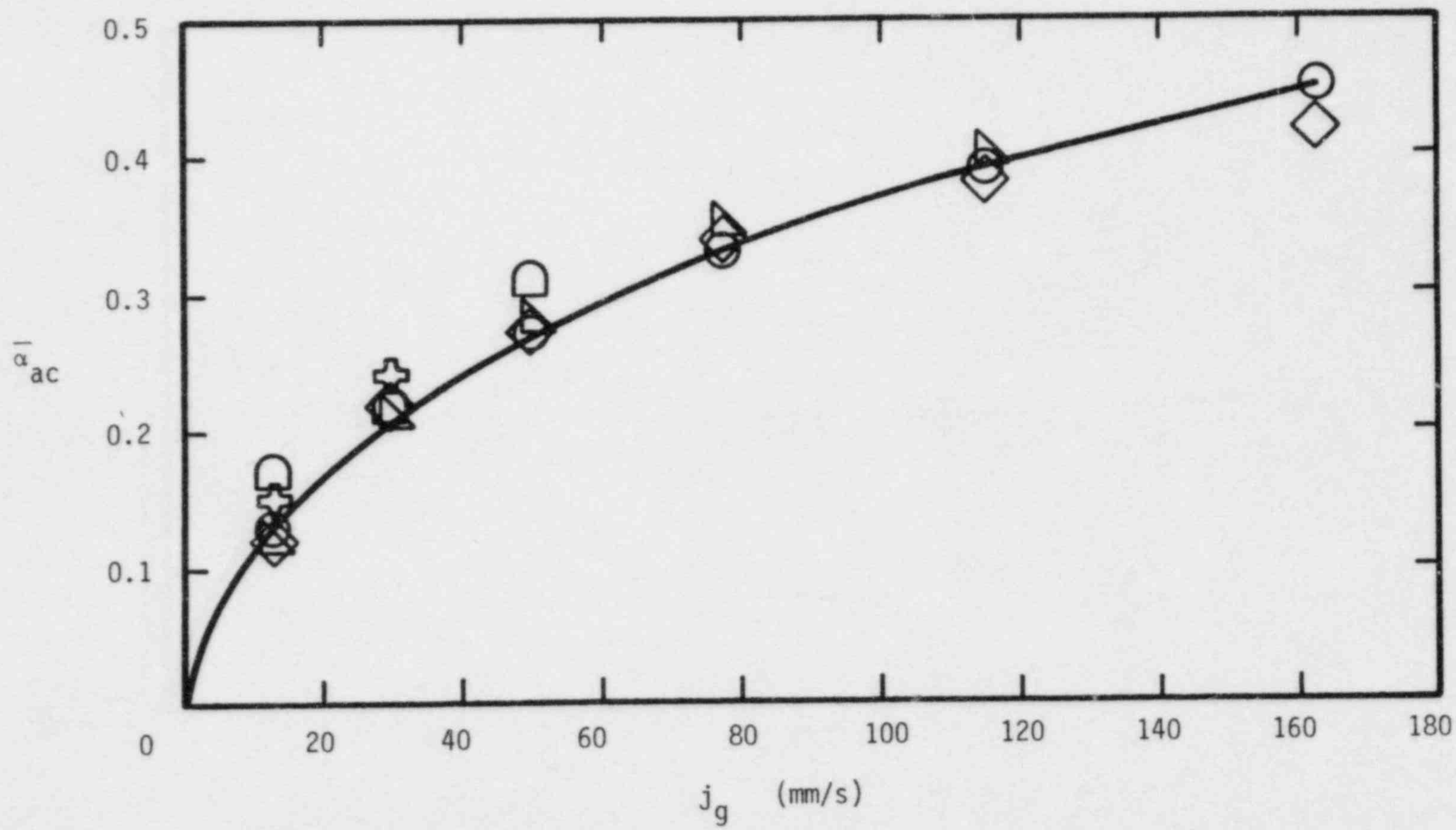

Figure F.19 Active Void Fractions for Mixture of 15 mm and 6 mm Nominal Diameter Particles

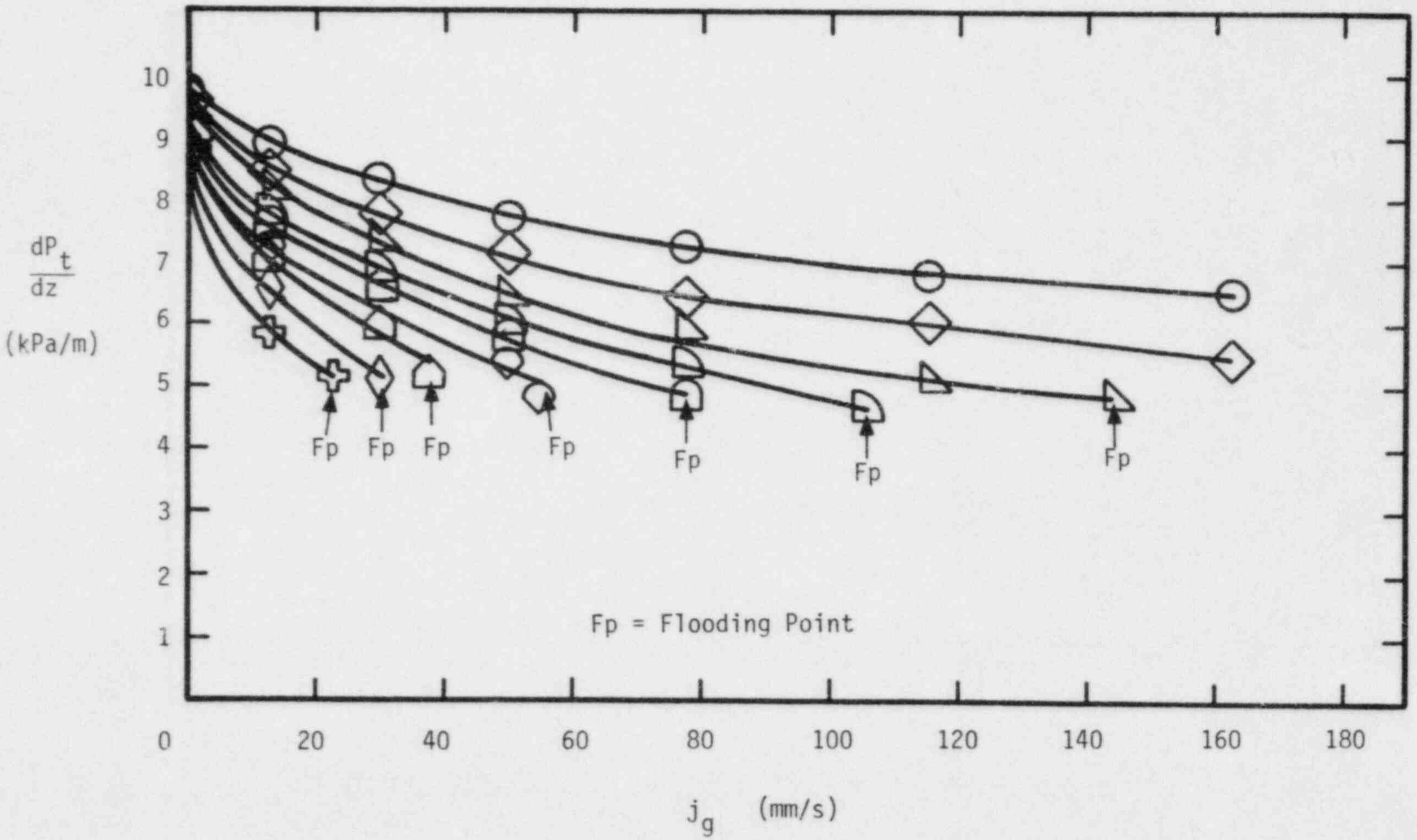

Figure F.20 Total Pressure Gradients for Mixture of 15 mm and 6 mm Nominal Diameter Particles

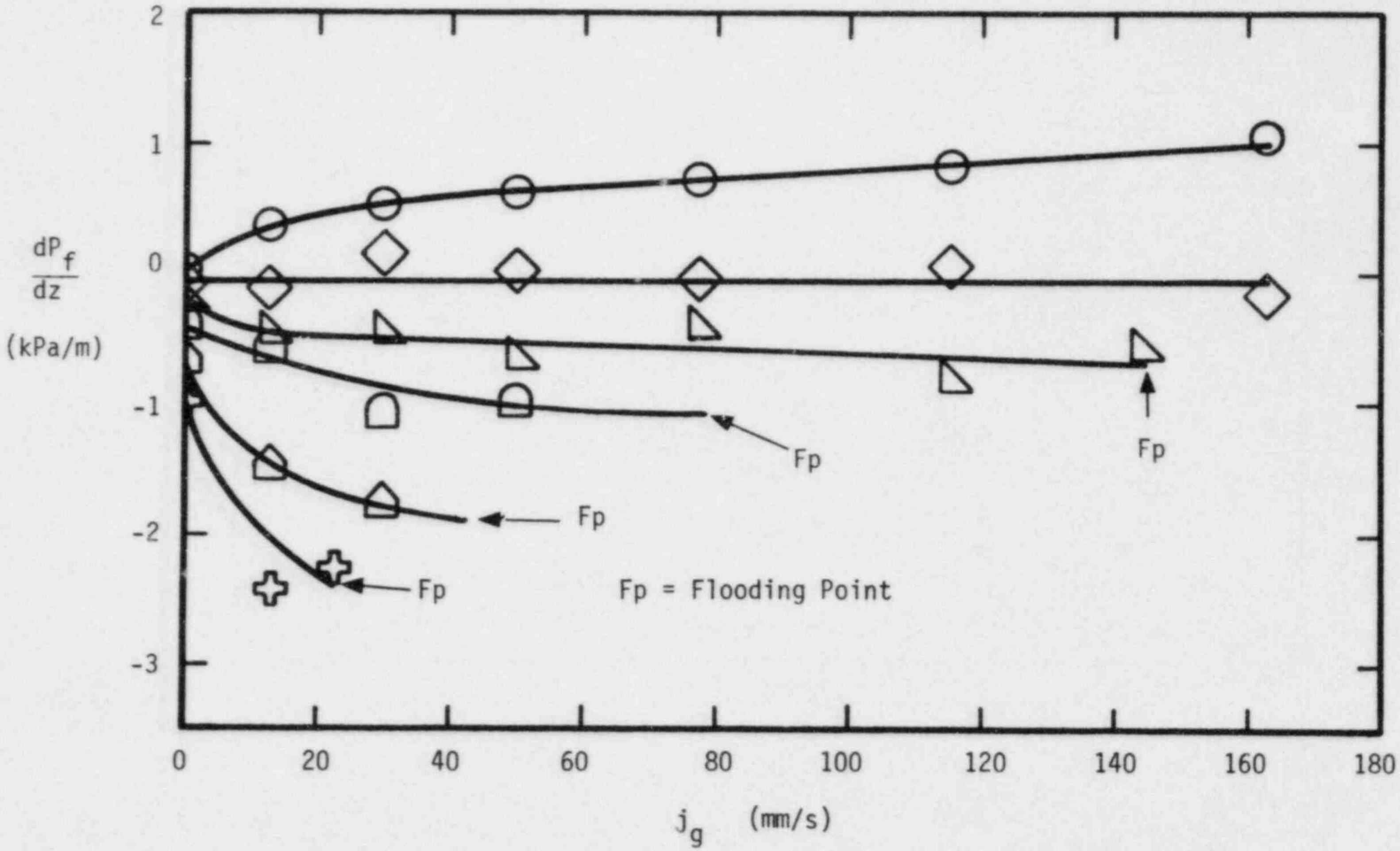

Figure F.21 Frictional Pressure Gradients for Mixture of 15 mm and 6 mm Nominal Diameter Particles

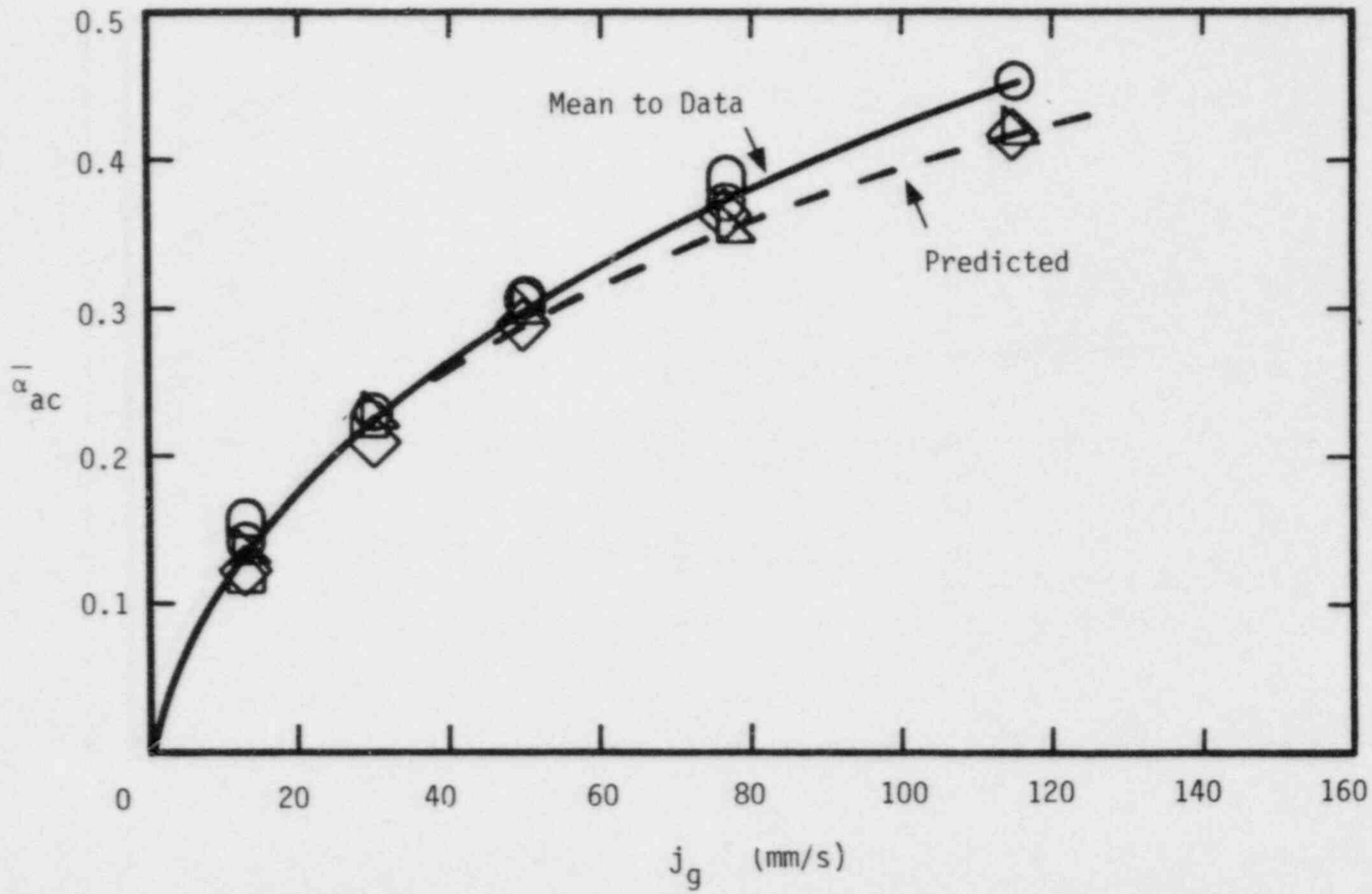

Figure F.22 Active Void Fractions for Mixture of 6,10,15,19 mm Nominal Diameter Particles

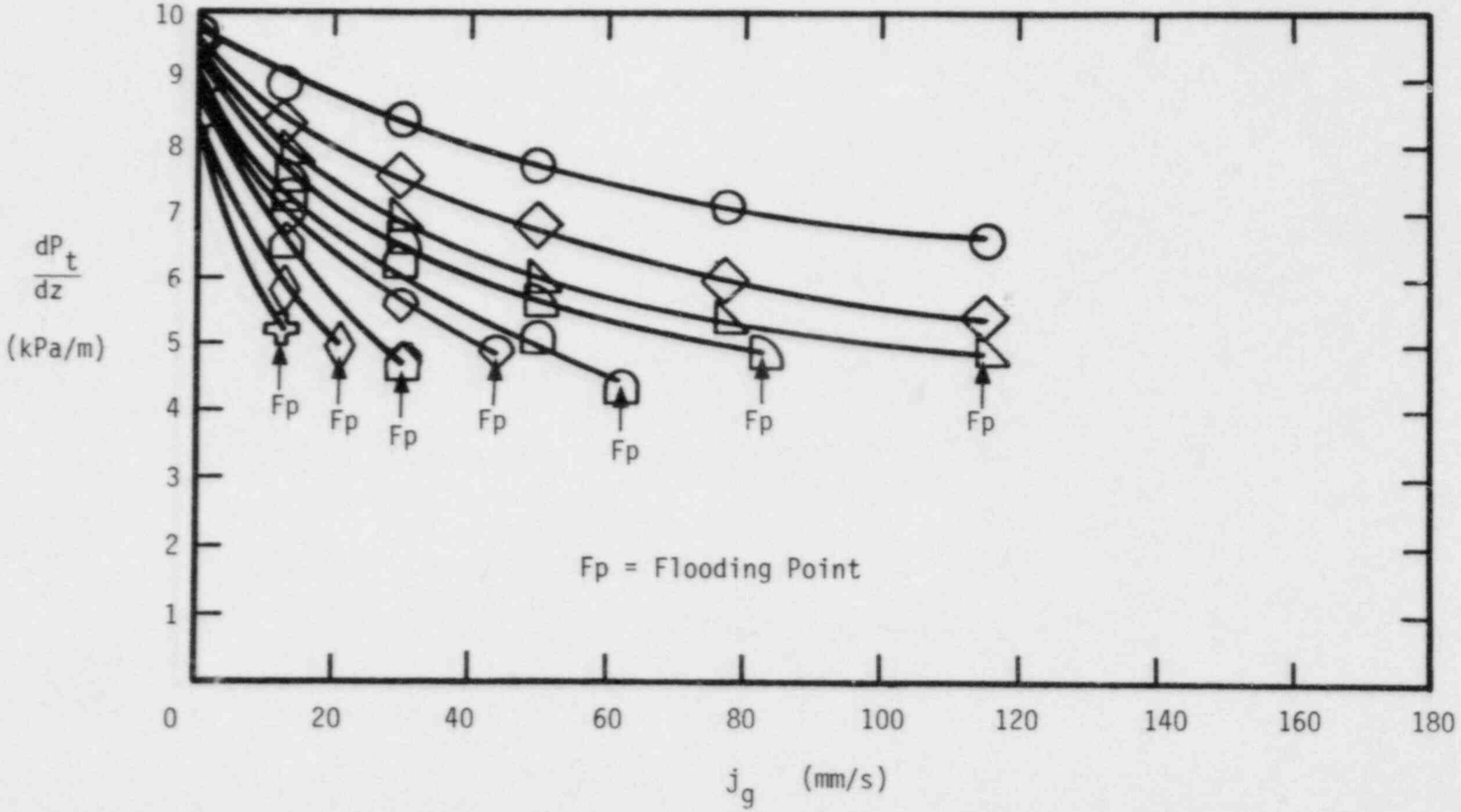

Figure F.23 Total Pressure Gradients for Mixture of 6,10,15,19 mm Nominal Diameter Particles

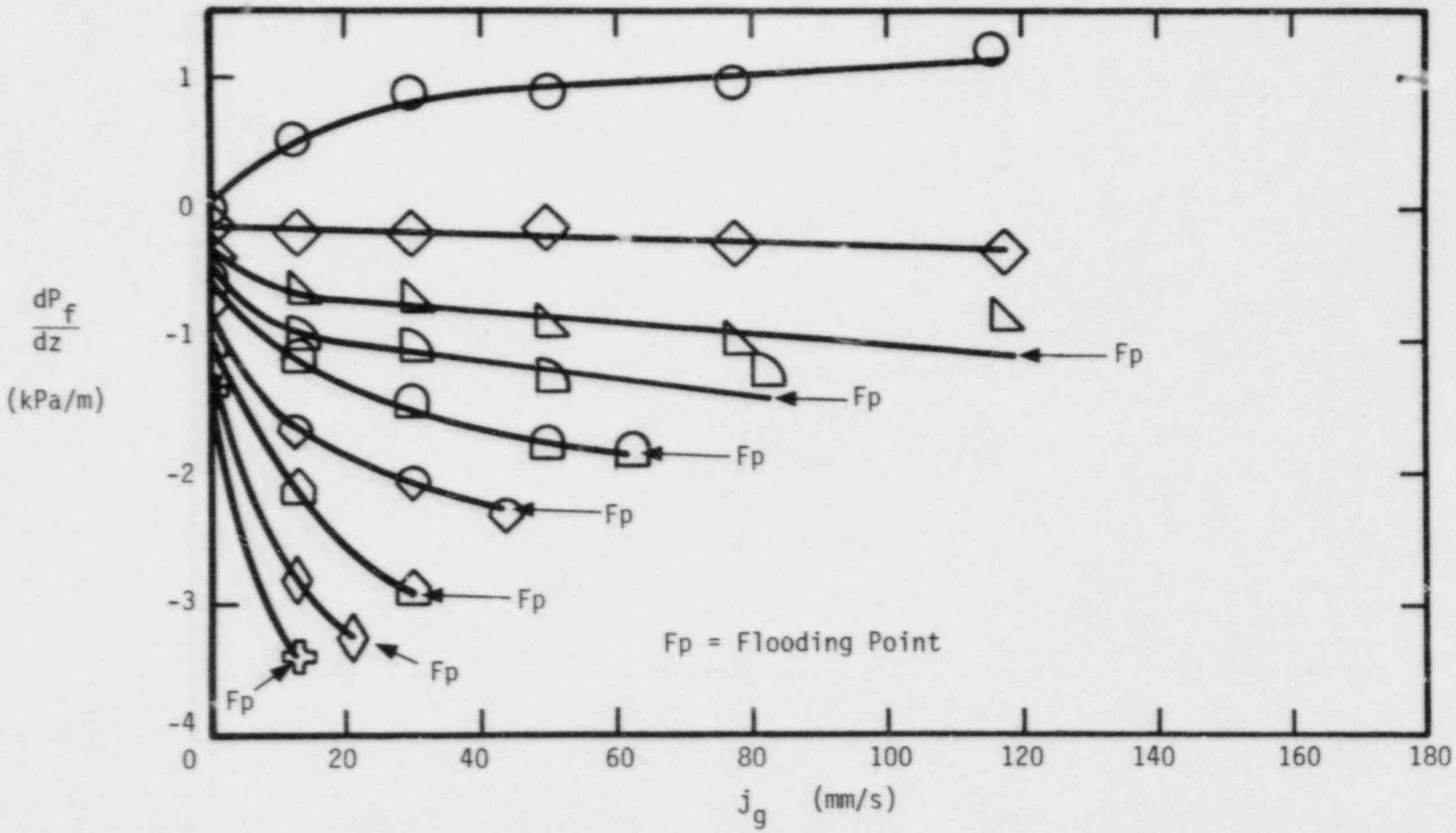

Figure F.24 Frictional Pressure Gradients for Mixture of 6,10,15,19 mm Nominal Diameter Particles

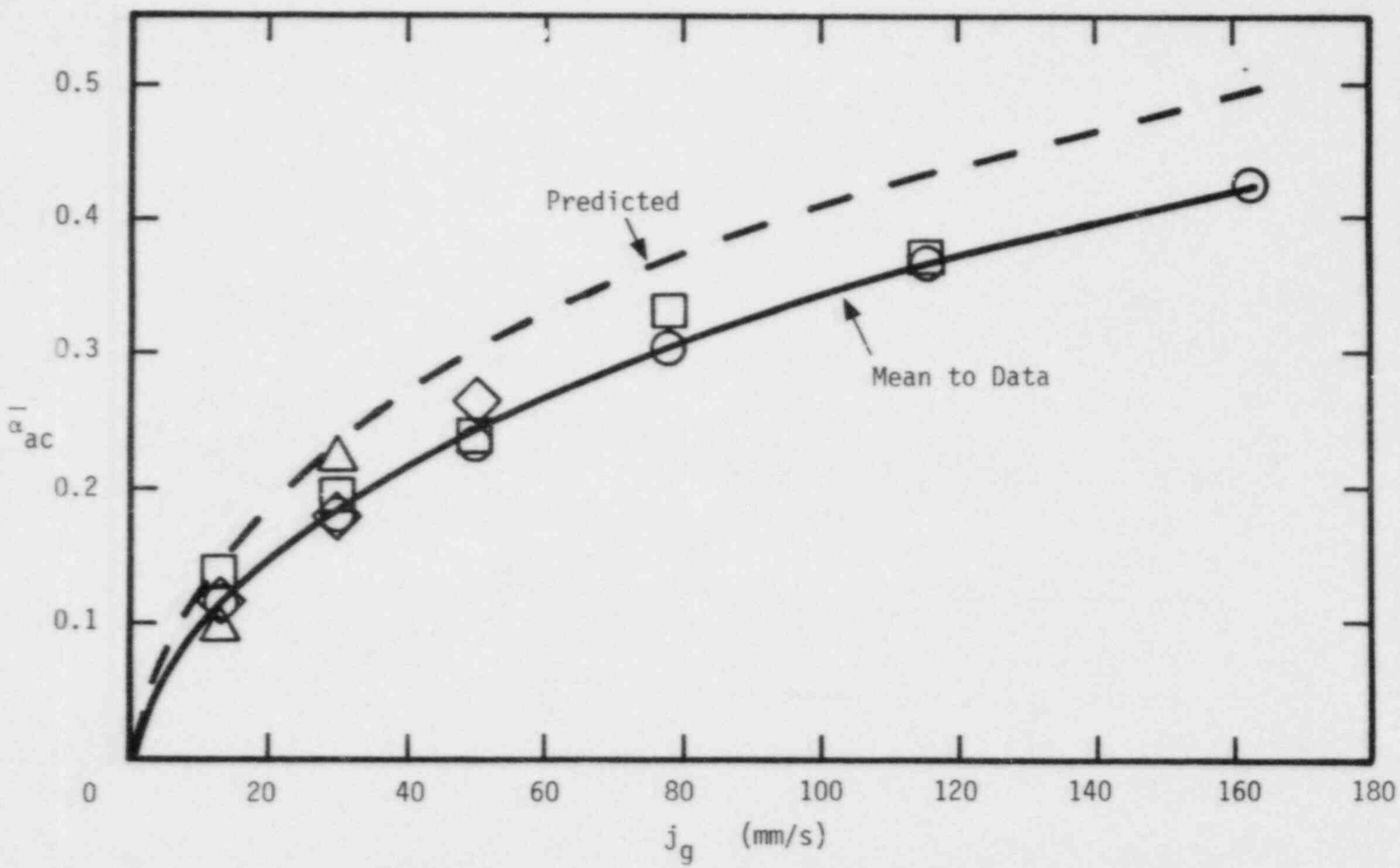

Figure F.25 Active Void Fractions for Mixture of 3,6,10,15,19 mm Nominal Diameter Particles

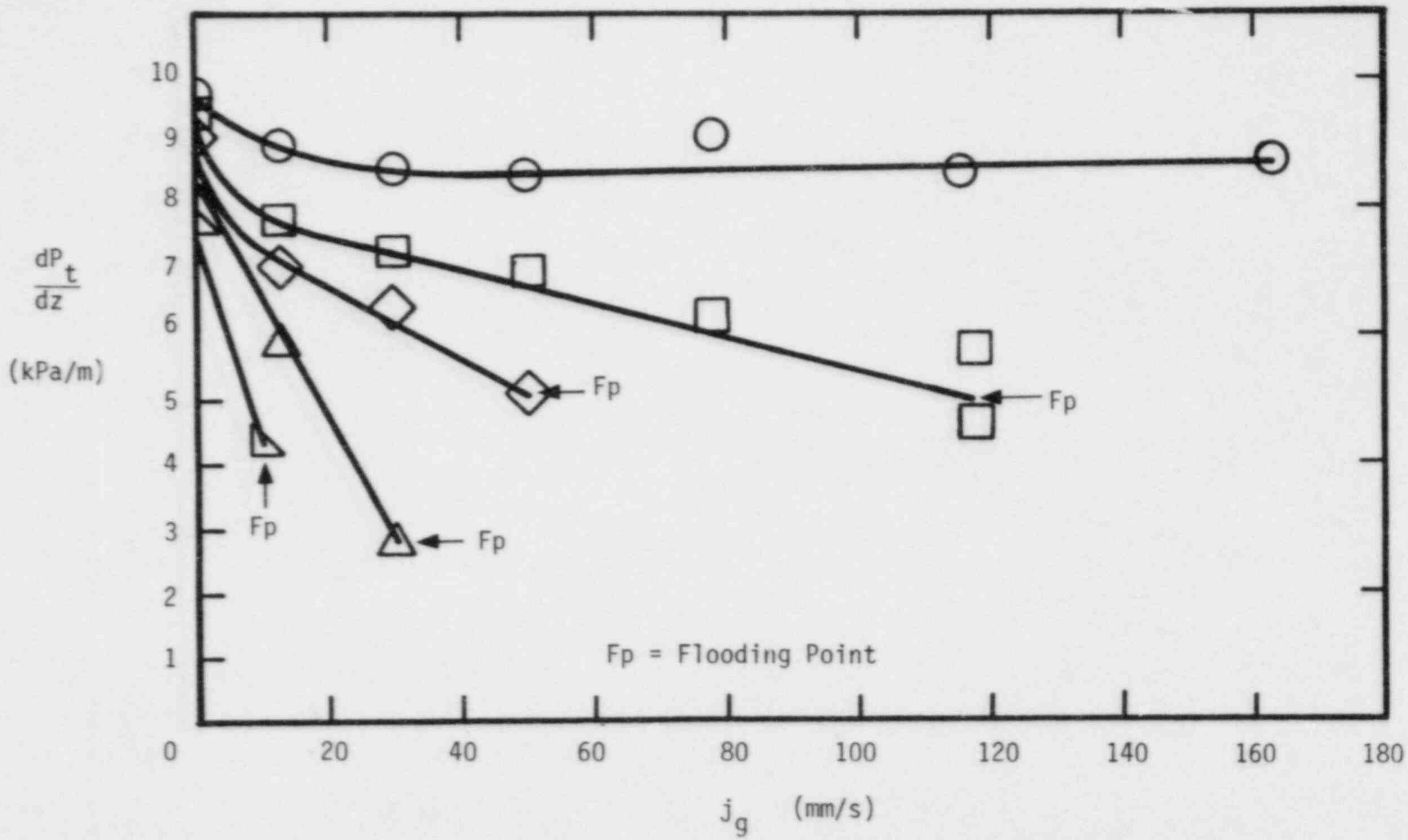

Figure F.26 Total Pressure Gradients for Mixture of 3,6,10,15,19 mm Nominal Diameter Particles

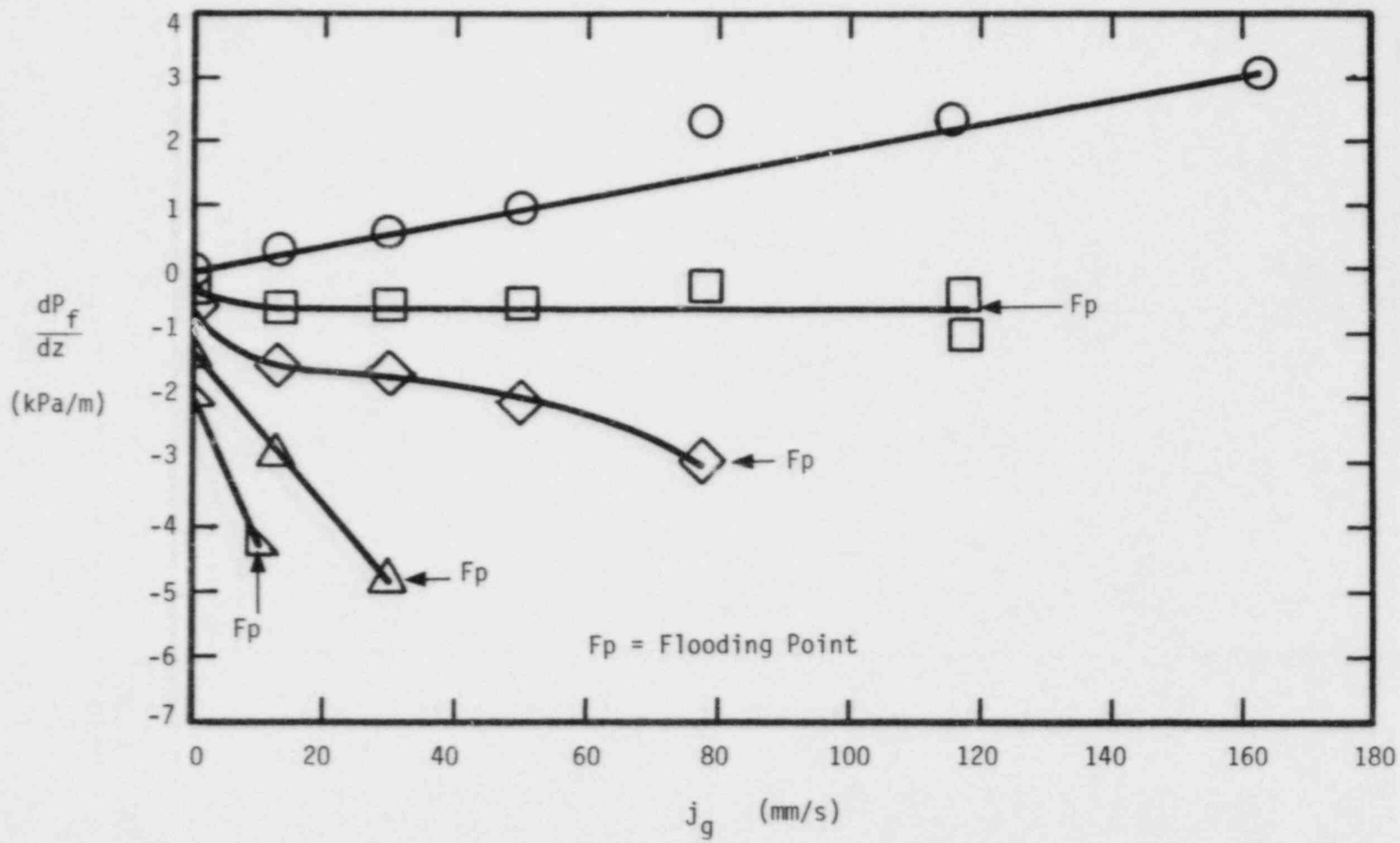

Figure F.27 Frictional Pressure Gradients for Mixture of 3,6,10,15,19 mm Nominal Diameter Particles

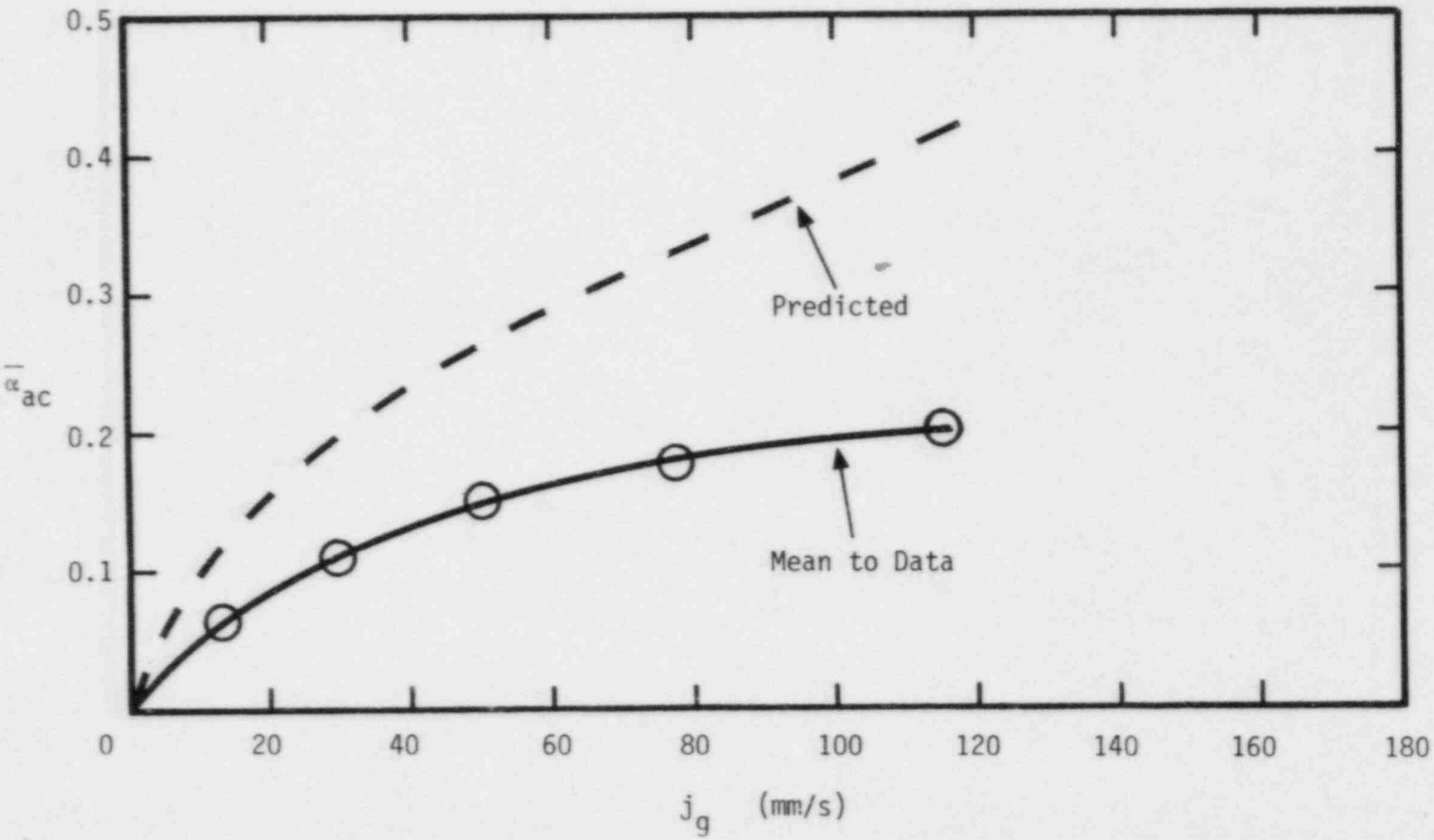

Figure F.28 Active Void Fractions for Mixture of 1,3,6,10,15,19 mm Nominal Diameter Particles

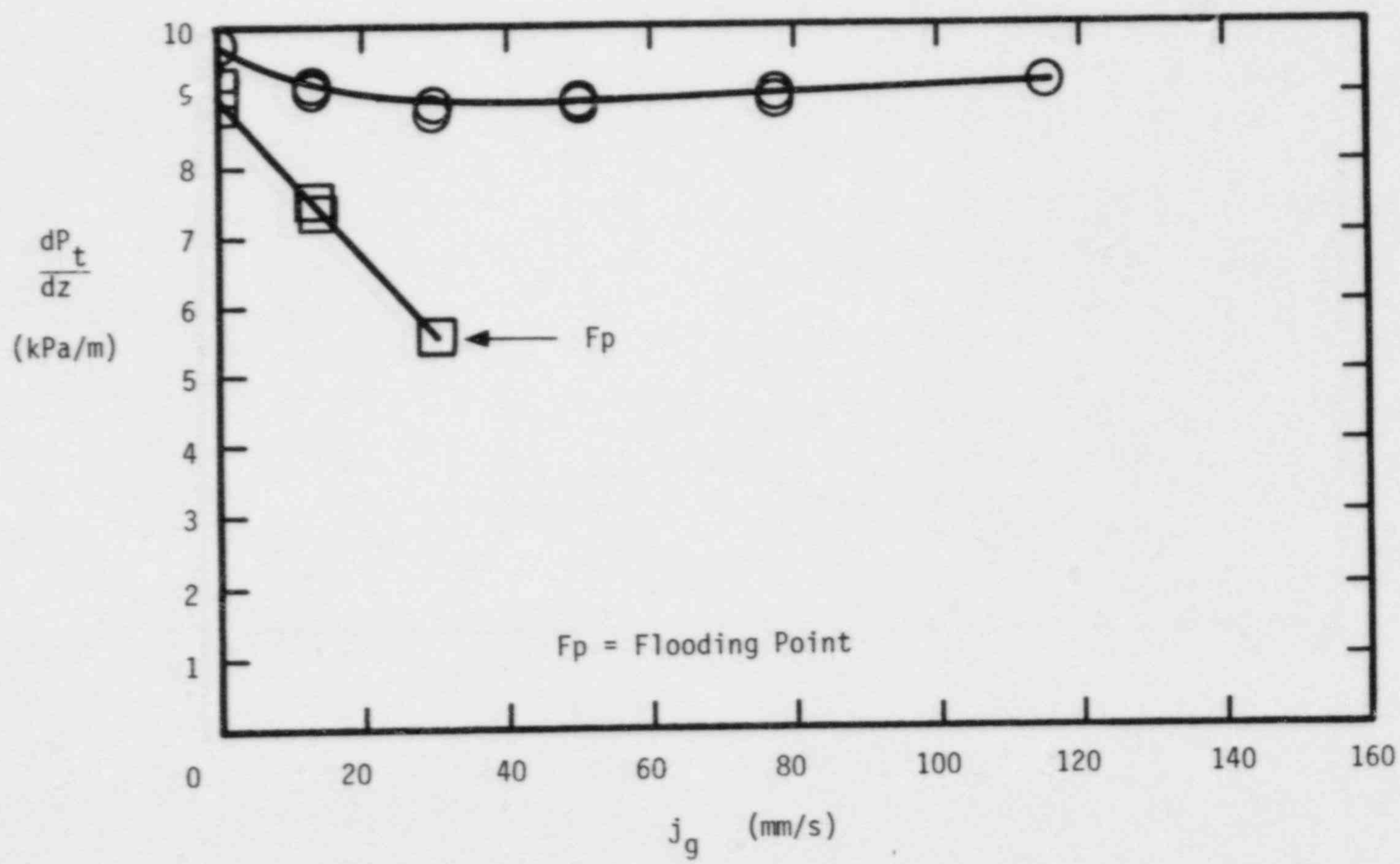

Figure F.29 Total Pressure Gradients for Mixture of 1,3,6,10,15,19 mm Nominal Diameter Particles

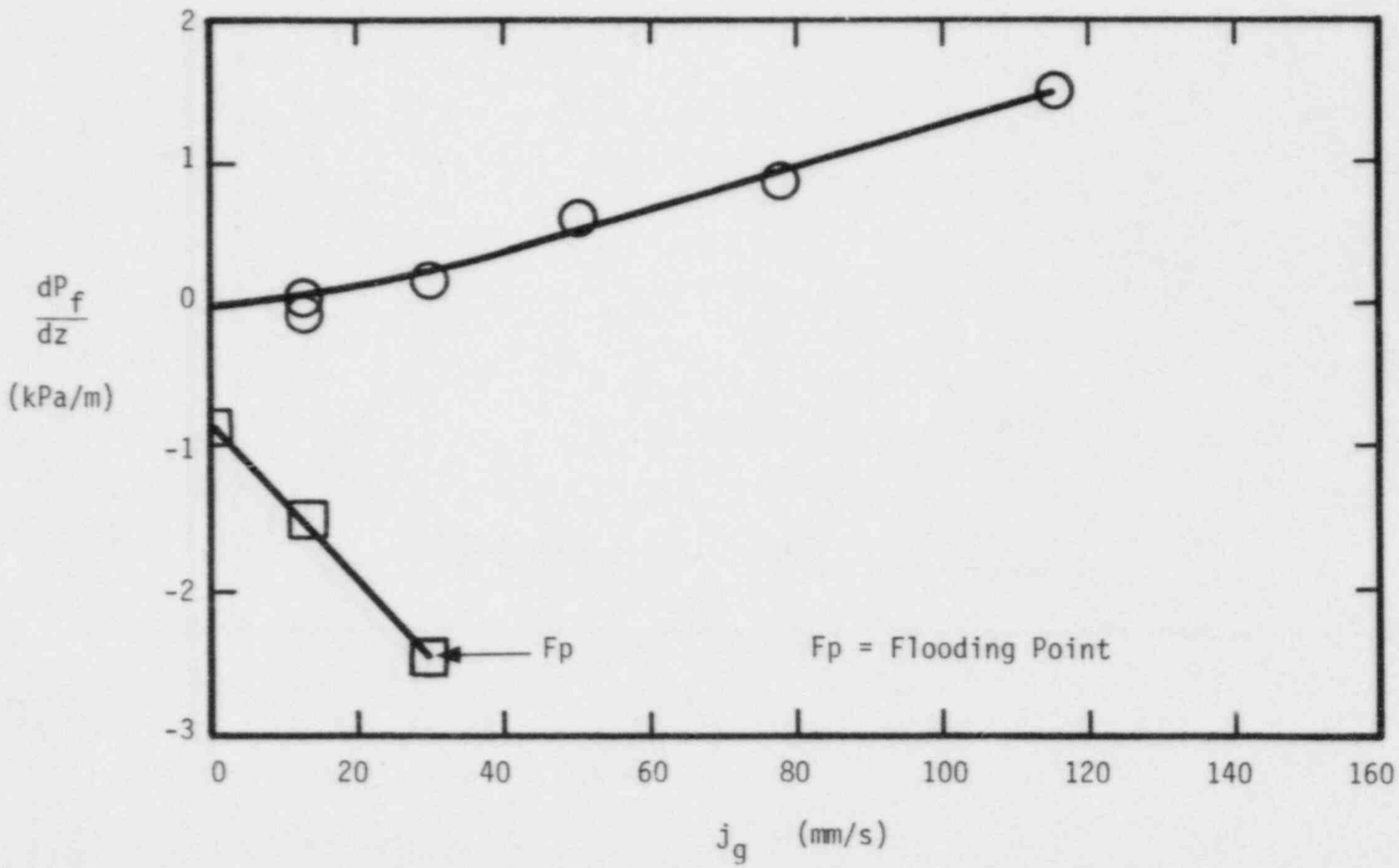

Figure F.30 Frictional Pressure Gradients for Mixture of 1,3,6,10,15,19 mm Nominal Diameter Particles

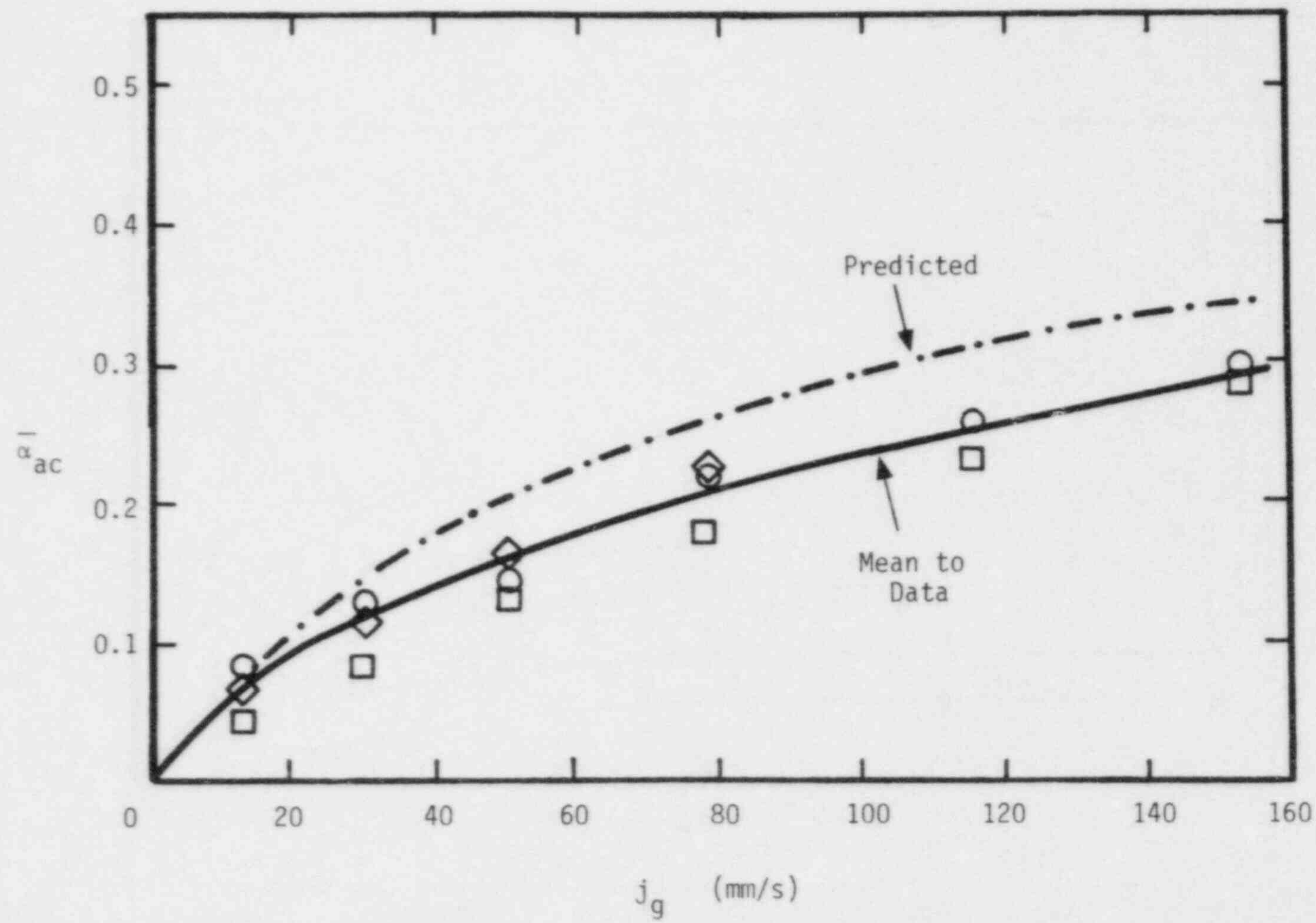

Figure F.31 Active Void Fraction for Mixture of 6 mm Nominal Diameter Spherical Particles and Non-Spherical Sharps

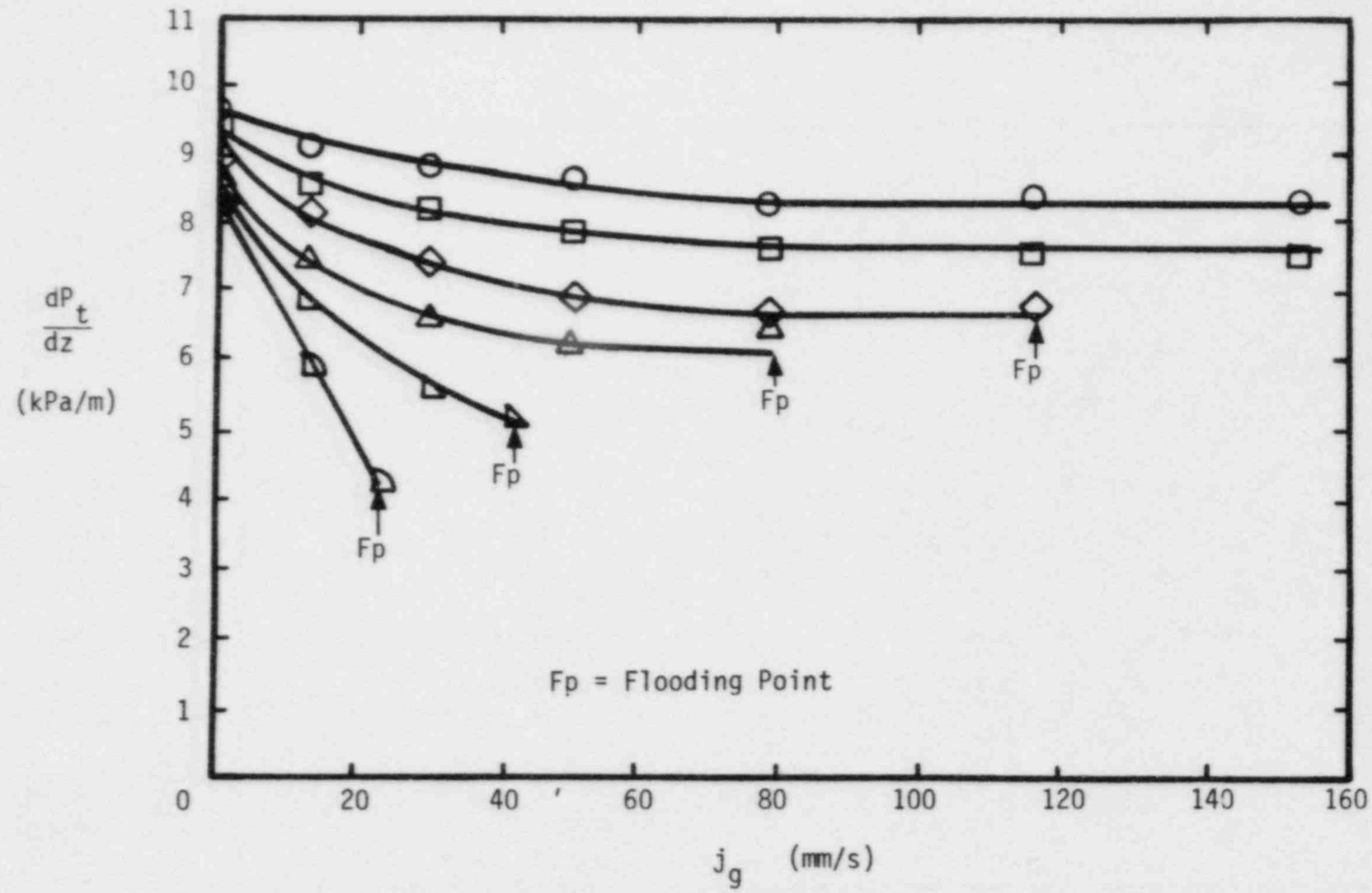

Figure F.32 Total Pressure Gradients for Mixture of 6 mm Nominal Diameter Spherical Particles and Non-Spherical Sharps

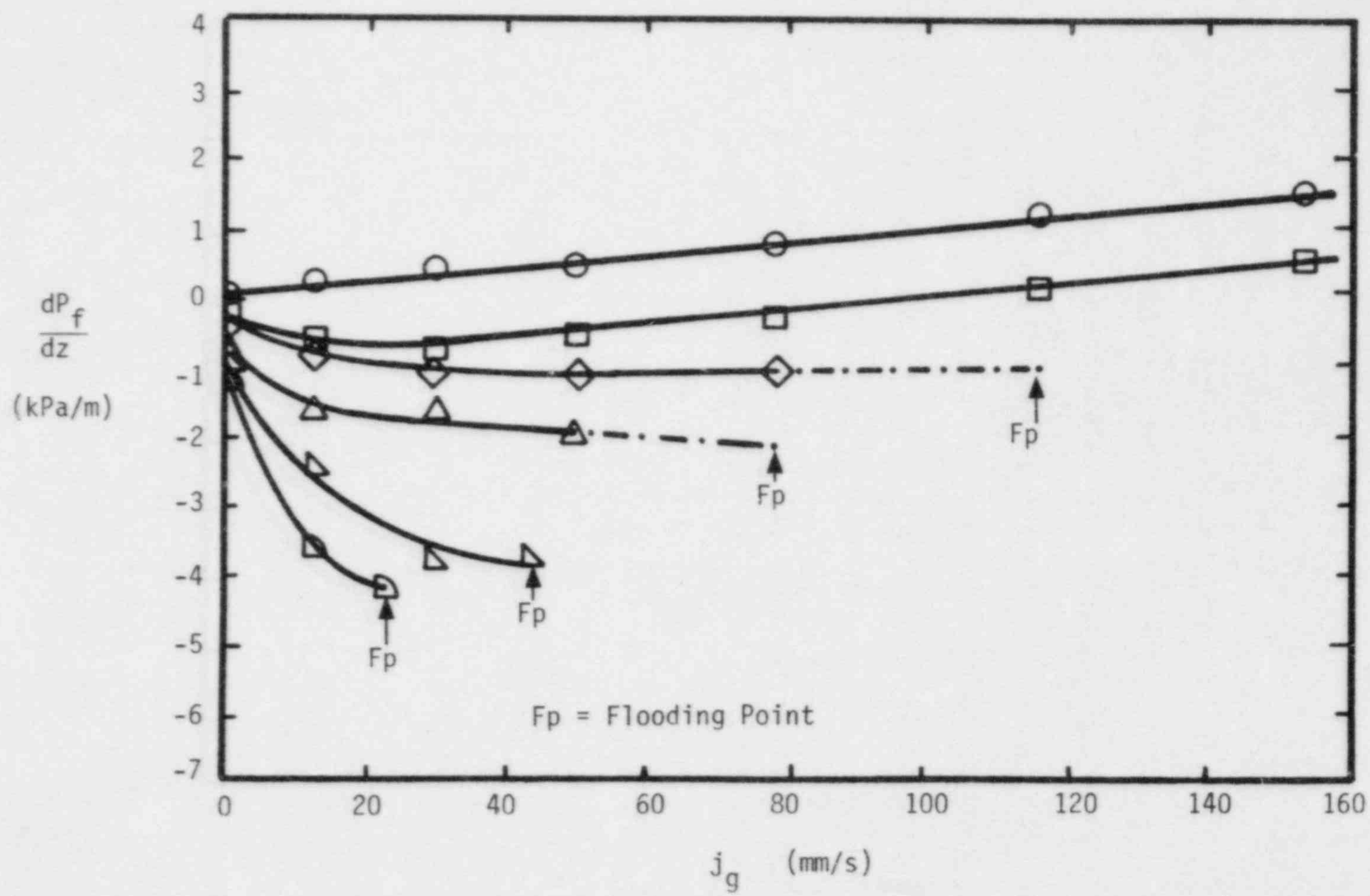

Figure F.33 Frictional Pressure Gradients for Mixture of 6 mm Nominal Diameter Spherical Particles and Non-Spherical Sharps

APPENDIX G: Listing of Void Fraction and Pressure Drop Data at and before Flooding

In this section, all void fraction and pressure drop data obtained in this work are listed. Data for beds composed of uniform size particles are given in Tables G.1 through G.5, and data for beds formed of mixtures of various size particles are given in Tables G.6 through G.11. When flooding of the particulate bed is observed, the superficial gas velocity at flooding is given for a particular superficial velocity of liquid. For beds formed of mixtures of various particle sizes, the composition of the bed is given by the particle volume fraction x_i for each constituent particle size, where the subscript i denotes the particle nominal diameter.

Table G.1 Void Fraction and Pressure Drop Data for a Bed Composed of 3 mm Nominal Diameter Particles

Bed Characteristics:

Spherical Particles: 3 mm Nominal Diameter

Mean Particle Diameter: 2.8 mm

Run Number: 00300

Superficial Liquid Velocity j_{ℓ} = 0.0 mm/s

Superficial Gas Velocity at Flooding j_g = —— mm/s

Superficial Gas Velocity	Particulate Bed			Overlying Liquid Layer		Average Pressure Gradient	
j_g (mm/s)	Bed Depth (mm)	Porosity ε	Average Active Void Fraction $\bar{\alpha}_{ac}$	Height (mm)	Average Void Fraction $\bar{\alpha}_o$	Total $\frac{dP_t}{dz}$ (kPa/m)	Frictional $\frac{dP_f}{dz}$ (kPa/m)
13.1	980	0.42	0.061	119	0.12	9.43	0.255
29.5	977	0.42	0.12	143	0.15	9.25	0.612
50.0	984	0.42	0.17	165	0.19	9.53	1.43
77.7	982	0.42	0.21	193	0.26	9.68	1.95
115.4	985	0.42	0.26	235	0.32	9.73	2.51
162.9	984	0.42	0.33	278	0.36	——	——

Table G.1 Void Fraction and Pressure Drop Data for a Bed Composed of 3 mm Nominal Diameter Particles (continued)

Bed Characteristics:

Spherical Particles: 3 mm Nominal Diameter

Mean Particle Diameter: 2.8 mm

Run Number: 00301

Superficial Liquid Velocity j_ℓ = 1.95 mm/s

Superficial Gas Velocity at Flooding j_g = 97 mm/s

Superficial Gas Velocity j_g (mm/s)	Particulate Bed			Overlying Liquid Layer		Average Pressure Gradient	
	Bed Depth (mm)	Porosity ϵ	Average Active Void Fraction $\bar{\alpha}_{ac}$	Height (mm)	Average Void Fraction $\bar{\alpha}_o$	Total $\frac{dP_t}{dz}$ (kPa/m)	Frictional $\frac{dP_f}{dz}$ (kPa/m)
0.0	994	0.43	0.00	154	0.00	9.49	-0.281
13.1	980	0.42	0.072	254	0.092	8.50	-0.572
29.5	978	0.42	0.12	343	0.13	8.41	-0.238
50.0	974	0.42	0.18	348	0.16	8.05	0.036
77.7	972	0.42	0.24	259	0.20	7.92	0.531
97.0	867	0.42	——	——	——	5.14	——

Table G.1 Void Fraction and Pressure Drop Data for a Bed Composed of 3 mm Nominal Diameter Particles (continued)

Bed Characteristics:

Spherical Particles: 3 mm Nominal Diameter

Mean Particle Diameter: 2.8 mm

Run Number: 00302

Superficial Liquid Velocity j_ℓ = 3.89 mm/s

Superficial Gas Velocity at Flooding j_g = 50 mm/s

Superficial Gas Velocity j_g (mm/s)	Particulate Bed			Overlying Liquid Layer		Average Pressure Gradient	
	Bed Depth (mm)	Porosity ϵ	Average Active Void Fraction $\bar{\alpha}_{ac}$	Height (mm)	Average Void Fraction $\bar{\alpha}_o$	Total $\frac{dP_t}{dz}$ (kPa/m)	Frictional $\frac{dP_f}{dz}$ (kPa/m)
0.0	979	0.42	0.00	171	0.00	9.12	-0.651
13.1	967	0.42	0.055	281	0.078	7.36	-1.87
29.5	969	0.42	0.12	303	0.12	7.09	-1.51
50.0	963	0.41	0.18	322	0.18	4.46	-3.55

Table G.1 Void Fraction and Pressure Drop Data for a Bed Composed of 3 mm Nominal Diameter Particles (continued)

Bed Characteristics:

Spherical Particles: 3 mm Nominal Diameter

Mean Particle Diameter: 2.8 mm

Run Number: 00303

Superficial Liquid Velocity j_{ℓ} = 5.84 mm/s

Superficial Gas Velocity at Flooding j_g = 30 mm/s

Superficial Gas Velocity	Particulate Bed			Overlying Liquid Layer		Average Pressure Gradient	
j_g (mm/s)	Bed Depth (mm)	Porosity ϵ	Average Active Void Fraction $\bar{\alpha}_{ac}$	Height (mm)	Average Void Fraction $\bar{\alpha}_o$	Total $\frac{dP_t}{dz}$ (kPa/m)	Frictional $\frac{dP_f}{dz}$ (kPa/m)
0.0	993	0.42	0.00	79	0.00	8.82	-0.951
13.1	980	0.42	0.080	271	0.069	5.82	-3.07
29.5	983	0.42	0.13	245	0.15	3.45	-5.05

Table G.1 Void Fraction and Pressure Drop Data for a Bed Composed of 3 mm Nominal Diameter Particles (continued)

Bed Characteristics:

Spherical Particles: 3 mm Nominal Diameter

Mean Particle Diameter: 2.8 mm

Run Number: 00304

Superficial Liquid Velocity j_{ℓ} = 7.78 mm/s

Superficial Gas Velocity at Flooding j_g = 16 mm/s

Superficial Gas Velocity	Particulate Bed			Overlying Liquid Layer		Average Pressure Gradient	
j_g (mm/s)	Bed Depth (mm)	Porosity ϵ	Average Active Void Fraction $\bar{\alpha}_{ac}$	Height (mm)	Average Void Fraction $\bar{\alpha}_o$	Total $\frac{dP_t}{dz}$ (kPa/m)	Frictional $\frac{dP_f}{dz}$ (kPa/m)
0.0	978	0.42	0.00	53	0.00	8.43	-1.34
10.0	963	0.41	0.097	326	0.056	5.58	-3.24
13.1	981	0.42	—	—	—	4.77	—
16.0	981	0.42	—	—	—	4.13	—

Table G.2 Void Fraction and Pressure Drop Data for a Bed Composed of 6 mm Nominal Diameter Particles

Bed Characteristics:

Spherical Particles: 6 mm Nominal Diameter

Mean Particle Diameter: 5.8 mm

Run Number: 00600

Superficial Liquid Velocity j_ℓ = 0.0 mm/s

Superficial Gas Velocity at Flooding j_g = —— mm/s

Superficial Gas Velocity	Particulate Bed			Overlying Liquid Layer		Average Pressure Gradient	
j_g (mm/s)	Bed Depth (mm)	Porosity ε	Average Active Void Fraction $\bar{\alpha}_{ac}$	Height (mm)	Average Void Fraction $\bar{\alpha}_o$	Total $\frac{dP_t}{dz}$ (kPa/m)	Frictional $\frac{dP_f}{dz}$ (kPa/m)
13.1	808	0.39	0.10	199	0.046	9.12	0.372
29.5	808	0.39	0.18	235	0.090	8.59	0.547
50.0	808	0.39	0.22	303	0.16	8.22	0.604
77.7	806	0.39	0.28	300	0.20	7.73	0.724
115.4	803	0.39	0.33	346	0.26	7.36	0.820
162.9	803	0.39	0.35	372	0.28	7.18	0.845

Table G.2 Void Fraction and Pressure Drop Data for a Bed Composed of 6 mm Nominal Diameter Particles (continued)

Bed Characteristics:

Spherical Particles: 6 mm Nominal Diameter

Mean Particle Diameter: 5.8 mm

Run Number: G0601

Superficial Liquid Velocity j_ℓ = 1.95 mm/s

Superficial Gas Velocity at Flooding j_g = —— mm/s

Superficial Gas Velocity j_g (mm/s)	Particulate Bed			Overlying Liquid Layer		Average Pressure Gradient	
	Bed Depth (mm)	Porosity ϵ	Average Active Void Fraction $\bar{\alpha}_{ac}$	Height (mm)	Average Void Fraction $\bar{\alpha}_o$	Total $\frac{dP_t}{dz}$ (kPa/m)	Frictional $\frac{dP_f}{dz}$ (kPa/m)
0.0	802	0.39	0.00	234	0.00	9.71	-0.065
13.1	799	0.38	0.11	217	0.074	8.70	-0.017
29.5	799	0.38	0.16	357	0.11	8.20	-0.027
50.0	799	0.38	0.22	345	0.16	7.59	-0.086
77.7	799	0.38	0.28	380	0.17	7.09	0.023
115.4	799	0.38	0.35	366	0.21	6.71	0.349
162.9	799	0.38	0.37	510	0.25	6.42	0.214

Table G.2 Void Fraction and Pressure Drop Data for a Bed Composed of 6 mm Nominal Diameter Particles (continued)

Bed Characteristics:

Spherical Particles: 6 mm Nominal Diameter

Mean Particle Diameter: 5.8 mm

Run Number: 00602

Superficial Liquid Velocity j_ℓ = 3.89 mm/s

Superficial Gas Velocity at Flooding j_g = —— mm/s

Superficial Gas Velocity j_g (mm/s)	Particulate Bed			Overlying Liquid Layer		Average Pressure Gradient	
	Bed Depth (mm)	Porosity ε	Average Active Void Fraction $\bar{\alpha}_{ac}$	Height (mm)	Average Void Fraction $\bar{\alpha}_o$	Total $\frac{dP}{dz}$ (kPa/m)	Frictional $\frac{dP_f}{dz}$ (kPa/m)
0.0	802	0.39	0.00	178	0.00	9.54	-0.227
13.1	802	0.39	0.083	465	0.056	8.46	-0.505
29.5	802	0.39	0.15	269	0.13	7.80	-0.559
50.0	802	0.39	0.22	270	0.14	7.04	-0.621
77.7	799	0.38	0.24	362	0.20	6.73	-0.670
115.4	799	0.38	0.30	422	0.29	5.71	-1.05
162.9	798	0.38	0.34	515	0.33	5.77	-0.668

Table G.2 Void Fraction and Pressure Drop Data for a Bed Composed of 6 mm Nominal Diameter Particles (continued)

Bed Characteristics:

Spherical Particles: 6 mm Nominal Diameter

Mean Particle Diameter: 5.8 mm

Run Number: 00603

Superficial Liquid Velocity j_ℓ = 5.84 mm/s

Superficial Gas Velocity at Flooding j_g = —— mm/s

Superficial Gas Velocity	Particulate Bed			Overlying Liquid Layer		Average Pressure Gradient	
j_g (mm/s)	Bed Depth (mm)	Porosity ε	Average Active Void Fraction $\bar{\alpha}_{ac}$	Height (mm)	Average Void Fraction $\bar{\alpha}_o$	Total $\frac{dP_t}{dz}$ (kPa/m)	Frictional $\frac{dP_f}{dz}$ (kPa/m)
0.0	808	0.39	0.00	148	0.00	9.45	-0.321
13.1	799	0.38	0.079	236	0.061	8.12	-0.876
29.5	802	0.39	0.15	331	0.090	7.20	-1.16
50.0	802	0.39	0.19	317	0.18	6.55	-1.35
77.7	796	0.38	0.23	467	0.22	5.87	-1.61
115.4	798	0.38	0.29	448	0.27	5.47	-1.85
162.9	795	0.38	0.35	495	0.33	4.12	-2.28

Table G.2 Void Fraction and Pressure Drop Data for a Bed Composed of 6 mm Nominal Diameter Particles (continued)

Bed Characteristics:

Spherical Particles: 6 mm Nominal Diameter

Mean Particle Diameter: 5.8 mm

Run Number: 00604

Superficial Liquid Velocity j_ℓ = 7.78 mm/s

Superficial Gas Velocity at Flooding j_g = 135 mm/s

Superficial Gas Velocity	Particulate Bed			Overlying Liquid Layer		Average Pressure Gradient	
j_g (mm/s)	Bed Depth (mm)	Porosity ε	Average Active Void Fraction $\bar{\alpha}_{ac}$	Height (mm)	Average Void Fraction $\bar{\alpha}_o$	Total $\frac{dP_t}{dz}$ (kPa/m)	Frictional $\frac{dP_f}{dz}$ (kPa/m)
0.0	808	0.39	0.00	184	0.00	9.27	-0.496
13.1	805	0.39	0.090	234	0.060	7.78	-1.21
29.5	808	0.39	0.16	273	0.11	6.77	-1.46
50.0	810	0.39	0.20	502	0.14	6.04	-1.76
77.7	808	0.39	0.26	497	0.17	5.35	-1.90
115.4	810	0.39	0.30	440	0.21	4.82	-2.03

Table G.2 Void Fraction and Pressure Drop Data for a Bed Composed of 6 mm Nominal Diameter Particles (continued)

Bed Characteristics:

Spherical Particles: 6 mm Nominal Diameter

Mean Particle Diameter: 5.8 mm

Run Number: 00605

Superficial Liquid Velocity j_ℓ = 9.73 mm/s

Superficial Gas Velocity at Flooding j_g = 83 mm/s

Superficial Gas Velocity j_g (mm/s)	Particulate Bed			Overlying Liquid Layer		Average Pressure Gradient	
	Bed Depth (mm)	Porosity ε	Average Active Void Fraction $\bar{\alpha}_{ac}$	Height (mm)	Average Void Fraction $\bar{\bar{\alpha}}_o$	Total $\frac{dP_t}{dz}$ (kPa/m)	Frictional $\frac{dP_f}{dz}$ (kPa/m)
0.0	802	0.39	0.00	221	0.00	9.06	-0.712
13.1	8.16	0.40	0.096	509	0.053	7.64	-1.20
29.5	816	0.40	0.16	506	0.090	6.54	-1.71
50.0	798	0.38	0.20	475	0.17	5.15	-2.66
77.7	804	0.39	0.22	379	0.23	4.82	-2.76

Table G.2 Void Fraction and Pressure Drop Data for a Bed Composed of 6 mm Nominal Diameter Particles (continued)

Bed Characteristics:

Spherical Particles: 6 mm Nominal Diameter

Mean Particle Diameter: 5.8 mm

Run Number: 00606

Superficial Liquid Velocity j_{ℓ} = 11.67 mm/s

Superficial Gas Velocity at Flooding j_g = 50 mm/s

Superficial Gas Velocity j_g (mm/s)	Particulate Bed			Overlying Liquid Layer		Average Pressure Gradient	
	Bed Depth (mm)	Porosity ε	Average Active Void Fraction $\bar{\alpha}_{ac}$	Height (mm)	Average Void Fraction $\bar{\alpha}_o$	Total $\frac{dP_t}{dz}$ (kPa/m)	Frictional $\frac{dP_f}{dz}$ (kPa/m)
0.0	802	0.39	0.00	206	0.00	8.83	-0.938
13.1	814	0.39	0.090	352	0.080	6.79	-2.10
29.5	814	0.39	0.16	419	0.10	5.63	-2.59
50.0	812	0.39	0.20	449	0.15	4.40	-3.46

Table G.2 Void Fraction and Pressure Drop Data for a Bed Composed of 6 mm Nominal Diameter Particles (continued)

Bed Characteristics:

Spherical Particles: 6 mm Nominal Diameter

Mean Particle Diameter: 5.8 mm

Run Number: 00607

Superficial Liquid Velocity j_ℓ = 13.62 mm/s

Superficial Gas Velocity at Flooding j_g = 30 mm/s

Superficial Gas Velocity	Particulate Bed			Overlying Liquid Layer		Average Pressure Gradient	
j_g (mm/s)	Bed Depth (mm)	Porosity ϵ	Average Active Void Fraction $\bar{\alpha}_{ac}$	Height (mm)	Average Void Fraction $\bar{\alpha}_o$	Total $\frac{dP_t}{dz}$ (kPa/m)	Frictional $\frac{dP_f}{dz}$ (kPa/m)
0.0	805	0.39	0.00	158	0.00	8.63	-1.14
13.1	806	0.39	0.087	346	0.077	6.23	-2.69
29.5	802	0.39	0.19	435	0.12	4.75	-3.15

Table G.2 Void Fraction and Pressure Drop Data for a Bed Composed of 6 mm Nominal Diameter Particles (continued)

Bed Characteristics:

Spherical Particles: 6 mm Nominal Diameter

Mean Particle Diameter: 5.8 mm

Run Number: 00608

Superficial Liquid Velocity j_ℓ = 15.56 mm/s

Superficial Gas Velocity at Flooding j_g = 16 mm/s

Superficial Gas Velocity j_g (mm/s)	Particulate Bed			Overlying Liquid Layer		Average Pressure Gradient	
	Bed Depth (mm)	Porosity ϵ	Average Active Void Fraction $\bar{\alpha}_{ac}$	Height (mm)	Average Void Fraction $\bar{\alpha}_o$	Total $\frac{dP_t}{dz}$ (kPa/m)	Frictional $\frac{dP_f}{dz}$ (kPa/m)
0.0	805	0.39	0.00	160	0.00	8.33	-1.45
13.1	805	0.39	0.088	305	0.074	5.59	-3.33

Table G.3 Void Fraction and Pressure Drop Data for a Bed Composed of 10 mm Nominal Diameter Particles

Bed Characteristics:

Spherical Particles: 10 mm Nominal Diameter

Mean Particle Diameter: 10.0 mm

Run Number: 01000

Superficial Liquid Velocity j_ℓ = 0.0 mm/s

Superficial Gas Velocity at Flooding j_g = —— mm/s

Superficial Gas Velocity	Particulate Bed			Overlying Liquid Layer		Average Pressure Gradient	
j_g (mm/s)	Bed Depth (mm)	Porosity ϵ	Average Active Void Fraction $\bar{\alpha}_{ac}$	Height (mm)	Average Void Fraction $\bar{\alpha}_o$	Total $\frac{dP_t}{dz}$ (kPa/m)	Frictional $\frac{dP_f}{dz}$ (kPa/m)
13.1	837	0.40	0.10	246	0.079	9.09	0.324
29.5	837	0.40	0.18	252	0.11	8.53	0.492
50.0	834	0.40	0.26	302	0.16	7.91	0.648
77.7	832	0.40	0.31	320	0.22	7.47	0.758
115.4	832	0.40	0.38	353	0.25	6.97	0.939
162.9	830	0.40	0.43	500	0.29	6.45	0.910

Table G.3 Void Fraction and Pressure Drop Data for a Bed Composed of 10 mm Nominal Diameter Particles (continued)

Bed Characteristics:

Spherical Particles: 10 mm Nominal Diameter

Mean Particle Diameter: 10.0 mm

Run Number: 01002

Superficial Liquid Velocity j_ℓ = 3.89 mm/s

Superficial Gas Velocity at Flooding j_g = —— mm/s

Superficial Gas Velocity	Particulate Bed			Overlying Liquid Layer		Average Pressure Gradient	
j_g (mm/s)	Bed Depth (mm)	Porosity ε	Average Active Void Fraction $\bar{\alpha}_{ac}$	Height (mm)	Average Void Fraction $\bar{\alpha}_o$	Total $\frac{dP_t}{dz}$ (kPa/m)	Frictional $\frac{dP_f}{dz}$ (kPa/m)
0.0	830	0.40	0.00	203	0.00	9.71	-0.065
13.1	830	0.40	0.095	269	0.082	8.77	-0.074
29.5	830	0.40	0.18	290	0.14	8.01	-0.046
50.0	830	0.40	0.24	354	0.15	7.47	0.026
77.7	830	0.40	0.32	326	0.22	6.68	-0.016
115.4	830	0.40	0.37	474	0.24	6.33	0.117
162.9	830	0.40	0.45	587	0.28	5.61	0.258

Table G.3 Void Fraction and Pressure Drop Data for a Bed Composed of 10 mm Nominal Diameter Particles (continued)

Bed Characteristics:

Spherical Particles: 10 mm Nominal Diameter

Mean Particle Diameter: 10.0 mm

Run Number: 01004

Superficial Liquid Velocity j_ℓ = 7.78 mm/s

Superficial Gas Velocity at Flooding j_g = —— mm/s

Superficial Gas Velocity j_g (mm/s)	Particulate Bed			Overlying Liquid Layer		Average Pressure Gradient	
	Bed Depth (mm)	Porosity ε	Average Active Void Fraction $\bar{\alpha}_{ac}$	Height (mm)	Average Void Fraction $\bar{\alpha}_o$	Total $\frac{dP_t}{dz}$ (kPa/m)	Frictional $\frac{dP_f}{dz}$ (kPa/m)
0.0	830	0.40	0.00	165	0.00	9.59	-0.178
13.1	830	0.40	0.11	254	0.087	8.41	-0.321
29.5	830	0.40	0.19	303	0.13	7.51	-0.371
50.0	830	0.40	0.25	342	0.19	6.65	-0.648
77.7	830	0.40	0.33	442	0.22	5.97	-0.617
115.4	830	0.40	0.38	543	0.27	5.03	-1.06
162.9	830	0.40	0.45	463	0.33	4.12	-1.24

Table G.3 Void Fraction and Pressure Drop Data for a Bed Composed of 10 mm Nominal Diameter Particles (continued)

Bed Characteristics:

Spherical Particles: 10 mm Nominal Diameter

Mean Particle Diameter: 10.0 mm

Run Number: 01005

Superficial Liquid Velocity j_ℓ = 9.73 mm/s

Superficial Gas Velocity at Flooding j_g = 163 mm/s

Superficial Gas Velocity j_g (mm/s)	Particulate Bed			Overlying Liquid Layer		Average Pressure Gradient	
	Bed Depth (mm)	Porosity ε	Average Active Void Fraction $\bar{\alpha}_{ac}$	Height (mm)	Average Void Fraction $\bar{\alpha}_o$	Total $\frac{dP_t}{dz}$ (kPa/m)	Frictional $\frac{dP_f}{dz}$ (kPa/m)
0.0	830	0.40	0.00	145	0.00	9.54	-0.226
13.1	830	0.40	0.10	257	0.086	8.31	-0.454
29.5	830	0.40	0.20	268	0.14	7.25	-0.557
50.0	830	0.40	0.26	352	0.16	6.47	-0.724
77.7	830	0.40	0.34	425	0.20	5.53	-0.930
115.4	830	0.40	0.40	480	0.25	5.05	-0.859
162.9	830	0.40	0.46	507	0.28	4.35	-0.979

Table G.3 Void Fraction and Pressure Drop Data for a Bed Composed of 10 mm Nominal Diameter Particles (continued)

Bed Characteristics:

Spherical Particles: 10 mm Nominal Diameter

Mean Particle Diameter: 10.0 mm

Run Number: 01006

Superficial Liquid Velocity j_ℓ = 11.67 mm/s

Superficial Gas Velocity at Flooding j_g = 115 mm/s

Superficial Gas Velocity	Particulate Bed			Overlying Liquid Layer		Average Pressure Gradient	
j_g (mm/s)	Bed Depth (mm)	Porosity ϵ	Average Active Void Fraction $\bar{\alpha}_{ac}$	Height (mm)	Average Void Fraction $\bar{\alpha}_o$	Total $\frac{dP_t}{dz}$ (kPa/m)	Frictional $\frac{dP_f}{dz}$ (kPa/m)
0.0	830	0.40	0.00	144	0.00	9.46	-0.307
13.1	830	0.40	0.12	250	0.084	7.96	-0.606
29.5	830	0.40	0.22	347	0.12	6.92	-0.721
50.0	830	0.40	0.27	439	0.16	6.03	-1.11
77.7	830	0.40	0.34	480	0.20	5.19	-1.27
115.4	830	0.40	0.39	447	0.26	4.30	-1.67

Table G.3 Void Fraction and Pressure Drop Data for a Bed Composed of 10 mm Nominal Diameter Particles (continued)

Bed Characteristics:

Spherical Particles: 10 mm Nominal Diameter

Mean Particle Diameter: 10.0 mm

Run Number: 01007

Superficial Liquid Velocity j_ℓ = 13.62 mm/s

Superficial Gas Velocity at Flooding j_g = 90 mm/s

Superficial Gas Velocity j_g (mm/s)	Particulate Bed			Overlying Liquid Layer		Average Pressure Gradient	
	Bed Depth (mm)	Porosity ϵ	Average Active Void Fraction $\overline{\alpha}_{ac}$	Height (mm)	Average Void Fraction $\overline{\alpha}_o$	Total $\frac{dP_t}{dz}$ (kPa/m)	Frictional $\frac{dP_f}{dz}$ (kPa/m)
0.0	833	0.40	0.00	207	0.00	9.37	-0.404
13.1	833	0.40	0.12	299	0.087	7.81	-0.813
29.5	833	0.40	0.20	326	0.14	6.68	-1.11
50.0	833	0.40	0.30	428	0.16	5.44	-1.41
77.7	830	0.40	0.37	465	0.20	4.58	-1.61

Table G.3 Void Fraction and Pressure Drop Data for a Bed Composed of 10 mm Nominal Diameter Particles (continued)

Bed Characteristics:

Spherical Particles: 10 mm Nominal Diameter

Mean Particle Diameter: 10.0 mm

Run Number: 01008

Superficial Liquid Velocity j_ℓ = 15.56 mm/s

Superficial Gas Velocity at Flooding j_g = 71 mm/s

Superficial Gas Velocity	Particulate Bed			Overlying Liquid Layer		Average Pressure Gradient	
j_g (mm/s)	Bed Depth (mm)	Porosity ε	Average Active Void Fraction $\bar{\alpha}_{ac}$	Height (mm)	Average Void Fraction $\bar{\alpha}_o$	Total $\frac{dP_t}{dz}$ (kPa/m)	Frictional $\frac{dP_f}{dz}$ (kPa/m)
0.0	832	0.40	0.00	164	0.00	9.25	-0.518
13.1	832	0.40	0.12	303	0.082	7.47	-1.09
29.5	832	0.40	0.21	356	0.12	6.29	-1.41
50.0	832	0.40	0.30	418	0.16	5.03	-1.79

Table G.3 Void Fraction and Pressure Drop Data for a Bed Composed of 10 mm Nominal Diameter Particles (continued)

Bed Characteristics:

Spherical Particles: 10 mm Nominal Diameter

Mean Particle Diameter: 10.0 mm

Run Number: 01009

Superficial Liquid Velocity j_ℓ = 17.51 mm/s

Superficial Gas Velocity at Flooding j_g = 60 mm/s

Superficial Gas Velocity j_g (mm/s)	Particulate Bed			Overlying Liquid Layer		Average Pressure Gradient	
	Bed Depth (mm)	Porosity ϵ	Average Active Void Fraction $\bar{\alpha}_{ac}$	Height (mm)	Average Void Fraction $\bar{\alpha}_o$	Total $\frac{dP_t}{dz}$ (kPa/m)	Frictional $\frac{dP_f}{dz}$ (kPa/m)
0.0	832	0.40	0.00	210	0.00	9.16	-0.615
13.1	832	0.40	0.10	338	0.082	7.26	-1.51
29.5	832	0.40	0.20	397	0.11	6.00	-1.82
50.0	832	0.40	0.22	496	0.17	5.42	-2.19

Table G.3 Void Fraction and Pressure Drop Data for a Bed Composed of 10 mm Nominal Diameter Particles (continued)

Bed Characteristics:

Spherical Particles: 10 mm Nominal Diameter

Mean Particle Diameter: 10.0 mm

Run Number: 01010

Superficial Liquid Velocity j_ℓ = 19.46 mm/s

Superficial Gas Velocity at Flooding j_g = 38 mm/s

Superficial Gas Velocity	Particulate Bed			Overlying Liquid Layer		Average Pressure Gradient	
j_g (mm/s)	Bed Depth (mm)	Porosity ε	Average Active Void Fraction $\bar{\alpha}_{ac}$	Height (mm)	Average Void Fraction $\bar{\alpha}_o$	Total $\frac{dP_t}{dz}$ (kPa/m)	Frictional $\frac{dP_f}{dz}$ (kPa/m)
0.0	832	0.40	0.00	201	0.00	8.96	-0.809
13.1	832	0.40	0.084	347	0.095	6.97	-1.98
29.5	832	0.40	0.21	444	0.11	5.32	-2.44

Table G.4 Void Fraction and Pressure Drop Data for a Bed Composed of 15 mm Nominal Diameter Particles

Bed Characteristics:

Spherical Particles: 15 mm Nominal Diameter

Mean Particle Diameter: 14.7 mm

Run Number: 01500

Superficial Liquid Velocity j_{ℓ} = 0.0 mm/s

Superficial Gas Velocity at Flooding j_g = —— mm/s

Superficial Gas Velocity	Particulate Bed			Overlying Liquid Layer		Average Pressure Gradient	
j_g (mm/s)	Bed Depth (mm)	Porosity ϵ	Average Active Void Fraction $\bar{\alpha}_{ac}$	Height (mm)	Average Void Fraction $\bar{\alpha}_o$	Total $\frac{dP_t}{dz}$ (kPa/m)	Frictional $\frac{dP_f}{dz}$ (kPa/m)
13.1	848	0.42	0.11	318	0.051	8.93	0.239
29.5	848	0.42	0.19	415	0.10	8.31	0.379
50.0	848	0.42	0.26	468	0.15	7.75	0.496
77.7	848	0.42	0.32	463	0.21	7.21	0.596
115.4	848	0.42	0.39	614	0.25	6.71	0.710
162.9	843	0.42	0.44	592	0.30	6.31	0.803

Table G.4 Void Fraction and Pressure Drop Data for a Bed Composed of 15 mm Nominal Diameter Particles (continued)

Bed Characteristics:

Spherical Particles: 15 mm Nominal Diameter

Mean Particle Diameter: 14.7 mm

Run Number: 01502

Superficial Liquid Velocity j_ℓ = 3.89 mm/s

Superficial Gas Velocity at Flooding j_g = —— mm/s

Superficial Gas Velocity j_g (mm/s)	Particulate Bed			Overlying Liquid Layer		Average Pressure Gradient	
	Bed Depth (mm)	Porosity ε	Average Active Void Fraction $\bar{\alpha}_{ac}$	Height (mm)	Average Void Fraction $\bar{\alpha}_o$	Total $\frac{dP_t}{dz}$ (kPa/m)	Frictional $\frac{dP_f}{dz}$ (kPa/m)
0.0	843	0.42	0.00	171	0.00	9.74	-0.032
13.1	843	0.42	0.11	239	0.083	8.70	-0.033
29.5	843	0.42	0.20	312	0.093	8.06	-0.227
50.0	843	0.42	0.27	329	0.15	7.36	0.205
77.7	843	0.42	0.32	486	0.20	6.81	0.192
115.4	843	0.42	0.38	521	0.25	6.21	0.130
162.9	843	0.42	0.46	545	0.29	5.59	0.260

Table G.4 Void Fraction and Pressure Drop Data for a Bed Composed of 15 mm Nominal Diameter Particles (continued)

Bed Characteristics:

Spherical Particles: 15 mm Nominal Diameter

Mean Particle Diameter: 14.7 mm

Run Number: 01504

Superficial Liquid Velocity j_ℓ = 7.78 mm/s

Superficial Gas Velocity at Flooding j_g = —— mm/s

Superficial Gas Velocity	Particulate Bed			Overlying Liquid Layer		Average Pressure Gradient	
j_g (mm/s)	Bed Depth (mm)	Porosity ε	Average Active Void Fraction $\bar{\alpha}_{ac}$	Height (mm)	Average Void Fraction $\bar{\alpha}_o$	Total $\frac{dP_t}{dz}$ (kPa/m)	Frictional $\frac{dP_f}{dz}$ (kPa/m)
0.0	845	0.42	0.00	219	0.00	9.69	-0.081
13.1	845	0.42	0.11	310	0.093	8.53	-0.221
29.5	845	0.42	0.20	311	0.14	7.73	-0.096
50.0	845	0.42	0.27	401	0.16	6.99	-0.157
77.7	845	0.42	0.32	429	0.20	6.39	-0.219
115.4	845	0.42	0.36	487	0.24	5.99	-0.270
162.9	845	0.42	0.41	471	0.30	5.68	-0.084

Table G.4 Void Fraction and Pressure Drop Data for a Bed Composed of 15 mm Nominal Diameter Particles (continued)

Bed Characteristics:

Spherical Particles: 15 mm Nominal Diameter

Mean Particle Diameter: 14.7 mm

Run Number: 01506

Superficial Liquid Velocity j_ℓ = 11.67 mm/s

Superficial Gas Velocity at Flooding j_g = —— mm/s

Superficial Gas Velocity j_g (mm/s)	Particulate Bed			Overlying Liquid Layer		Average Pressure Gradient	
	Bed Depth (mm)	Porosity ε	Average Active Void Fraction $\bar{\alpha}_{ac}$	Height (mm)	Average Void Fraction $\bar{\alpha}_o$	Total $\frac{dP_t}{dz}$ (kPa/m)	Frictional $\frac{dP_f}{dz}$ (kPa/m)
0.0	845	0.42	0.00	176	0.00	9.58	-0.194
13.1	845	0.42	0.12	248	0.088	8.19	-0.404
29.5	845	0.42	0.22	319	0.14	7.36	-0.312
50.0	845	0.42	0.29	337	0.16	6.63	-0.357
77.7	845	0.42	0.34	416	0.22	6.07	-0.443
115.4	845	0.42	0.43	449	0.27	5.65	-0.605
162.9	845	0.42	0.47	436	0.32	5.11	-0.588

Table G.4 Void Fraction and Pressure Drop Data for a Bed Composed of 15 mm Nominal Diameter Particles (continued)

Bed Characteristics:

Spherical Particles: 15 mm Nominal Diameter

Mean Particle Diameter: 14.7 mm

Run Number: 01508

Superficial Liquid Velocity j_{ℓ} = 15.56 mm/s

Superficial Gas Velocity at Flooding j_g = 153 mm/s

Superficial Gas Velocity j_g (mm/s)	Particulate Bed			Overlying Liquid Layer		Average Pressure Gradient	
	Bed Depth (mm)	Porosity ε	Average Active Void Fraction $\bar{\alpha}_{ac}$	Height (mm)	Average Void Fraction $\bar{\alpha}_o$	Total $\frac{dP_t}{dz}$ (kPa/m)	Frictional $\frac{dP_f}{dz}$ (kPa/m)
0.0	845	0.42	0.00	195	0.00	9.46	-0.307
13.1	845	0.42	0.14	297	0.069	7.93	-0.488
29.5	845	0.42	0.20	286	0.13	6.99	-0.870
50.0	845	0.42	0.28	324	0.18	6.21	-0.836
77.7	845	0.42	0.35	412	0.22	5.60	-1.19
115.4	845	0.42	0.42	449	0.26	4.87	-1.07
153.0	845	0.42	0.46	494	0.31	4.59	-1.47

Table G.4 Void Fraction and Pressure Drop Data for a Bed Composed of 15 mm Nominal Diameter Particles (continued)

Bed Characteristics:

Spherical Particles: 15 mm Nominal Diameter

Mean Particle Diameter: 14.7 mm

Run Number: 01509

Superficial Liquid Velocity j_ℓ = 17.51 mm/s

Superficial Gas Velocity at Flooding j_g = 124 mm/s

Superficial Gas Velocity j_g (mm/s)	Particulate Bed			Overlying Liquid Layer		Average Pressure Gradient	
	Bed Depth (mm)	Porosity ϵ	Average Active Void Fraction $\bar{\alpha}_{ac}$	Height (mm)	Average Void Fraction $\bar{\alpha}_o$	Total $\frac{dP_t}{dz}$ (kPa/m)	Frictional $\frac{dP_f}{dz}$ (kPa/m)
0.0	845	0.42	0.00	186	0.00	9.41	-0.356
13.1	845	0.42	0.091	301	0.072	7.83	-1.05
29.5	845	0.42	0.21	317	0.14	6.86	-0.833
50.0	845	0.42	0.28	342	0.19	6.28	-0.926
77.7	845	0.42	0.33	557	0.21	5.52	-1.17
124.0	845	0.42	0.37	625	0.26	4.87	-1.26

Table G.4 Void Fraction and Pressure Drop Data for a Bed Composed of 15 mm Nominal Diameter Particles (continued)

Bed Characteristics:

Spherical Particles: 15 mm Nominal Diameter

Mean Particle Diameter: 14.7 mm

Run Number: 01510

Superficial Liquid Velocity j_ℓ = 19.46 mm/s

Superficial Gas Velocity at Flooding j_g = 99 mm/s

Superficial Gas Velocity j_g (mm/s)	Particulate Bed			Overlying Liquid Layer		Average Pressure Gradient	
	Bed Depth (mm)	Porosity ε	Average Active Void Fraction $\bar{\alpha}_{ac}$	Height (mm)	Average Void Fraction $\bar{\alpha}_o$	Total $\frac{dP_t}{dz}$ (kPa/m)	Frictional $\frac{dP_f}{dz}$ (kPa/m)
0.0	845	0.42	0.00	158	0.00	9.35	-0.421
13.1	845	0.42	0.12	290	0.085	7.68	-0.928
29.5	845	0.42	0.22	398	0.12	6.66	-0.964
50.0	845	0.42	0.31	423	0.17	6.07	-0.675
77.7	845	0.42	0.36	464	0.21	5.40	-0.857
99.0	845	0.42	0.43	415	0.26	4.64	-0.934

Table G.5 Void Fraction and Pressure Drop Data for a Bed Composed of 19 mm Nominal Diameter Particles

Bed Characteristics:

Spherical Particles: 19 mm Nominal Diameter

Mean Particle Diameter: 19.1 mm

Run Number: 01900

Superficial Liquid Velocity $j_\ell = 0.0$ mm/s

Superficial Gas Velocity at Flooding $j_g =$ —— mm/s

Superficial Gas Velocity	Particulate Bed			Overlying Liquid Layer		Average Pressure Gradient	
j_g (mm/s)	Bed Depth (mm)	Porosity ε	Average Active Void Fraction $\bar{\alpha}_{ac}$	Height (mm)	Average Void Fraction $\bar{\alpha}_o$	Total $\frac{dP_t}{dz}$ (kPa/m)	Frictional $\frac{dP_f}{dz}$ (kPa/m)
13.1	823	0.40	0.12	215	0.060	8.82	0.239
29.5	823	0.40	0.20	256	0.12	8.17	0.313
50.0	823	0.40	0.26	298	0.17	7.60	0.380
77.7	823	0.40	0.32	338	0.21	7.07	0.431
115.4	823	0.40	0.38	404	0.29	6.55	0.528
162.9	823	0.40	0.43	446	0.33	6.07	0.492

Table G.5 Void Fraction and Pressure Drop Data for a Bed Composed of 19 mm Nominal Diameter Particles (continued)

Bed Characteristics:

Spherical Particles: 19 mm Nominal Diameter

Mean Particle Diameter: 19.1 mm

Run Number: 01902

Superficial Liquid Velocity j_ℓ = 3.89 mm/s

Superficial Gas Velocity at Flooding j_g = — mm/s

Superficial Gas Velocity j_g (mm/s)	Particulate Bed			Overlying Liquid Layer		Average Pressure Gradient	
	Bed Depth (mm)	Porosity ϵ	Average Active Void Fraction $\bar{\alpha}_{ac}$	Height (mm)	Average Void Fraction $\bar{\alpha}_o$	Total $\frac{dP_t}{dz}$ (kPa/m)	Frictional $\frac{dP_f}{dz}$ (kPa/m)
0.0	820	0.40	0.00	176	0.00	9.75	-0.016
13.1	820	0.40	0.11	238	0.078	8.62	-0.046
29.5	820	0.40	0.19	304	0.12	7.96	-0.006
50.0	820	0.40	0.27	317	0.17	7.28	0.134
77.7	820	0.40	0.31	356	0.23	6.89	0.165
115.4	820	0.40	0.37	402	0.28	6.29	0.084
162.9	820	0.40	0.45	513	0.30	5.73	0.308

Table G.5 Void Fraction and Pressure Drop Data for a Bed Composed of 19 mm Nominal Diameter Particles (continued)

Bed Characteristics:

Spherical Particles: 19 mm Nominal Diameter

Mean Particle Diameter: 19.1 mm

Run Number: 01904

Superficial Liquid Velocity j_ℓ = 7.78 mm/s

Superficial Gas Velocity at Flooding j_g = —— mm/s

Superficial Gas Velocity j_g (mm/s)	Particulate Bed			Overlying Liquid Layer		Average Pressure Gradient	
	Bed Depth (mm)	Porosity ϵ	Average Active Void Fraction $\bar{\alpha}_{ac}$	Height (mm)	Average Void Fraction $\bar{\alpha}_o$	Total $\frac{dP_t}{dz}$ (kPa/m)	Frictional $\frac{dP_f}{dz}$ (kPa/m)
0.0	820	0.40	0.00	160	0.00	9.71	-0.065
13.1	820	0.40	0.11	218	0.65	8.41	-0.246
29.5	820	0.40	0.20	310	0.12	7.73	-0.086
50.0	820	0.40	0.27	358	0.17	7.13	-0.041
77.7	820	0.40	0.31	320	0.25	6.58	-0.191
115.4	820	0.40	0.36	426	0.28	6.03	-0.204
162.9	820	0.40	0.43	387	0.34	5.35	-0.220

Table G.5 Void Fraction and Pressure Drop Data for a Bed Composed of 19 mm Nominal Diameter Particles (continued)

Bed Characteristics:

Spherical Particles: 19 mm Nominal Diameter

Mean Particle Diameter: 19.1 mm

Run Number: 01906

Superficial Liquid Velocity j_ℓ = 11.67 mm/s

Superficial Gas Velocity at Flooding j_g = —— mm/s

Superficial Gas Velocity j_g (mm/s)	Particulate Bed			Overlying Liquid Layer		Average Pressure Gradient	
	Bed Depth (mm)	Porosity ε	Average Active Void Fraction $\bar{\alpha}_{ac}$	Height (mm)	Average Void Fraction $\bar{\alpha}_o$	Total $\frac{dP_t}{dz}$ (kPa/m)	Frictional $\frac{dP_f}{dz}$ (kPa/m)
0.0	817	0.40	0.00	188	0.00	9.64	-0.129
13.1	817	0.40	0.13	292	0.098	8.19	-0.273
29.5	817	0.40	0.21	336	0.13	7.49	-0.202
50.0	817	0.40	0.26	366	0.16	6.89	-0.313
77.7	817	0.40	0.32	405	0.24	6.21	-0.416
115.4	817	0.40	0.38	422	0.27	5.68	-0.404
162.9	817	0.40	0.43	485	0.30	4.93	-0.640

Table G.5 Void Fraction and Pressure Drop Data for a Bed Composed of 19 mm Nominal Diameter Particles (continued)

Bed Characteristics:

Spherical Particles: 19 mm Nominal Diameter

Mean Particle Diameter: 19.1 mm

Run Number: 01908

Superficial Liquid Velocity j_ℓ = 15.56 mm/s

Superficial Gas Velocity at Flooding j_g = —— mm/s

Superficial Gas Velocity j_g (mm/s)	Particulate Bed			Overlying Liquid Layer		Average Pressure Gradient	
	Bed Depth (mm)	Porosity ε	Average Active Void Fraction $\bar{\alpha}_{ac}$	Height (mm)	Average Void Fraction $\bar{\alpha}_o$	Total $\frac{dP_t}{dz}$ (kPa/m)	Frictional $\frac{dP_f}{dz}$ (kPa/m)
0.0	817	0.40	0.00	188	0.00	9.54	-0.227
13.1	817	0.40	0.12	283	0.10	7.96	-0.621
29.5	817	0.40	0.21	354	0.13	7.23	-0.529
50.0	817	0.40	0.27	366	0.16	6.54	-0.600
77.7	817	0.40	0.33	385	0.22	5.95	-0.646
115.4	817	0.40	0.40	444	0.26	5.05	-0.839
162.9	817	0.40	0.47	503	0.29	4.48	-0.713

Table G.5 Void Fraction and Pressure Drop Data for a Bed Composed of 19 mm Nominal Diameter Particles (continued)

Bed Characteristics:

Spherical Particles: 19 mm Nominal Diameter

Mean Particle Diameter: 19.1 mm

Run Number: 01910

Superficial Liquid Velocity j_ℓ = 19.46 mm/s

Superficial Gas Velocity at Flooding j_g = 191 mm/s

Superficial Gas Velocity	Particulate Bed			Overlying Liquid Layer		Average Pressure Gradient	
j_g (mm/s)	Bed Depth (mm)	Porosity ε	Average Active Void Fraction $\bar{\alpha}_{ac}$	Height (mm)	Average Void Fraction $\bar{\alpha}_o$	Total $\frac{dP_t}{dz}$ (kPa/m)	Frictional $\frac{dP_f}{dz}$ (kPa/m)
0.0	817	0.40	0.00	193	0.00	9.45	-0.324
13.1	817	0.40	0.11	315	0.12	7.72	-0.973
29.5	817	0.40	0.18	350	0.15	7.02	-1.01
50.0	817	0.40	0.25	417	0.18	6.31	-1.03
77.7	817	0.40	0.32	518	0.20	5.56	-1.08
115.4	817	0.40	0.40	566	0.26	4.64	-1.19
162.9	817	0.40	——	638	0.29	4.35	——

Table G.6 Void Fraction and Pressure Drop Data for a Bed Composed of a Mixture of 6 mm and 10 mm Nominal Diameter Particles

Bed Characteristics:

Spherical Particles: 10 mm and 6 mm Nominal Diameter Mixture

Mean Particle Diameter: 7.8 mm

Run Number: 61000

Superficial Liquid Velocity j_ℓ = 0.0 mm/s

Superficial Gas Velocity at Flooding j_g = —— mm/s

Superficial Gas Velocity	Particulate Bed			Overlying Liquid Layer		Average Pressure Gradient	
j_g (mm/s)	Bed Depth (mm)	Porosity ε	Average Active Void Fraction $\bar{\alpha}_{ac}$	Height (mm)	Average Void Fraction $\bar{\alpha}_o$	Total $\frac{dP_t}{dz}$ (kPa/m)	Frictional $\frac{dP_f}{dz}$ (kPa/m)
13.1	854	0.36	0.12	195	0.056	9.08	0.497
29.5	854	0.36	0.20	232	0.10	8.51	0.716
50.0	854	0.36	0.27	277	0.17	7.96	0.825
77.7	854	0.36	0.34	324	0.23	7.39	0.979
115.4	854	0.36	0.41	370	0.27	6.88	1.06
162.9	851	0.36	0.45	420	0.32	6.62	1.22

Table G.6 Void Fraction and Pressure Drop Data for a Bed Composed of a Mixture of 6 mm and 10 mm Nominal Diameter Particles (continued)

Bed Characteristics:

Spherical Particles: 10 mm and 6 mm Nominal Diameter Mixture

Mean Particle Diameter: 7.8 mm

x_6= 0.280 x_{10}= 0.720

Run Number: 61002

Superficial Liquid Velocity j_ℓ= 3.89 mm/s

Superficial Gas Velocity at Flooding j_g= —— mm/s

Superficial Gas Velocity	Particulate Bed			Overlying Liquid Layer		Average Pressure Gradient	
j_g (mm/s)	Bed Depth (mm)	Porosity ε	Average Active Void Fraction $\bar{\alpha}_{ac}$	Height (mm)	Average Void Fraction $\bar{\alpha}_o$	Total $\frac{dP_t}{dz}$ (kPa/m)	Frictional $\frac{dP_f}{dz}$ (kPa/m)
0.0	852	0.36	0.00	172	0.00	9.59	-0.178
13.1	852	0.36	0.12	254	0.075	8.48	-0.147
29.5	852	0.36	0.20	331	0.10	7.83	-0.036
50.0	852	0.36	0.25	347	0.15	7.20	-0.101
77.7	850	0.36	0.31	483	0.22	6.36	-0.401
115.4	854	0.36	0.38	588	0.25	5.76	-0.342
162.9	849	0.36	0.43	543	0.29	5.13	-0.479

Table G.6 Void Fraction and Pressure Drop Data for a Bed Composed of a Mixture of 6 mm and 10 mm Nominal Diameter Particles (continued)

Bed Characteristics:

Spherical Particles: 10 mm and 6 mm Nominal Diameter Mixture

Mean Particle Diameter: 7.8 mm

x_6 = 0.280 x_{10} = 0.720

Run Number: 61003

Superficial Liquid Velocity j_ℓ = 5.84 mm/s

Superficial Gas Velocity at Flooding j_g = 163 mm/s

Superficial Gas Velocity	Particulate Bed			Overlying Liquid Layer		Average Pressure Gradient	
j_g (mm/s)	Bed Depth (mm)	Porosity ε	Average Active Void Fraction $\bar{\alpha}_{ac}$	Height (mm)	Average Void Fraction $\bar{\alpha}_o$	Total $\frac{dP_t}{dz}$ (kPa/m)	Frictional $\frac{dP_f}{dz}$ (kPa/m)
0.0	849	0.36	0.00	159	0.00	9.53	-0.243
13.1	845	0.36	0.12	251	0.095	8.22	-0.397
29.5	845	0.36	0.19	337	0.12	7.36	-0.586
50.0	845	0.36	0.25	412	0.18	6.58	-0.793
77.7	845	0.36	0.31	471	0.23	5.97	-0.803
115.4	845	0.36	0.34	550	0.25	5.31	-1.13
162.9	845	0.36	——	571	——	4.70	——

Table G.6 Void Fraction and Pressure Drop Data for a Bed Composed of a Mixture of 6 mm and 10 mm Nominal Diameter Particles (continued)

Bed Characteristics:

Spherical Particles: 10 mm and 6 mm Nominal Diameter Mixture

Mean Particle Diameter: 7.8 mm

x_6 = 0.280 x_{10} = 0.720

Run Number: 61004

Superficial Liquid Velocity j_ℓ = 7.78 mm/s

Superficial Gas Velocity at Flooding j_g = 115 mm/s

Superficial Gas Velocity	Particulate Bed			Overlying Liquid Layer		Average Pressure Gradient	
j_g (mm/s)	Bed Depth (mm)	Porosity ε	Average Active Void Fraction $\bar{\alpha}_{ac}$	Height (mm)	Average Void Fraction $\bar{\alpha}_o$	Total $\frac{dP_t}{dz}$ (kPa/m)	Frictional $\frac{dP_f}{dz}$ (kPa/m)
0.0	848	0.36	0.00	142	0.00	9.35	-0.421
13.1	847	0.36	0.12	231	0.11	7.91	-0.724
29.5	847	0.36	0.20	306	0.14	6.97	-0.898
50.0	845	0.36	0.26	343	0.17	6.15	-1.08
77.7	845	0.36	0.32	464	0.22	5.23	-1.46
115.4	845	0.36	0.41	569	0.24	4.42	-1.34

Table G.6 Void Fraction and Pressure Drop Data for a Bed Composed of a Mixture of 6 mm and 10 mm Nominal Diameter Particles (continued)

Bed Characteristics:

Spherical Particles: 10 mm and 6 mm Nominal Diameter Mixture

Mean Particle Diameter: 7.8 mm

x_6 = 0.280 x_{10} = 0.720

Run Number:

Superficial Liquid Velocity j_ℓ = 9.73 mm/s

Superficial Gas Velocity at Flooding j_g = 83 mm/s

Superficial Gas Velocity j_g (mm/s)	Particulate Bed			Overlying Liquid Layer		Average Pressure Gradient	
	Bed Depth (mm)	Porosity ε	Average Active Void Fraction $\bar{\alpha}_{ac}$	Height (mm)	Average Void Fraction $\bar{\alpha}_o$	Total $\frac{dP_t}{dz}$ (kPa/m)	Frictional $\frac{dP_f}{dz}$ (kPa/m)
0.0	845	0.36	0.00	158	0.00	9.27	-0.502
13.1	845	0.36	0.12	250	0.10	7.57	-1.00
29.5	845	0.36	0.22	398	0.13	6.47	-1.15
50.0	845	0.36	0.28	424	0.17	5.63	-1.42
83.0	845	0.36	0.37	457	0.21	4.59	-1.57

Table G.6 Void Fraction and Pressure Drop Data for a Bed Composed of a Mixture of 6 mm and 10 mm Nominal Diameter Particles (continued)

Bed Characteristics:

Spherical Particles: 10 mm and 6 mm Nominal Diameter Mixture

Mean Particle Diameter: 7.8 mm

x_6 = 0.280 x_{10} = 0.720

Run Number: 61006

Superficial Liquid Velocity j_ℓ = 11.67 mm/s

Superficial Gas Velocity at Flooding j_g = 65 mm/s

Superficial Gas Velocity j_g (mm/s)	Particulate Bed			Overlying Liquid Layer		Average Pressure Gradient	
	Bed Depth (mm)	Porosity ε	Average Active Void Fraction $\bar{\alpha}_{ac}$	Height (mm)	Average Void Fraction $\bar{\alpha}_o$	Total $\frac{dP_t}{dz}$ (kPa/m)	Frictional $\frac{dP_f}{dz}$ (kPa/m)
0.0	845	0.36	0.00	166	0.00	9.09	-0.679
13.1	845	0.36	0.14	270	0.11	7.20	-1.25
29.5	845	0.36	0.21	397	0.14	5.97	-1.75
50.0	845	0.36	0.25	447	0.20	5.10	-2.29
65.0	845	0.36	0.34	476	0.20	4.25	-2.21

Table G.6 Void Fraction and Pressure Drop Data for a Bed Composed of a Mixture of 6 mm and 10 mm Nominal Diameter Particles (continued)

Bed Characteristics:

Spherical Particles: 10 mm and 6 mm Nominal Diameter Mixture

Mean Particle Diameter: 7.8 mm

x_6 = 0.280 x_{10} = 0.720

Run Number: 61007

Superficial Liquid Velocity j_ℓ = 13.62 mm/s

Superficial Gas Velocity at Flooding j_g = 46 mm/s

Superficial Gas Velocity j_g (mm/s)	Particulate Bed			Overlying Liquid Layer		Average Pressure Gradient	
	Bed Depth (mm)	Porosity ε	Average Active Void Fraction $\bar{\alpha}_{ac}$	Height (mm)	Average Void Fraction $\bar{\alpha}_o$	Total $\frac{dP_t}{dz}$ (kPa/m)	Frictional $\frac{dP_f}{dz}$ (kPa/m)
0.0	844	0.36	0.00	154	0.00	8,95	-0.825
13.1	844	0.36	0.13	288	0.11	6.71	-1.79
29.5	844	0.36	0.22	404	0.15	5.39	-2.28
46.0	844	0.36	0.27	470	0.19	4.58	-2.64

Table G.6 Void Fraction and Pressure Drop Data for a Bed Composed of a Mixture of 6 mm and 10 mm Nominal Diameter Particles (continued)

Bed Characteristics:

Spherical Particles: 10 mm and 6 mm Nominal Diameter Mixture

Mean Particle Diameter: 7.8 mm

x_6 = 0.280 x_{10} = 0.720

Run Number: 61008

Superficial Liquid Velocity j_ℓ = 15.56 mm/s

Superficial Gas Velocity at Flooding j_g = 30 mm/s

Superficial Gas Velocity	Particulate Bed			Overlying Liquid Layer		Average Pressure Gradient	
j_g (mm/s)	Bed Depth (mm)	Porosity ϵ	Average Active Void Fraction $\bar{\alpha}_{ac}$	Height (mm)	Average Void Fraction $\bar{\alpha}_o$	Total $\frac{dP_t}{dz}$ (kPa/m)	Frictional $\frac{dP_f}{dz}$ (kPa/m)
0.0	844	0.36	0.00	161	0.00	8.75	-1.02
13.1	844	0.36	0.13	338	0.092	6.16	-2.34
29.5	844	0.36	0.24	420	0.15	4.80	-2.62

Table G.6 Void Fraction and Pressure Drop Data for a Bed Composed of a Mixture of 6 mm and 10 mm Nominal Diameter Particles (continued)

Bed Characteristics:

Spherical Particles: 10 mm and 6 mm Nominal Diameter Mixture

Mean Particle Diameter: 7.8 mm

x_6 = 0.280 x_{10} = 0.720

Run Number: 61009

Superficial Liquid Velocity j_ℓ = 17.51 mm/s

Superficial Gas Velocity at Flooding j_g = 21 mm/s

Superficial Gas Velocity	Particulate Bed			Overlying Liquid Layer		Average Pressure Gradient	
j_g (mm/s)	Bed Depth (mm)	Porosity ε	Average Active Void Fraction $\bar{\alpha}_{ac}$	Height (mm)	Average Void Fraction $\bar{\alpha}_o$	Total $\frac{dP_t}{dz}$ (kPa/m)	Frictional $\frac{dP_f}{dz}$ (kPa/m)
0.0	844	0.36	0.00	148	0.00	8.49	-1.28
13.1	844	0.36	0.13	307	0.11	5.69	-2.85
21.0	844	0.36	0.21	336	0.11	4.41	-3.19

Table G.6 Void Fraction and Pressure Drop Data for a Bed Composed of a Mixture of 6 mm and 10 mm Nominal Diameter Particles (continued)

Bed Characteristics:

Spherical Particles: 10 mm and 6 mm Nominal Diameter Mixture

Mean Particle Diameter: 7.8 mm

x_6 = 0.280 x_{10} = 0.720

Run Number: 61010

Superficial Liquid Velocity j_ℓ = 19.46 mm/s

Superficial Gas Velocity at Flooding j_g = 14.3 mm/s

Superficial Gas Velocity j_g (mm/s)	Particulate Bed			Overlying Liquid Layer		Average Pressure Gradient	
	Bed Depth (mm)	Porosity ϵ	Average Active Void Fraction $\bar{\alpha}_{ac}$	Height (mm)	Average Void Fraction $\bar{\alpha}_o$	Total $\frac{dP_t}{dz}$ (kPa/m)	Frictional $\frac{dP_f}{dz}$ (kPa/m)
0.0	844	0.36	0.00	170	0.00	8.10	-1.67
10.0	844	0.36	0.14	319	0.088	5.58	-2.86
13.1	844	0.36	0.13	319	0.14	5.13	-3.39
14.3	844	0.36	0.18	545	0.084	4.58	-3.47

Table G.7 Void Fraction and Pressure Drop Data for a Bed Composed of a Mixture of 6 mm and 15 mm Nominal Diameter Particles

Bed Characteristics:

Spherical Particles: 15 mm and 6 mm Nominal Diameter Mixture

Mean Particle Diameter: 10.3 mm

$x_6 = 0.156$ $x_{15} = 0.844$

Run Number: 61500

Superficial Liquid Velocity $j_\ell = 0.0$ mm/s

Superficial Gas Velocity at Flooding $j_g =$ — mm/s

Superficial Gas Velocity j_g (mm/s)	Particulate Bed			Overlying Liquid Layer		Average Pressure Gradient	
	Bed Depth (mm)	Porosity ϵ	Average Active Void Fraction $\bar{\alpha}_{ac}$	Height (mm)	Average Void Fraction $\bar{\alpha}_o$	Total $\frac{dP_t}{dz}$ (kPa/m)	Frictional $\frac{dP_f}{dz}$ (kPa/m)
13.1	858	0.38	0.13	203	0.048	8.90	0.366
29.5	853	0.37	0.21	253	0.12	8.28	0.527
50.0	851	0.37	0.27	294	0.16	7.72	0.614
77.7	850	0.37	0.33	340	0.21	7.25	0.726
115.4	850	0.37	0.39	387	0.27	6.76	0.817
162.9	849	0.37	0.45	444	0.32	6.47	1.08

Table G.7 Void Fraction and Pressure Drop Data for a Bed Composed of a Mixture of 6 mm and 15 mm Nominal Diameter Particles (continued)

Bed Characteristics:

Spherical Particles: 15 mm and 6 mm Nominal Diameter Mixture

Mean Particle Diameter: 10.3 mm

x_6= 0.156 x_{15}= 0.844

Run Number: 61502

Superficial Liquid Velocity j_ℓ= 3.89 mm/s

Superficial Gas Velocity at Flooding j_g= —— mm/s

Superficial Gas Velocity	Particulate Bed			Overlying Liquid Layer		Average Pressure Gradient	
j_g (mm/s)	Bed Depth (mm)	Porosity ε	Average Active Void Fraction $\bar{\alpha}_{ac}$	Height (mm)	Average Void Fraction $\bar{\alpha}_o$	Total $\frac{dP_t}{dz}$ (kPa/m)	Frictional $\frac{dP_f}{dz}$ (kPa/m)
0.0	847	0.37	0.00	173	0.00	9.69	-0.081
13.1	847	0.37	0.12	263	0.086	8.44	-0.116
29.5	847	0.37	0.22	326	0.11	7.76	0.141
50.0	847	0.37	0.27	309	0.19	7.12	0.002
77.7	847	0.37	0.34	402	0.23	6.41	-0.056
115.4	847	0.37	0.38	409	0.26	6.02	0.054
162.9	847	0.37	0.42	538	0.28	5.45	-0.181

Table G.7 Void Fraction and Pressure Drop Data for a Bed Composed of a Mixture of 6 mm and 15 mm Nominal Diameter Particles (continued)

Bed Characteristics:

Spherical Particles: 15 mm and 6 mm Nominal Diameter Mixture

Mean Particle Diameter: 10.3 mm

x_6 = 0.156 x_{15} = 0.844

Run Number: 61504

Superficial Liquid Velocity j_ℓ = 7.78 mm/s

Superficial Gas Velocity at Flooding j_g = 144 mm/s

Superficial Gas Velocity	Particulate Bed			Overlying Liquid Layer		Average Pressure Gradient	
j_g (mm/s)	Bed Depth (mm)	Porosity ϵ	Average Active Void Fraction $\bar{\alpha}_{ac}$	Height (mm)	Average Void Fraction $\bar{\alpha}_o$	Total $\frac{dP_t}{dz}$ (kPa/m)	Frictional $\frac{dP_f}{dz}$ (kPa/m)
0.0	847	0.37	0.00	163	0.00	9.53	-0.243
13.1	847	0.37	0.12	247	0.075	8.10	-0.456
29.5	847	0.37	0.21	319	0.12	7.30	-0.465
50.0	847	0.37	0.28	403	0.17	6.41	-0.681
77.7	847	0.37	0.35	464	0.22	5.92	-0.454
115.4	847	0.37	0.40	449	0.26	5.06	-0.853
144.0	847	0.37	0.53	468	0.28	4.79	-0.589

Table G.7 Void Fraction and Pressure Drop Data for a Bed Composed of a Mixture of 6 mm and 15 mm Nominal Diameter Particles (continued)

Bed Characteristics:

Spherical Particles: 15 mm and 6 mm Nominal Diameter Mixture

Mean Particle Diameter: 10.3 mm

x_6= 0.156 x_{15}= 0.844

Run Number: 61505

Superficial Liquid Velocity j_ℓ= 9.73 mm/s

Superficial Gas Velocity at Flooding j_g= 106 mm/s

Superficial Gas Velocity j_g (mm/s)	Particulate Bed			Overlying Liquid Layer		Average Pressure Gradient	
	Bed Depth (mm)	Porosity ϵ	Average Active Void Fraction $\bar{\alpha}_{ac}$	Height (mm)	Average Void Fraction $\bar{\alpha}_o$	Total $\frac{dP_t}{dz}$ (kPa/m)	Frictional $\frac{dP_f}{dz}$ (kPa/m)
0.0	844	0.37	0.00	152	0.00	9.45	-0.324
13.1	844	0.37	0.16	248	0.088	7.72	-0.503
29.5	844	0.37	0.21	304	0.12	6.86	-0.901
50.0	844	0.37	0.30	405	0.16	6.03	-0.790
77.7	844	0.37	0.39	440	0.21	5.32	-0.608
106.0	844	0.37	0.37	489	0.22	4.64	-1.54

Table G.7 Void Fraction and Pressure Drop Data for a Bed Composed of a Mixture of 6 mm and 15 mm Nominal Diameter Particles (continued)

Bed Characteristics:

Spherical Particles: 15 mm and 6 mm Nominal Diameter Mixture

Mean Particle Diameter: 10.3 mm

$x_6 = 0.156$ $x_{15} = 0.844$

Run Number: 61506

Superficial Liquid Velocity $j_\ell = 11.67$ mm/s

Superficial Gas Velocity at Flooding $j_g = 78$ mm/s

Superficial Gas Velocity	Particulate Bed			Overlying Liquid Layer		Average Pressure Gradient	
j_g (mm/s)	Bed Depth (mm)	Porosity ε	Average Active Void Fraction $\bar{\alpha}_{ac}$	Height (mm)	Average Void Fraction $\bar{\alpha}_o$	Total $\frac{dP_t}{dz}$ (kPa/m)	Frictional $\frac{dP_f}{dz}$ (kPa/m)
0.0	846	0.37	0.00	172	0.00	9.33	-0.437
13.1	846	0.37	0.17	271	0.088	7.54	-0.573
29.5	846	0.37	0.22	313	0.13	6.55	-1.10
50.0	846	0.37	0.31	366	0.15	5.73	-1.03
77.7	846	0.37	——	489	0.18	4.82	——

Table G.7 Void Fraction and Pressure Drop Data for a Bed Composed of a Mixture of 6 mm and 15 mm Nominal Diameter Particles (continued)

Bed Characteristics:

Spherical Particles: 15 mm and 6 mm Nominal Diameter Mixture

Mean Particle Diameter: 10.3 mm

x_6= 0.156 x_{15}= C.844

Run Number: 61507

Superficial Liquid Velocity j_ℓ= 13.62 mm/s

Superficial Gas Velocity at Flooding j_g= 55 mm/s

Superficial Gas Velocity	Particulate Bed			Overlying Liquid Layer		Average Pressure Gradient	
j_g (mm/s)	Bed Depth (mm)	Porosity ϵ	Average Active Void Fraction $\bar{\alpha}_{ac}$	Height (mm)	Average Void Fraction $\bar{\alpha}_o$	Total $\frac{dP_t}{dz}$ (kPa/m)	Frictional $\frac{dP_f}{dz}$ (kPa/m)
0.0	844	0.37	0.00	156	0.00	9.22	-0.550
13.1	844	0.37	0.16	260	0.10	7.15	-1.11
29.5	844	0.37	0.24	335	0.11	6.24	-1.24
50.0	844	0.37	0.29	429	0.17	5.34	-1.65
55.0	844	0.37	——	433	——	4.80	——

Table G.7 Void Fraction and Pressure Drop Data for a Bed Composed of a Mixture of 6 mm and 15 mm Nominal Diameter Particles (continued)

Bed Characteristics:

Spherical Particles: 15 mm and 6 mm Nominal Diameter Mixture

Mean Particle Diameter: 10.3 mm

x_6 = 0.156 x_{15} = 0.844

Run Number: 61508

Superficial Liquid Velocity j_ℓ = 15.56 mm/s

Superficial Gas Velocity at Flooding j_g = 41.5 mm/s

Superficial Gas Velocity	Particulate Bed			Overlying Liquid Layer		Average Pressure Gradient	
j_g (mm/s)[¶]	Bed Depth (mm)	Porosity ϵ	Average Active Void Fraction $\bar{\alpha}_{ac}$	Height (mm)	Average Void Fraction $\bar{\alpha}_o$	Total $\frac{dP_t}{dz}$ (kPa/m)	Frictional $\frac{dP_f}{dz}$ (kPa/m)
0.0	844	0.37	0.00	152	0.00	9.08	-0.696
13.1	844	0.37	0.13	304	0.10	7.00	-1.49
29.5	844	0.37	0.21	401	0.13	5.89	-1.79
37.5	844	0.37	——	440	——	5.11	——

Table G.7 Void Fraction and Pressure Drop Data for a Bed Composed of a Mixture of 6 mm and 15 mm Nominal Diameter Particles (continued)

Bed Characteristics:

Spherical Particles: 15 mm and 6 mm Nominal Diameter Mixture

Mean Particle Diameter: 10.3 mm

$x_6 = 0.156$ $x_{15} = 0.844$

Run Number: 61509

Superficial Liquid Velocity $j_\ell = 17.51$ mm/s

Superficial Gas Velocity at Flooding $j_g = 30$ mm/s

Superficial Gas Velocity j_g (mm/s)	Particulate Bed			Overlying Liquid Layer		Average Pressure Gradient	
	Bed Depth (mm)	Porosity ε	Average Active Void Fraction $\bar{\alpha}_{ac}$	Height (mm)	Average Void Fraction $\bar{\alpha}_o$	Total $\frac{dP_t}{dz}$ (kPa/m)	Frictional $\frac{dP_f}{dz}$ (kPa/m)
0.0	844	0.37	0.00	199	0.00	8.90	-0.873
13.1	844	0.37	0.14	392	0.088	6.49	-1.88
29.5	844	0.37	0.23	413	0.13	5.14	-2.39

Table G.7 Void Fraction and Pressure Drop Data for a Bed Composed of a Mixture of 6 mm and 15 mm Nominal Diameter Particles (continued)

Bed Characteristics:

Spherical Particles: 15 mm and 6 mm Nominal Diameter Mixture

Mean Particle Diameter: 10.3 mm

x_6 = 0.156 x_{15} = 0.844

Run Number: 61510

Superficial Liquid Velocity j_ℓ = 19.46 mm/s

Superficial Gas Velocity at Flooding j_g = 23 mm/s

Superficial Gas Velocity	Particulate Bed			Overlying Liquid Layer		Average Pressure Gradient	
j_g (mm/s)	Bed Depth (mm)	Porosity ε	Average Active Void Fraction $\bar{\alpha}_{ac}$	Height (mm)	Average Void Fraction $\bar{\alpha}_o$	Total $\frac{dP_t}{dz}$ (kPa/m)	Frictional $\frac{dP_f}{dz}$ (kPa/m)
0.0	844	0.37	0.00	174	0.00	8.77	-1.00
13.1	844	0.37	0.15	398	0.092	5.86	-2.42
23.0	844	0.37	0.24	443	0.11	5.14	-2.29

Table G.8 Void Fraction and Pressure Drop Data for a Bed Composed of a Mixture of 6, 10, 15, and 19 mm Nominal Diameter Particles

Bed Characteristics:

Spherical Particles: 6,10,15,19 mm Nominal Diameter Mixture

Mean Particle Diameter: 9.9 mm

$x_6 = 0.20$ $x_{10} = 0.30$ $x_{15} = 0.30$ $x_{19} = 0.20$

Run Number: 00AM1

Superficial Liquid Velocity $j_\ell = 0.0$ mm/s

Superficial Gas Velocity at Flooding $j_g =$ —— mm/s

Superficial Gas Velocity	Particulate Bed			Overlying Liquid Layer		Average Pressure Gradient	
j_g (mm/s)	Bed Depth (mm)	Porosity ε	Average Active Void Fraction $\bar{\alpha}_{ac}$	Height (mm)	Average Void Fraction $\bar{\alpha}_o$	Total $\frac{dP_t}{dz}$ (kPa/m)	Frictional $\frac{dP_f}{dz}$ (kPa/m)
13.1	855	0.35	0.14	305	0.039	8.93	0.546
29.5	852	0.34	0.23	341	0.056	8.40	0.897
50.0	852	0.34	0.31	385	0.11	7.67	0.895
77.7	852	0.34	0.37	424	0.15	7.09	0.945
115.4	847	0.34	0.45	477	0.19	6.57	1.21

Table G.8 Void Fraction and Pressure Drop Data for a Bed Composed of a Mixture of 6, 10, 15, and 19 mm Nominal Diameter Particles (continued)

Bed Characteristics:

Spherical Particles: 6,10,15,19 mm Nominal Diameter Mixture

Mean Particle Diameter: 9.9 mm

x_6= 0.20 x_{10}= 0.30 x_{15}= 0.30 x_{19}= 0.20

Run Number: 02AM1

Superficial Liquid Velocity j_ℓ= 3.89 mm/s

Superficial Gas Velocity at Flooding j_g= —— mm/s

Superficial Gas Velocity j_g (mm/s)	Particulate Bed			Overlying Liquid Layer		Average Pressure Gradient	
	Bed Depth (mm)	Porosity ϵ	Average Active Void Fraction $\bar{\alpha}_{ac}$	Height (mm)	Average Void Fraction $\bar{\alpha}_o$	Total $\frac{dP_t}{dz}$ (kPa/m)	Frictional $\frac{dP_f}{dz}$ (kPa/m)
0.0	850	0.34	0.00	175	0.00	9.66	-0.113
13.1	850	0.34	0.13	236	0.047	8.36	-0.192
29.5	847	0.34	0.21	304	0.10	7.55	-0.192
50.0	850	0.34	0.29	389	0.14	6.79	-0.162
77.7	848	0.34	0.36	358	0.18	5.97	-0.270
115.4	848	0.34	0.42	472	0.23	5.39	-0.324

Table G.8 Void Fraction and Pressure Drop Data for a Bed Composed of a Mixture of 6, 10, 15, and 19 mm Nominal Diameter Particles (continued)

Bed Characteristics:

Spherical Particles: 6,10,15,19 mm Nominal Diameter Mixture

Mean Particle Diameter: 9.9 mm

x_6= 0.20 x_{10}= 0.30 x_{15}= 0.30 x_{19}= 0.20

Run Number: 04AM1

Superficial Liquid Velocity j_ℓ= 7.78 mm/s

Superficial Gas Velocity at Flooding j_g= 115 mm/s

Superficial Gas Velocity j_g (mm/s)	Particulate Bed			Overlying Liquid Layer		Average Pressure Gradient	
	Bed Depth (mm)	Porosity ε	Average Active Void Fraction $\bar{\alpha}_{ac}$	Height (mm)	Average Void Fraction $\bar{\alpha}_o$	Total $\frac{dP_t}{dz}$ (kPa/m)	Frictional $\frac{dP_f}{dz}$ (kPa/m)
0.0	848	0.34	0.00	196	0.00	9.46	-0.307
13.1	848	0.34	0.14	305	0.070	7.81	-0.648
29.5	845	0.34	0.23	328	0.12	6.84	-0.702
50.0	845	0.34	0.30	438	0.14	5.95	-0.917
77.7	845	0.34	0.35	473	0.18	5.32	-1.01
115.4	845	0.34	0.42	545	0.21	4.85	-0.844

Table G.8 Void Fraction and Pressure Drop Data for a Bed Composed of a Mixture of 6, 10, 15, and 19 mm Nominal Diameter Particles (continued)

Bed Characteristics:

Spherical Particles: 6,10,15,19 mm Nominal Diameter Mixture

Mean Particle Diameter: 9.9 mm

x_6= 0.20 x_{10}= 0.30 x_{15}= 0.30 x_{19}= 0.20

Run Number: 05AM1

Superficial Liquid Velocity j_ℓ = 9.73 mm/s

Superficial Gas Velocity at Flooding j_g = 83 mm/s

Superficial Gas Velocity j_g (mm/s)	Particulate Bed			Overlying Liquid Layer		Average Pressure Gradient	
	Bed Depth (mm)	Porosity ε	Average Active Void Fraction $\bar{\alpha}_{ac}$	Height (mm)	Average Void Fraction $\bar{\alpha}_o$	Total $\frac{dP_t}{dz}$ (kPa/m)	Frictional $\frac{dP_f}{dz}$ (kPa/m)
13.1	843	0.34	0.14	278	0.082	7.46	-0.966
29.5	843	0.34	0.22	334	0.10	6.57	-1.07
50.0	843	0.34	0.30	425	0.16	5.60	-1.27
83.0	843	0.34	0.38	541	0.19	4.84	-1.25

Table G.8 Void Fraction and Pressure Drop Data for a Bed Composed of a Mixture of 6, 10, 15, and 19 mm Nominal Diameter Particles (continued)

Bed Characteristics:

Spherical Particles: 6,10,15,19 mm Nominal Diameter Mixture

Mean Particle Diameter: 9.9 mm

x_6 = 0.20 x_{10} = 0.30 x_{15} = 0.30 x_{19} = 0.20

Run Number: 06AM1

Superficial Liquid Velocity j_ℓ = 11.67 mm/s

Superficial Gas Velocity at Flooding j_g = 62 mm/s

Superficial Gas Velocity	Particulate Bed			Overlying Liquid Layer		Average Pressure Gradient	
j_g (mm/s)	Bed Depth (mm)	Porosity ϵ	Average Active Void Fraction $\bar{\alpha}_{ac}$	Height (mm)	Average Void Fraction $\bar{\alpha}_o$	Total $\frac{dP_t}{dz}$ (kPa/m)	Frictional $\frac{dP_f}{dz}$ (kPa/m)
0.0	847	0.34	0.00	213	0.00	9.22	-0.550
13.1	847	0.34	0.15	355	0.066	7.09	-1.18
29.5	847	0.34	0.22	386	0.10	6.11	-1.48
50.0	843	0.34	0.30	492	0.14	5.06	-1.80
62.0	843	0.34	0.37	568	0.15	4.29	-1.86

Table G.8 Void Fraction and Pressure Drop Data for a Bed Composed of a Mixture of 6, 10, 15, and 19 mm Nominal Diameter Particles (continued)

Bed Characteristics:

Spherical Particles: 6,10,15,19 mm Nominal Diameter Mixture

Mean Particle Diameter: 9.9 mm

$x_6 = 0.20$ $x_{10} = 0.30$ $x_{15} = 0.30$ $x_{19} = 0.20$

Run Number: 07AM1

Superficial Liquid Velocity $j_\ell = 13.62$ mm/s

Superficial Gas Velocity at Flooding $j_g = 44$ mm/s

Superficial Gas Velocity	Particulate Bed			Overlying Liquid Layer		Average Pressure Gradient	
j_g (mm/s)	Bed Depth (mm)	Porosity ϵ	Average Active Void Fraction $\bar{\alpha}_{ac}$	Height (mm)	Average Void Fraction $\bar{\alpha}_o$	Total $\frac{dP_t}{dz}$ (kPa/m)	Frictional $\frac{dP_f}{dz}$ (kPa/m)
0.0	843	0.34	0.00	170	0.00	9.01	-0.760
13.1	843	0.34	0.12	279	0.086	6.86	-1.70
29.5	843	0.34	0.22	413	0.11	5.58	-2.10
44.0	843	0.34	0.27	442	0.14	4.85	-2.32

Table G.8 Void Fraction and Pressure Drop Data for a Bed Composed of a Mixture of 6, 10, 15, and 19 mm Nominal Diameter Particles (continued)

Bed Characteristics:

Spherical Particles: 6,10,15,19 mm Nominal Diameter Mixture

Mean Particle Diameter: 9.9 mm

x_6 = 0.20 x_{10} = 0.30 x_{15} = 0.30 x_{19} = 0.20

Run Number: 08AM1

Superficial Liquid Velocity j_ℓ = 15.56 mm/s

Superficial Gas Velocity at Flooding j_g = 30 mm/s

Superficial Gas Velocity	Particulate Bed			Overlying Liquid Layer		Average Pressure Gradient	
j_g (mm/s)	Bed Depth (mm)	Porosity ε	Average Active Void Fraction $\bar{\alpha}_{ac}$	Height (mm)	Average Void Fraction $\bar{\alpha}_o$	Total $\frac{dP_t}{dz}$ (kPa/m)	Frictional $\frac{dP_f}{dz}$ (kPa/m)
0.0	843	0.34	0.00	182	0.00	8.75	-1.02
13.1	843	0.34	0.12	317	0.085	6.47	-2.16
29.5	843	0.34	0.23	498	0.10	4.63	-2.91

Table G.8 Void Fraction and Pressure Drop Data for a Bed Composed of a Mixture of 6, 10, 15, and 19 mm Nominal Diameter Particles (continued)

Bed Characteristics:

Spherical Particles: 6,10,15,19 mm Nominal Diameter Mixture

Mean Particle Diameter: 9.9 mm

x_6= 0.20 x_{10}= 0.30 x_{15}= 0.30 x_{19}= 0.20

Run Number: 09AM1

Superficial Liquid Velocity j_ℓ = 17.51 mm/s

Superficial Gas Velocity at Flooding j_g = 21 mm/s

Superficial Gas Velocity	Particulate Bed			Overlying Liquid Layer		Average Pressure Gradient	
j_g (mm/s)	Bed Depth (mm)	Porosity ϵ	Average Active Void Fraction $\bar{\alpha}_{ac}$	Height (mm)	Average Void Fraction $\bar{\alpha}_o$	Total $\frac{dP_t}{dz}$ (kPa/m)	Frictional $\frac{dP_f}{dz}$ (kPa/m)
0.0	843	0.34	0.00	175	0.00	8.59	-1.18
13.1	843	0.34	0.11	364	0.077	5.86	-2.81
21.0	843	0.34	0.16	436	0.092	4.97	-3.25

Table G.8 Void Fraction and Pressure Drop Data for a Bed Composed of a Mixture of 6, 10, 15, and 19 mm Nominal Diameter Particles (continued)

Bed Characteristics:

Spherical Particles: 6,10,15,19 mm Nominal Diameter Mixture

Mean Particle Diameter: 9.9 mm

x_6 = 0.20 x_{10} = 0.30 x_{15} = 0.30 x_{19} = 0.20

Run Number: 10AM1

Superficial Liquid Velocity j_ℓ = 19.46 mm/s

Superficial Gas Velocity at Flooding j_g = 13.1 mm/s

Superficial Gas Velocity	Particulate Bed			Overlying Liquid Layer		Average Pressure Gradient	
j_g (mm/s)	Bed Depth (mm)	Porosity ϵ	Average Active Void Fraction $\bar{\alpha}_{ac}$	Height (mm)	Average Void Fraction $\bar{\alpha}_o$	Total $\frac{dP_t}{dz}$ (kPa/m)	Frictional $\frac{dP_f}{dz}$ (kPa/m)
0.0	843	0.34	0.00	172	0.00	8.38	-1.39
13.1	843	0.34	0.12	388	0.10	5.21	-3.39

Table G.9 Void Fraction and Pressure Drop Data for a Bed Composed of a Mixture of 3, 6, 10, 15, and 19 mm Nominal Diameter Particles

Bed Characteristics:

Spherical Particles: 3,6,10,15,19 mm Nominal Diameter Mixture

Mean Particle Diameter: 5.4 mm

x_3= 0.16 x_6= 0.21 x_{10}= 0.21 x_{15}= 0.21 x_{19}= 0.21

Run Number: 00AM2

Superficial Liquid Velocity j_ℓ = 0.0 mm/s

Superficial Gas Velocity at Flooding j_g = —— mm/s

Superficial Gas Velocity	Particulate Bed			Overlying Liquid Layer		Average Pressure Gradient	
j_g (mm/s)	Bed Depth (mm)	Porosity ε	Average Active Void Fraction $\bar{\alpha}_{ac}$	Height (mm)	Average Void Fraction $\bar{\alpha}_o$	Total $\frac{dP_t}{dz}$ (kPa/m)	Frictional $\frac{dP_f}{dz}$ (kPa/m)
13.1	850	0.29	0.12	486	0.037	8.96	0.307
29.5	850	0.29	0.18	512	0.067	8.61	0.596
50.0	846	0.28	0.23	555	0.11	8.48	0.960
77.7	841	0.28	0.30	606	0.17	9.12	2.31
115.4	841	0.28	0.37	646	0.20	8.56	2.35
162.9	844	0.28	0.42	690	0.24	8.72	3.09

Table G.9 Void Fraction and Pressure Drop Data for a Bed Composed of a Mixture of 3, 6, 10, 15, and 19 mm Nominal Diameter Particles (continued)

Bed Characteristics:

Spherical Particles: 3,6,10,15,19 mm Nominal Diameter Mixture

Mean Particle Diameter: 5.4 mm

x_3= 0.16 x_6= 0.21 x_{10}= 0.21 x_{15}= 0.21 x_{19}= 0.21

Run Number: 01AM2

Superficial Liquid Velocity j_ℓ = 1.95 mm/s

Superficial Gas Velocity at Flooding j_g = 115 mm/s

Superficial Gas Velocity	Particulate Bed			Overlying Liquid Layer		Average Pressure Gradient	
j_g (mm/s)	Bed Depth (mm)	Porosity ε	Average Active Void Fraction $\bar{\alpha}_{ac}$	Height (mm)	Average Void Fraction $\bar{\alpha}_o$	Total $\frac{dP_t}{dz}$ (kPa/m)	Frictional $\frac{dP_f}{dz}$ (kPa/m)
0.0	845	0.28	0.00	166	0.00	9.48	-0.291
13.1	836	0.27	0.14	220	0.005	7.81	-0.619
29.5	836	0.27	0.19	243	0.11	7.33	-0.551
50.0	836	0.27	0.23	274	0.18	6.96	-0.543
77.7	836	0.27	0.33	315	0.22	6.28	-0.270
115.4	845	0.28	0.37	446	0.28	5.76	-0.411

Table G.9 Void Fraction and Pressure Drop Data for a Bed Composed of a Mixture of 3, 6, 10, 15, and 19 mm Nominal Diameter Particles (continued)

Bed Characteristics:

Spherical Particles: 3,6,10,15,19 mm Nominal Diameter Mixture

Mean Particle Diameter: 5.4 mm

x_3= 0.16 x_6= 0.21 x_{10}= 0.21 x_{15}= 0.21 x_{19}= 0.21

Run Number: 02AM2

Superficial Liquid Velocity j_ℓ= 3.89 mm/s

Superficial Gas Velocity at Flooding j_g= 50 mm/s

Superficial Gas Velocity	Particulate Bed			Overlying Liquid Layer		Average Pressure Gradient	
j_g (mm/s)	Bed Depth (mm)	Porosity ε	Average Active Void Fraction $\bar{\alpha}_{ac}$	Height (mm)	Average Void Fraction $\bar{\alpha}_o$	Total $\frac{dP_t}{dz}$ (kPa/m)	Frictional $\frac{dP_f}{dz}$ (kPa/m)
0.0	848	0.28	0.00	170	0.00	9.17	-0.599
13.1	846	0.28	0.11	269	0.065	7.13	-1.54
29.5	846	0.28	0.17	341	0.11	6.45	-1.62
50.0	845	0.28	0.26	409	0.16	5.08	-2.11

Table G.9 Void Fraction and Pressure Drop Data for a Bed Composed of a Mixture of 3, 6, 10, 15, and 19 mm Nominal Diameter Particles (continued)

Bed Characteristics:

Spherical Particles: 3,6,10,15,19 mm Nominal Diameter Mixture

Mean Particle Diameter: 5.4 mm

x_3 = 0.16 x_6 = 0.21 x_{10} = 0.21 x_{15} = 0.21 x_{19} = 0.21

Run Number: 03AM2

Superficial Liquid Velocity j_ℓ = 5.84 mm/s

Superficial Gas Velocity at Flooding j_g = 30 mm/s

Superficial Gas Velocity	Particulate Bed			Overlying Liquid Layer		Average Pressure Gradient	
j_g (mm/s)	Bed Depth (mm)	Porosity ϵ	Average Active Void Fraction $\bar{\alpha}_{ac}$	Height (mm)	Average Void Fraction $\bar{\alpha}_o$	Total $\frac{dP_t}{dz}$ (kPa/m)	Frictional $\frac{dP_f}{dz}$ (kPa/m)
0.0	836	0.27	0.00	204	0.00	8.43	-1.34
13.1	836	0.27	0.095	359	0.050	5.90	-2.94
29.5	836	0.27	0.22	523	0.11	2.78	-4.83

Table G.9 Void Fraction and Pressure Drop Data for a Bed Composed of a Mixture of 3, 6, 10, 15, and 19 mm Nominal Diameter Particles (continued)

Bed Characteristics:

Spherical Particles: 3,6,10,15,19 mm Nominal Diameter Mixture

Mean Particle Diameter: 5.4 mm

x_3= 0.16 x_6= 0.21 x_{10}= 0.21 x_{15}= 0.21 x_{19}= 0.21

Run Number: 04AM2

Superficial Liquid Velocity j_ℓ = 7.78 mm/s

Superficial Gas Velocity at Flooding j_g = 10.0 mm/s

Superficial Gas Velocity j_g (mm/s)	Particulate Bed			Overlying Liquid Layer		Average Pressure Gradient	
	Bed Depth (mm)	Porosity ε	Average Active Void Fraction $\bar{\alpha}_{ac}$	Height (mm)	Average Void Fraction $\bar{\alpha}_o$	Total $\frac{dP_t}{dz}$ (kPa/m)	Frictional $\frac{dP_f}{dz}$ (kPa/m)
0.0	836	0.27	0.00	184	0.00	7.76	-2.01
10.0	836	0.27	0.12	289	0.059	4.32	-4.30

Table G.10 Void Fraction and Pressure Drop Data for a Bed Composed of a Mixture of 1, 3, 6, 10, 15, and 19 mm Nominal Diameter Particles

Bed Characteristics:

Spherical Particles: 1,3,6,10,15,19 mm Nominal Diameter Mixture

Mean Particle Diameter: 3.1 mm

Run Number: 00AM3

Superficial Liquid Velocity j_ℓ = 0.0 mm/s

Superficial Gas Velocity at Flooding j_g = —— mm/s

x_1 = 0.10 x_3 = 0.15 x_6 = 0.25 x_{10} = 0.25 x_{15} = 0.15 x_{19} = 0.10

Superficial Gas Velocity j_g (mm/s)	Particulate Bed			Overlying Liquid Layer		Average Pressure Gradient	
	Bed Depth (mm)	Porosity ϵ	Average Active Void Fraction $\bar{\alpha}_{ac}$	Height (mm)	Average Void Fraction $\bar{\alpha}_o$	Total $\frac{dP_t}{dz}$ (kPa/m)	Frictional $\frac{dP_f}{dz}$ (kPa/m)
13.1	765	0.27	0.069	524	0.044	9.16	0.063
29.5	765	0.27	0.11	580	0.071	8.88	0.183
50.0	768	0.27	0.15	619	0.13	8.93	0.614
77.7	770	0.27	0.18	658	0.18	8.91	0.857
115.4	770	0.27	0.22	551	0.25	9.14	1.47

Table G.10 Void Fraction and Pressure Drop Data for a Bed Composed of a Mixture of 1, 3, 6, 10, 15, and 19 mm Nominal Diameter Particles (continued)

Bed Characteristics:

Spherical Particles: 1,3,6,10,15,19 mm Nominal Diameter Mixture

Mean Particle Diameter: 3.1 mm

Run Number: 01AM3

Superficial Liquid Velocity j_ℓ = 1.95 mm/s

Superficial Gas Velocity at Flooding j_g = 30 mm/s

x_1 = 0.10 x_3 = 0.15 x_6 = 0.25 x_{10} = 0.25 x_{15} = 0.15 x_{19} = 0.10

Superficial Gas Velocity j_g (mm/s)	Particulate Bed			Overlying Liquid Layer		Average Pressure Gradient	
	Bed Depth (mm)	Porosity ε	Average Active Void Fraction $\bar{\alpha}_{ac}$	Height (mm)	Average Void Fraction $\bar{\alpha}_o$	Total $\frac{dP_t}{dz}$ (kPa/m)	Frictional $\frac{dP_f}{dz}$ (kPa/m)
0.0	767	0.27	0.00	408	0.00	8.90	-0.874
13.1	767	0.27	0.089	318	0.055	7.33	-1.57
29.5	767	0.27	0.18	446	0.092	5.55	-2.46

Table G.11 Void Fraction and Pressure Drop Data for a Bed Composed of a Mixture of 6 mm Nominal Diameter Spherical Particles and Non-Spherical Sharps

Bed Characteristics:

Particles: Non-Spherical Sharps and 6 mm Nominal Diameter Spherical Particles Mixture

Mean Particle Diameter: 3.4 mm

x_S= 0.50 x_6= 0.50

Run Number: 06S00

Superficial Liquid Velocity j_ℓ = 0.0 mm/s

Superficial Gas Velocity at Flooding j_g = —— mm/s

Superficial Gas Velocity	Particulate Bed			Overlying Liquid Layer		Average Pressure Gradient	
j_g (mm/s)	Bed Depth (mm)	Porosity ϵ	Average Active Void Fraction $\bar{\alpha}_{ac}$	Height (mm)	Average Void Fraction $\bar{\alpha}_o$	Total $\frac{dP_t}{dz}$ (kPa/m)	Frictional $\frac{dP_f}{dz}$ (kPa/m)
13.1	379	0.38	0.084	507	0.043	9.19	0.234
29.5	376	0.37	0.12	551	0.10	8.96	0.395
50.0	373	0.37	0.14	460	0.16	8.74	0.353
77.7	373	0.37	0.22	499	0.21	8.31	0.675
115.4	373	0.37	0.26	542	0.26	8.41	1.16
153.0	373	0.37	0.30	564	0.28	8.31	1.43

Table G.11 Void Fraction and Pressure Drop Data for a Bed Composed of a Mixture of 6 mm Nominal Diameter Spherical Particles and Non-Spherical Sharps (continued)

Bed Characteristics:

Particles: Non-Spherical Sharps and 6 mm Nominal Diameter Spherical Particles Mixture

Mean Particle Diameter: 3.4 mm

x_S= 0.50 x_6= 0.50

Run Number: 06S01

Superficial Liquid Velocity j_ℓ= 1.95 mm/s

Superficial Gas Velocity at Flooding j_g= —— mm/s

Superficial Gas Velocity j_g (mm/s)	Particulate Bed			Overlying Liquid Layer		Average Pressure Gradient	
	Bed Depth (mm)	Porosity ε	Average Active Void Fraction $\bar{\alpha}_{ac}$	Height (mm)	Average Void Fraction $\bar{\alpha}_o$	Total $\frac{dP_t}{dz}$ (kPa/m)	Frictional $\frac{dP_f}{dz}$ (kPa/m)
0.0	369	0.36	0.00	311	0.00	9.51	-0.259
13.1	369	0.36	0.044	370	0.068	8.67	-0.676
29.5	369	0.36	0.077	406	0.12	8.25	-0.769
50.0	369	0.36	0.13	471	0.17	7.89	-0.600
77.7	369	0.36	0.18	538	0.23	7.67	-0.385
115.4	369	0.36	0.23	573	0.23	7.60	0.065
153.0	369	0.36	0.28	649	0.29	7.54	0.513

Table G.11 Void Fraction and Pressure Drop Data for a Bed Composed of a Mixture of 6 mm Nominal Diameter Spherical Particles and Non-Spherical Sharps (continued)

Bed Characteristics:

Particles: Non-Spherical Sharps and 6 mm Nominal Diameter Spherical Particles Mixture

Mean Particle Diameter: 3.4 mm

$x_S = 0.50$ $x_6 = 0.50$

Run Number: 06S02

Superficial Liquid Velocity j_ℓ = 3.89 mm/s

Superficial Gas Velocity at Flooding j_g = 115 mm/s

Superficial Gas Velocity j_g (mm/s)	Particulate Bed			Overlying Liquid Layer		Average Pressure Gradient	
	Bed Depth (mm)	Porosity ϵ	Average Active Void Fraction $\bar{\alpha}_{ac}$	Height (mm)	Average Void Fraction $\bar{\alpha}_o$	Total $\frac{dP_t}{dz}$ (kPa/m)	Frictional $\frac{dP_f}{dz}$ (kPa/m)
0.0	373	0.37	0.00	288	0.00	9.32	-0.153
13.1	373	0.37	0.068	364	0.060	8.19	-0.926
29.5	373	0.37	0.12	428	0.11	7.51	-1.14
50.0	373	0.37	0.16	481	0.16	7.02	-1.16
77.7	373	0.37	0.22	548	0.22	6.66	-0.936
115.4	373	0.37	——	548	0.32	6.79	——

Table G.11 Void Fraction and Pressure Drop Data for a Bed Composed of a Mixture of 6 mm Nominal Diameter Spherical Particles and Non-Spherical Sharps (continued)

Bed Characteristics:

Particles: Non-Spherical Sharps and 6 mm Nominal Diameter Spherical Particles Mixture

Mean Particle Diameter: 3.4 mm

$x_S = 0.50$ $x_6 = 0.50$

Run Number: 06S03

Superficial Liquid Velocity $j_\ell = 5.84$ mm/s

Superficial Gas Velocity at Flooding $j_g = 78$ mm/s

Superficial Gas Velocity j_g (mm/s)	Particulate Bed			Overlying Liquid Layer		Average Pressure Gradient	
	Bed Depth (mm)	Porosity ϵ	Average Active Void Fraction $\bar{\alpha}_{ac}$	Height (mm)	Average Void Fraction $\bar{\alpha}_o$	Total $\frac{dP_t}{dz}$ (kPa/m)	Frictional $\frac{dP_f}{dz}$ (kPa/m)
0.0	365	0.36	0.00	329	0.00	8.99	-0.776
13.1	365	0.36	0.063	390	0.079	7.47	-1.69
29.5	365	0.36	0.14	458	0.11	6.66	-1.71
50.0	365	0.36	0.15	490	0.15	6.24	-2.07
77.7	365	0.36	——	530	0.25	6.50	——

Table G.11 Void Fraction and Pressure Drop Data for a Bed Composed of a Mixture of 6 mm Nominal Diameter Spherical Particles and Non-Spherical Sharps (continued)

Bed Characteristics:

Particles: Non-Spherical Sharps and 6 mm Nominal Diameter Spherical Particles Mixture

Mean Particle Diameter: 3.4 mm

$x_S = 0.50$ $x_6 = 0.50$

Run Number: 06504

Superficial Liquid Velocity $j_\ell = 7.78$ mm/s

Superficial Gas Velocity at Flooding $j_g = 42$ mm/s

Superficial Gas Velocity j_g (mm/s)	Particulate Bed			Overlying Liquid Layer		Average Pressure Gradient	
	Bed Depth (mm)	Porosity ϵ	Average Active Void Fraction $\bar{\alpha}_{ac}$	Height (mm)	Average Void Fraction $\bar{\alpha}_o$	Total $\frac{dP_t}{dz}$ (kPa/m)	Frictional $\frac{dP_f}{dz}$ (kPa/m)
0.0	372	0.37	0.00	311	0.00	8.73	-1.04
13.1	372	0.37	0.041	383	0.082	6.89	-2.48
29.5	372	0.37	0.13	476	0.12	5.63	-3.84
41.8	372	0.37	0.14	550	0.16	5.24	-3.77

Table G.11 Void Fraction and Pressure Drop Data for a Bed Composed of a Mixture of 6 mm Nominal Diameter Spherical Particles and Non-Spherical Sharps (continued)

Bed Characteristics:

Particles: Non-Spherical Sharps and 6 mm Nominal Diameter Spherical Particles Mixture

Mean Particle Diameter: 3.4 mm

$x_S = 0.50$ $x_6 = 0.50$

Run Number: 06S05

Superficial Liquid Velocity $j_\ell = 9.73$ mm/s

Superficial Gas Velocity at Flooding $j_g = 23$ mm/s

Superficial Gas Velocity j_g (mm/s)	Particulate Bed			Overlying Liquid Layer		Average Pressure Gradient	
	Bed Depth (mm)	Porosity ϵ	Average Active Void Fraction $\bar{\alpha}_{ac}$	Height (mm)	Average Void Fraction $\bar{\alpha}_o$	Total $\frac{dP_t}{dz}$ (kPa/m)	Frictional $\frac{dP_f}{dz}$ (kPa/m)
0.0	369	0.36	0.00	342	0.00	8.44	-1.33
13.1	369	0.36	0.018	419	0.080	5.95	-3.64
22.9	369	0.36	0.12	559	0.10	4.27	-4.28

NRC FORM 335 (7-77)

U.S. NUCLEAR REGULATORY COMMISSION

BIBLIOGRAPHIC DATA SHEET

1. REPORT NUMBER (Assigned by DDC): NUREG/CR-3995

2. (Leave blank)

3. RECIPIENT'S ACCESSION NO.

4. TITLE AND SUBTITLE (Add Volume No., if appropriate)
Hydrodynamics of Counter-Current Two Phase Flow Through Porous Media

5. DATE REPORT COMPLETED
MONTH: May | YEAR: 1984

DATE REPORT ISSUED
MONTH: December | YEAR: 1984

6. (Leave blank)

7. AUTHOR(S)
J.S. Marshall and V.K. Dhir

8. (Leave blank)

9. PERFORMING ORGANIZATION NAME AND MAILING ADDRESS (Include Zip Code)
School of Engineering and Applied Sciences
University of California, Los Angeles
Los Angeles, CA 90024

10. PROJECT/TASK/WORK UNIT NO.

11. CONTRACT NO.
G-04-81-025

12. SPONSORING ORGANIZATION NAME AND MAILING ADDRESS (Include Zip Code)
Division of Accident Evaluation
Office of Nuclear Regulatory Research
U.S. Nuclear Regulatory Commission
Washington, D.C. 20555

13. TYPE OF REPORT
Technical Topical Report

PERIOD COVERED (Inclusive dates)
Jan 1983 - Dec. 1983

14. (Leave blank)

15. SUPPLEMENTARY NOTES

16. ABSTRACT (200 words or less) Understanding of the hydrodynamic characteristics and flow limitations of two phase flow through porous media is necessary to evaluate the coolability of a top flooded degraded nuclear reactor core. In the present work, an analytical and experimental investigation of counter-current two phase flow through 80-100 cm deep porous layers composed of both uniform size spherical particles (nominal diameters 1-19 mm), mixtures of spherical particles and nonspherical "sharps" has been performed. The porous layers were formed in a 20 cm diameter plexiglass tube. Water and air were used as the test fluids, with superficial velocities ranging from 0-19.5 mm/s and 0-163 mm/s, respectively. Bed porosity, mean particle diameter, flooding limits, and void fraction and pressure gradient at flooding were investigated. An analytical approach based upon geometrical models was used to derive expressions for porosity and mean particle diameter. An empirical correlation has been found for the flooding data which is slightly different than that found in the literature. The effect of coupling of the overlying liquid layer with the bed and of axial gas injection upon the flooding limit were also studied. The results of these hydrodynamic investigations were applied to obtai[illegible] dryout heat flux in bottom and volume heated particulate beds.

17. KEY WORDS AND DOCUMENT ANALYSIS

17a. DESCRIPTORS

Thermohydraulics
Heat Transfer
Debris Bed Coolability
Severe Accidents

17b. IDENTIFIERS/OPEN-ENDED TERMS

18. AVAILABILITY STATEMENT
Unlimited

19. SECURITY CLASS (This report): Unclassified

20. SECURITY CLASS (This page): Unclassified

21. NO. OF PAGES

22. PRICE
$

NRC FORM 335 (7-77)

UNITED STATES
NUCLEAR REGULATORY COMMISSION
WASHINGTON, D.C. 20555

OFFICIAL BUSINESS
PENALTY FOR PRIVATE USE, $300

FOURTH CLASS MAIL
POSTAGE & FEES PAID
USNRC
WASH. D.C.
PERMIT No. G-67

120555078877 1 IANIR2
US NRC
ADM-DIV OF TIDC
POLICY & PUB MGT BR-PDR NUREG
W-501
WASHINGTON DC 20555